Characterization of Infectious Human Prions

by

Claudia Y. Acevedo Morantes

A thesis submitted in partial fulfillment of the requirements for the
degree of

Doctor of Philosophy

Department of Biochemistry
University of Alberta

ABSTRACT

Human prion diseases present as sporadic, familial, infectious, or iatrogenic forms. They include diseases such as Creutzfeldt-Jakob disease (CJD), Gerstmann-Sträussler-Scheinker syndrome (GSS), and Fatal Familial Insomnia (FFI). The wide range of phenotypic variation in human prion diseases is caused by aberrantly folded versions of the prion protein, termed PrP^{Sc}. Evidence indicates that distinct aggregated forms with heterogeneous morphologies regarding length, width, shape, longitudinal twist, and the number of protofilaments exist, which originate during prion replication. However, the insolubility of PrP^{Sc} and its propensity to aggregate make it inaccessible to high-resolution techniques. Another piece of the puzzle is that prions have different proteinase K (PK)-cleavage sites and distinct pathogenic mechanisms, characterized by diverse symptoms, despite an identical primary structure.

Thus, the proposed hypothesis of this study is that human prions have different PK-cleavage sites despite an identical primary structure, suggesting that prion types exist due to different pathological protein conformations. The central objective of this study is to evaluate the intrinsic heterogeneity between sporadic and familial forms of human prions by characterizing their structural conformations, via electron microscopy (EM) approaches. It is expected that these results will provide new knowledge regarding the conformational structure of these particles and serves as a platform to evaluate the current proposed structural models. Previous studies have used in vitro- and rodent- derived prions to elucidate the structure of prions and the heterogeneity of fibrils in sample populations. Hence, this study is based on the rationale that, regardless that these models have contributed and will continue to contribute in our understanding of the molecular basis of the

structural organization of diverse prion species, these conformers are imperfect substitutes to prions derived from human brain.

To accomplish this objective, I used tilted-beam–transmission electron microscopy (TB-TEM), to determine the mass-per-length (MPL) of PrP^{Sc} fibrils. This data can be used to determine the number of protofilaments per fibril, establish the intrinsic heterogeneity of individual samples, and provide a platform to evaluate the current proposed models for prion fibrils.

The main findings of this work were to delineate a biochemical profile of each human PrP species based on their limited proteolysis, electrophoretic mobility, TEM imaging and MPL measurements. Thus, MPL measurements determined from PrP^{Sc} fibrils of sCJD and fCJD, showed a value of ~60 kDa/nm, suggesting that PrP^{Sc} fibrils are composed of more than one protofilament. Bioassays in transgenic humanized PrP mice (TgHu(PrP)) also confirmed the infectious nature of these PrP^{Sc} species. These results also suggested that no significant differences are present in the structural conformation of PrP^{Sc} fibrils derived from sCJD and fCJD.

PrP species derived from brain tissue of a patient diagnosed with GSS and with the alanine to valine mutation at codon 117 (A117V), and the common methionine to valine polymorphism at codon 129 (M129V), were examined by a series of enzymatic digestions, electrophoretic mobility and TEM imaging. The presence of PK- and thermolysin (TL)- resistant fragments of ~7 kDa/nm and ~16 kDa/nm, respectively was revealed. Although no significant differences were found regarding the amount of PrP species derived from cortex and cerebellum, enzymatic digestions exhibited that PrP species from cortex were more sensitive to PK-digestion when compared with those derived from cerebellum. These findings suggest that brain tropism might have an effect in the structural conformation of PrP species, regardless that they present the same neuropathological features. Evaluation of the infectivity of these particles in Tg(HuPrP) mice, also revealed that these

particles maintained their infectious nature, a hallmark of prion particles. Elucidating the structure of prion proteins may aid the design of effective structure-based therapies against different proteinopathies.

PREFACE

The research conducted for this thesis is the result of my original work and form part of international research collaboration, led by Professor Holger Wille at the University of Alberta. The chapters that compose this thesis contain unpublished data, and are in preparation to be submitted for publication.

The research project, of which this thesis is a part received ethics approval from the University of Alberta Research Ethics Board, Project Name: "Human prions and other misfolded proteins-analyzing the molecular structure of the misfolded conformers" (Study ID: Pro00042442).

The Health Research Ethics Board - Biomedical Panel has reviewed this project and found it to be acceptable within the limitations of human experimentation. The membership of the Health Research Ethics Board (HREB) - Biomedical Panel complies with the membership requirements for research ethics boards as defined in Division 5 of the Food and Drug Regulations and the Tri Council Policy Statement. The HREB - Biomedical Panel carries out its functions in a manner consistent with Good Clinical Practices and the Canadian General Standards Board (CAN/CGSB-101.1-2013).

Animal studies were conducted following the Canadian Council on Animal Care Guidelines and Policies with approval from the Health Sciences Care and Use Committee of the University of Alberta Research Ethics Board; Project name: "Structural biology of infectious mammalian prions", AUP00000884.

ACKNOWLEDGEMENTS

"Some people pass through our lives for a season to teach us
lessons that could never be learned if they stayed"

Mandy Hale

First, I would like to thank the selection committee of graduate students in the department of Biochemistry at the University of Alberta, for initially accepting my application in the program. Special thanks to Kimberly Arndt and Dr. David Stuart for their help and guidance during these years. I am very grateful also to the Faculty of Graduate Studies and Research (FGSR) at the University of Alberta for selecting me to receive the University of Alberta Doctoral Recruitment Scholarship.

I would like to thank my supervisor, Dr. Holger Wille, for providing me invaluable advice throughout the development of this project. Accept my heartfelt gratitude for your support and counseling during these years. I am filled with gratitude to the members of my Thesis Committee, Dr. Michael Overduin and Dr. Bernard Lemire, for their time, support and useful suggestions. In addition, I thank Dr. Andrew MacMillan from the Department of Biochemistry at the University of Alberta, and Dr. Candace Mathiason from the Department of Microbiology, Immunology and Pathology at the Colorado State University, for accepting being the examiners in my PhD defense.

I would like to express my gratitude to my colleagues at the Centre for Prions and Protein Folding Diseases at the University of Alberta, especially thanks to Brian Tancowny, who enormously helped me with the bioassays. Many thanks also to Dr. Xiongyao Wang, who patiently trained me in the use of the electron microscope, as well as to Dr. Yong-Liang Wang for his support and commitment to keep the electron microscope properly running. Thanks also to Dr. Xinli Tang, who kindly has provided the antibodies used in this project.

I am deeply grateful to my family and friends for their unconditional support. Thanks for always be there.

TABLE OF CONTENTS

LIST OF FIGURES

CHAPTER 1. INTRODUCTION

CHAPTER 2. EXPERIMENTAL PROCEDURES

CHAPTER 3. CHARACTERIZATION OF FAMILIAL CREUTZFELDT-JAKOB DISEASE (fCJD) WITH A MUTATION AT CODON E200K AND A POLYMORPHISM AT CODON M129V OF PRION PROTEIN GENE

CHAPTER 4 CHARACTERIZATION OF SPORADIC CREUTZFELDT-JAKOB DISEASE (sCJD) PRION SPECIES BY LIMITED PROTEOLYSIS AND MPL MEASUREMENTS

CHAPTER 5. CHARACTERIZATION OF GERSTMANN-STRÄUSSLER-SCHEINKER (GSS) SYNDROME WITH A MUTATION AT CODON A117V AND POLYMORPHISM M129V OF PRION PROTEIN GENE

CHAPTER 6. CONCLUSSIONS

Supplemental Material

LIST OF TABLES

LIST OF ABBREVIATIONS (Alphabetical order)

ADC   Apparent diffusion coefficient (ADC)

BSE   Bovine spongiform encephalopathies

CJD   Creutzfeldt-Jakob disease

CNS   Central nervous system

CSF   Cerebrospinal fluid

CT   Computed tomography (scan of the brain)

DWI   Diffusion-weighted imaging

EEG   Electroencephalogram

fCJD   Familial [inherited, genetic] Creutzfeldt-Jakob disease

FFI   Fatal Familial Insomnia

FI   Fatal Insomnia

FLAIR   Fluid-attenuated inversion recovery

FWHM   Full-width at half-maximum

GSS   Gerstmann-Sträussler-Scheinker syndrome

MPL   Mass-per-length

MRI   Magnetic resonance imaging

PE   Pronase E

PK   Proteinase K

PRNP   Prion gene

PrP^C Normal cellular isoform of prion protein

PrPres   Prion protein resistant to proteinase K (PK)-digestion

PrP^{Sc} Abnormal isoform of prion protein

PSWCs   Periodic-sharp wave complexes

recPrP   Recombinant prion protein

sCJD   Sporadic Creutzfeldt-Jakob disease

sPrP^{Sc}	Prion protein sensitive to digestion by proteinase K (PK)
ssNMR	Solid-state nuclear magnetic resonance
TB-TEM	Tilted-Beam -Transmission electron microscopy
TEM	Transmission electron microscopy
Tg	Transgenic
Tg(HuPrP)	Transgenic mice expressing human prion protein
TL	Thermolysin
TMV	Tobacco mosaic virus
TSEs	Transmissible spongiform encephalopathies
vCJD	Variant Creutzfeldt-Jakob disease
WT	Wild-type

GLOSSARY OF MEDICAL TERMS (Alphabetical order)

Akinetic mutism:	A state in which a person is unable to speak (mute) or move (akinetic). Akinetic mutism is often due to damage to the frontal lobes of the brain
Apraxia:	The inability to execute a voluntary motor movement despite being able to perform normal muscle function
Ataxia:	Poor coordination and unsteadiness due to the brain's failure to regulate the body's posture and regulate the strength and direction of limb movements
Bradykinesia:	Slow movement. Bradykinesia is often associated with an impaired ability to adjust the body's position
Bradyphrenia:	A slow thought process. Bradyphrenia can be a side effect of certain psychiatric medications
Dysarthria:	Difficult or unclear articulation of speech
Dyspnea:	Difficult or labored breathing; shortness of breath. Dyspnea is a sign of serious disease of the airway, lungs, or heart
Dysphagia:	Difficulty swallowing. Dysphagia is due to abnormal nerve or muscle control
Ideomotor apraxia:	Disorder characterized by deficits in properly performing tool-use pantomimes and communicative gestures
Infratentorial region:	Region of the brain that contains the cerebellum
Myoclonus:	A condition of abnormal contraction of muscles or portion of muscles
Oliguria:	Less urination than normal
Parenchyma:	The key element of an organ essential to its functioning, as distinct from the capsule that encompasses it and other supporting structures

Pyramidal: Refers to upper motor neurons that originate in the cerebral cortex and terminate in the spinal cord or brainstem

Supratentorial region: Region of the brain that contains the cerebrum

Tetraparesis: A condition in which all four limbs are weak

Source: www.medicinenet.com

CHAPTER 1

INTRODUCTION

1.1. The prion protein: overview

Prion encephalopathies, also known as transmission spongiform encephalopathies (TSEs), are a family of rare progressive neurodegenerative disorders afflicting humans and other mammals. These diseases are characterized by neuropathological changes that include: vacuolation, astrocytosis, neuronal loss and the development of amyloid plaques in the brain. The prion protein is most highly expressed in the central nervous system (CNS), but it can be found in other tissues and cell types as well, including secondary lymphoid organs, muscle, blood and sites of chronic inflammation [1–3].

Misfolding of normally soluble, functional peptides and proteins and their subsequent conversion into fibrillar aggregates, of which the archetype example are amyloid fibrils, are associated with approximately 50 disorders. It is known that the misfolded PrP^{Sc} is the causative agent of TSEs. The term "prion (PrP)" is a contraction created by Stanley Prusiner [4] for "proteinaceous infectious particle", which refers to the abnormal conformational conformer, PrP^{Sc}. In a process that is not fully understood, the misfolded, disease causing, prion scrapie isoform PrP^{Sc}, binds to the monomeric, non-infectious, cellular prion isoform PrP^{C} and promotes its conversion into PrP^{Sc}. It has been hypothesized that in a self-perpetuating process these newly misfolded proteins, in turn, act as templates for the conversion of more PrP^{C} into PrP^{Sc}. These cascades of events induce an exponential accumulation of PrP^{Sc} in the CNS. As a consequence, the abnormal protein isoform aggregates into densely packed β-sheets, an abnormal fold called amyloid. These polypeptide aggregates form plaques that are thought to cause "entanglement" of neurofibrils and interfere with synapse function, leading to neurodegeneration. Eventually, many microscopic, sponge-like holes (vacuoles) can be seen in the brain, resulting in progressive deterioration, cell death and dementia [5].

1.1.1. The prion protein: historical background. Proteins were first recognized as a distinct class of biological molecules by Antoine Fourcroy in 1789 [67]. Nearly a century later, in 1838, Dutch chemist Gerhardus Johannes Mulder carried out elemental analyses of several proteins and determined their primary composition. He proposed that proteins share a single common core substance, called "Grundstoff", synthesized by plants, transferred intact into herbivores and consequently into carnivores. G.J Mulder also proposed that albuminous proteins have the same empirical formula C400H620N100O120P1S1, with variations in their own content of sulfur and phosphorus atoms [7]. The Swedish chemist Jöns Jacob Berzelius supported Mulder's theory, and proposed the name "protein" derived from the Greek word "prota", meaning "of primary importance". Subsequently, extensive research would take to the discovery of other proteins, to elucidate their composition, and hence the amino acids as the basic chemical building blocks that make up proteins.

Simultaneously, advances in other fields like microbiology, lead to a systematic discovery and classification of microorganisms, among which were: i) the initial classification of bacteria by Ferdinand Cohn, in 1875 [8]; ii) Koch's postulates, which were derived in 1890, from Robert Koch's work, and which continue to guide microbiologists today [9]; iii) findings that antibodies conferred immunity against pathogens by Paul Ehrlich in 1891 [10]; iv) identification of viruses, including elucidation of the structure of tobacco mosaic virus (TMV) [11]; v) the observation that viral replication requires nucleic acid [12]; and vi) cracking the genetic code [13], which eventually would lay the groundwork and become the "central dogma of molecular biology".

Since the mid-20th century, extensive research has been done in elucidating protein structures and function, and the atomic interaction that governs their folding and conformation. However, regardless of our increasing knowledge in protein folding, predicting the mechanisms involved in the process continues to challenge researchers today. In this regards, the prion protein defies the biochemical and biological paradigms and challenges the "central dogma of molecular biology", which establish that the information in genes flows into proteins, a two-step process known as transcription and translation (DNA → RNA → protein). This is not the first time when the central dogma has been the subject of scrutiny. In 1970, Francis Crick challenged the central dogma in

response to the discovery of retrotranscribing genetic elements (where the information transfer goes from RNA → DNA). Crick realized that, in spite of its biological implications, reverse transcription was an integral part of the cell cycle. Here, prion protein puts the central dogma under scrutiny again, and places the actual "exclusion principle" at another level, the lateral information transfer, based on self-propagating changes in a protein [14].

The old dogma facing new tricks: the maneuver of proteins as pathogens. The story of prions began in the 18th century when the first case of a "strange disease" was reported in a Spanish Merino sheep in 1732. The affected sheep presented abnormal behavior such as altered gaits, excessive licking, and intense itching that compelled the affected animals to compulsively scrape against fences, rocks, or trees [15]. Hence, the name "scrapie" was derived from the pathological itching sensation in the affected animals. Scrapie would become later a member of a new class of neurological disorders known as TSEs, that puzzled the scientific community for around 60 years.

Initial findings that viruses contain RNA or DNA, that are capable of encoding their replication factors, and were infectious [16], drifted the first theories of TSE etiology toward a "slow virus" [17–19]. It was not until 1953 when the accidental outcome of an experiment would help to shed light in deciphering the nature of prions. Dr. William S Gordon, a veterinarian at Moredun Research Institute (Edinburgh, Scotland) was working alongside other researchers on the development of a vaccine against louping-ill virus (LIV), an acute viral agent that is restricted mostly to ovines and that is characterized by a biphasic fever, depression, ataxia, muscular incoordination, tremors, posterior paralysis, coma, and death [20]. Gordon's team used formalin to inactive the louping-ill virus in brain and spleen samples, obtained from infected animals. They used these treated tissues to vaccinate healthy animals [21]. Formalin inactivated the virus but not the scrapie agent that was unknowingly present in the samples. Hence, the vaccinated animals developed scrapie and died two years later. In 1920, German neurologists Hans Gerhard Creutzfeldt and Alfons Maria Jakob described for the first time a human neurological disorder of unknown etiology [22,23], giving it the name Creutzfeldt-Jakob disease (CJD). It appears that the initial diagnostic described in their first paper did not match the current criteria for CJD. It seems that at least two of the patients in the initial studies were afflicted by unusual neuropathological findings associated with other disorders

[24,25]. A few years later, in 1936, neurologists Ernst Sträussler, Josef Gerstmann, and Ilya Scheinker, would describe a rare neurological disease with brain lesions similar to that seen in sheep scrapie disease in members of an Austrian family. Initially reported as CJD, it would later be known as Gerstmann-Sträussler-Scheinker syndrome (GSS) [26], a condition characterized by plaque-like deposits in the cerebral cortex, basal ganglia, and (most extremely) in all layers of the cerebellum. Subsequently, four categories of CJD were reported: 1) sporadic CJD (sCJD), caused by the spontaneous misfolding of the prion protein [27]; 2) familial CJD (fCJD), originated by an inherited mutation in the prion protein gene *PRNP* [28]; 3) iatrogenic or acquired CJD (iCJD) described in 1974, when a patient received a corneal transplant from an infected cadaver [29,30]; and 4) variant CJD (vCJD), reported in the mid-1990s in the UK, as a type of acquired CJD, presumed to be caused by consumption of prion-contaminated food [31].

In the early 1950s, Australian officers patrolling the Eastern Highlands of Papua New Guinea reported a "new disease" afflicting the Fore tribes in the region [32]. The term kuru derives from the Fore word kuria or guria (to shake or to tremble), due to the body twitching and loss of coordination that are the classic symptoms of the disease. It is also known as the "laughing sickness" due to the compulsive, pathologic bursts of laughter [33]. It is now widely accepted that kuru was transmitted among members of the Fore tribe of Papua New Guinea via ritual cannibalism. The corpses of family members were traditionally cooked and eaten, where women and children usually consumed the brain; thus, the disease was more prevalent among them [33].

Like scrapie, CJD and kuru would not be categorized as a TSE for many years, regardless that their infectious nature was demonstrated by inoculating infected samples obtained from scrapie-affected sheep into healthy animals and transmitting the disease [34,35]. Veterinary neuropathologist William Hadlow was the first to recognize similarities between kuru and scrapie [36]. Based on his observations that brain histology of kuru-affected patients was similar to that seen in scrapie-infected sheep, Dr. Hadlow suggested a comprehensive study of the disease to virologist Daniel Carleton Gajdusek. Thus, Gajdusek in collaboration with Drs. Vincent Zigas, Michael Alpers (an Australian doctor) and Joe Gibbs (expert in neurological disorders), aimed efforts to understand the pathology of the disease. They inoculated chimpanzees with kuru brain samples,

obtained from an 11-year Fore girl who had died of kuru. After two years, one of the chimps, Daisy, developed the disease [37]. Here, Gajdusek demonstrated the transmissibility nature of the infectious agent and its ability to cross the species barrier. This finding was a significant advancement in human medicine, leading to the award of the Nobel Prize in Physiology or Medicine to Gajdusek in 1976 [37].

In 1968, A.G. Dickinson investigated the differential incubation periods that certain mouse strains exhibited when inoculated with the same scrapie brain homogenate. By using basic genetics, he found the locus that controls the time between exposure of mice to the scrapie agent and the onset of disease. He named this locus *Sinc* (scrapie incubation). Later shown to be the PrP gene [38]. Meanwhile, researchers from different fields collaborated to elucidate the stability of scrapie. Major efforts were made to inactivate the scrapie agent by ionization, UV radiation, extreme heat, high pressures, and by other methods that were known to inactivate viruses and bacteria [4,39–41]. While trying to isolate the scrapie agent from formalin-fixed tissue, I.H. Pattison would provide evidence that the scrapie agent was of protein origin [42]. In 1967, J.S. Griffith would become the first researcher to boldly proposed that proteins could be infectious pathogens and postulated scrapie as an infectious proteinaceous agent [43]. Many researchers followed in Griffith's footsteps and gathered data that continued to support the hypothesis of scrapie as an infectious protein [19,44,45].

However, it would be Stanley B. Prusiner and coworkers who demonstrated the infectious nature of scrapie, when they purified infectious particles from scrapie-infected hamster brains. S.B. Prusiner coined the term "prion" to designate the "proteinaceous infectious" particles. Here, Prusiner pushed the "protein-only" hypothesis to a rebellious new level, and in 1997 he would win the Nobel Prize [4]. Prusiner and coworkers bolstered their prion hypothesis by inactivating the infectious proteinaceous particles using several techniques that destroyed proteins [46,47]. At the same time, they reinforced previous findings that methods that destroy nucleic acids, such as potent radiation and nucleases, failed to inactivate prions [19].

There was another piece of the puzzle that was overlooked by the scientific community, and that should have revealed striking differences between the prion agent and typical pathogens: the fact that CJD has a genetic component of transmissibility [48,49]. In 1989, Owen and coworkers, demonstrated for the first time, that mutations in the *PRNP* gene are associated with inherited CJD. In this study, a 144-bp insertion in the *PRNP* gene was identified in affected members of a family with inherited CJD. This insertion results in six-extra octapeptide repeats in the N-terminal region of the protein [50].

In 1983, fatal familial insomnia (FFI), a rare prion disease, would be reported by Dr. Ignazio Roiter, an Italian neurologist and sleep expert [51]. Dr. Roiter received a patient at the University of Bologna hospital's sleep Institute; the man known only as Silvano, showed symptoms of insomnia, followed by a progressive memory loss. A similar case was previously reported in Venice, Italy, in 1765, where the first FFI case was reported. Today, it is well known that this disease has two forms: 1) an autosomal dominant inherited isoform, called fatal familial insomnia (FFI), and 2) a variant called sporadic fatal insomnia (sFI) that can be developed spontaneously as a non-inherited mutation [52].

In an attempt to identify a unique scrapie virus-associated messenger RNA in tissues of infected animals, Bruce Chesebro and coworkers synthesized an oligonucleotide probe complementary to the mRNA sequence corresponding to the amino acid sequence of the prion protein, PrP 27-30. A complementary DNA clone corresponding to PrP 27-30 was obtained from infected mice brains. These results were in agreement with a previous published sequence of PrP 27-30. The cDNA clone hybridized to a single 2.4-2.5 kb mRNA from both normal and scrapie-infected brain [53]. Another line of genetic evidence would come from Charles Weissman, S.B. Prusiner, and coworkers, when they isolated a cDNA clone corresponding to a pathogenic PrP fragment from a scrapie-infected hamster brain cDNA library. Southern blot hybridization with a PrP cDNA probe revealed a single gene, called *Prn-p*, with the same restriction pattern in normal and scrapie-infected brain DNA. Similar results were found in murine and human DNA. Enzymatic digestion with PK yielded an amino-terminal truncated- 27-30 kDa fragment of about 140 amino acids [54,55]. Afterwards, they created knockout mice lacking functional PrP genes, which displayed

resistance to scrapie infection and therefore, incapable of propagating the scrapie agent, demonstrating the requirement of PrP[C] for prion infection [56]. Although these findings supported the "prion protein-only hypothesis", there was still a strong reticence to accept them. In the following years, supporting evidence continued to grow and provided in-depth insights into the infectious nature of PrP particles, to name a few:

- In the late 1980s, throughout the United Kingdom, cattle were fed with meat containing the remains of other cattle who spontaneously developed the scrapie-associated disease, later called bovine spongiform encephalopathy (BSE), also known as mad cow disease. Following the BSE outbreak Wilesmith and coworkers were the first research group in identifying scrapie as the causative agent of the BSE epidemic [57].

- In 1993, Prusiner and coworkers found that prions do not stimulate the humoral immune response. Because, it seems that PrP[Sc] is composed of identical amino acid sequence to the cellular PrP[C], the specific immune system displays a natural tolerance [58,59], although lymphoid organs are strongly implicated in the preclinical stages of the disease [59].

- In 1996, Collinge and coworkers would identify a new variant CJD (nvCJD) strain, with characteristics resembling those of BSE transmitted to other species of animals, such as mice, domestic cats and macaques [60].

- In 1998, Jean Manson and Richard Moore using classical genetic analysis, demonstrated that polymorphisms in the *Prnp-p* locus (which contains the PrP[C] gene) controlled incubation time length in prion-infected mice, and that the *Sinc(Prn-i)* (locus controlling mouse scrapie incubation time) and *Prn-p* loci are congruent [61].

- Original studies of spontaneous *de novo* generation of infectious prions have provided the strongest evidence that these particles are misfolded proteins that lack nucleic acid and can

cause disease. In these studies, infectious prions were generated whether by incubating PrP^{Sc} with its normal counterpart PrP^{C} following overnight shaking [62], or by protein misfolding cyclic amplification (PMCA), an innovative technique that uses a serial rounds of cycles of ultrasound sonication and shaking [63]. These findings gave support to the "protein-only" hypothesis postulated by Prusiner, establishing that prions are capable of self-replicating and propagate by conveying the infectious protein conformation to its normally folded counterpart [64].

- In 2013, Jiyan Ma and coworkers conducted the most convincing experiment to date in support of the "prion-only hypothesis": generation of PK-resistant infectious prions (PrPres) from recombinant prion protein (recPrP) expressed in bacteria [65]. These findings have become a breakthrough in prion research, as previous skepticism dismissed initial *de novo* prion experiments arguing that they relied on PrP^{C} derived from living animals as they might harbor a putative TSE virus. These findings revealed that PMCA is sufficient to initiate a series of self-perpetuating PK-resistant and infectious prions.

Subsequently, the discovery of yeast and filamentous fungi prion proteins, as well as the development of new technologies would shed light into the structural biochemistry and propagation of prions, data that eventually would lay the groundwork for the biochemical and structural bases of mammalian prions.

1.1.2. The "prion protein-only" hypothesis. The "prion protein-only" hypothesis states that the disease is a consequence from the conformational change of a normal isoform of a prion protein (PrP^{C}) into a misfolded, protease-resistant, pathogenic isoform called PrP^{Sc}; without implications from a virus or bacteria [66]. From the initial report of prion diseases, it was evident that the causative infectious agents of these disorders were different from standard pathogens (viruses and bacteria). Several approaches were undertaken to probe the infectious nature of the scrapie agent by using methods well known to inactivate nucleic acids (DNA or RNA). The results from these studies concluded that conditions in which nucleic acids were inactive, did not have any effect on the

infectivity of the scrapie agent. Conversely, protein denaturants were effective at reducing infectivity titers, with complete inactivation requiring extremely harsh conditions, such as 5 h of autoclaving at 134 °C or treatment with 2 N NaOH. These findings indicate that the infectious agent is most likely not DNA or RNA-based [47,67].

1.2. Prions in humans and other species

Prion diseases affect several mammalian species, including humans. The existence of prion strains was initially challenging to rationalize within the "protein-only" hypothesis framework, which relies on the idea that the causative agent in these diseases was composed only by misfolded proteins. In particular, considering that in most cases, strain variation has been documented within the same animal species (expressing a single cellular prion protein [PrP^C] sequence) [68]. Current evidence suggests that prion strain-specific phenotypes can be encoded by different protein conformational arrangements and glycosylation patterns (63). The ability of a protein to encode phenotypic information has important biological implications. The appearance of a new human prion disease, variant CJD, and the clear experimental evidence that it is caused by exposure to BSE has highlighted the need to understand the molecular basis of prion propagation, pathogenesis, and the barriers limiting inter-mammalian transmission [66].

1.2.1. Filamentous fungal and yeast prions: an unforeseen support to the "prion protein-only hypothesis". The concept of prion as an infectious self-propagating protein isoform received unexpected support from the simplest eukaryotic organisms -yeast and filamentous fungi. Initially, the term "prion" was used to describe the infectious agent responsible for several neurodegenerative diseases found in mammals. Since then, the term has expanded after the discovery of prions-like proteins in single-celled organisms with a cellular organization similar to that of higher organisms [19]. An enzyme whose active and modified form is necessary for its maturation might also be a prion (Table 1). The feasibility and rapid growth of yeast and filamentous fungal prions have greatly accelerated studies investigating their propagation and

structural conformation, data that have provided biochemical and structural bases for mammalian prion strains [19].

1.2.1.1. The filamentous fungal prion [HET-s]. A member of the Fungi kingdom, *Podospora anserina*, an ascomycete filamentous fungus, would shed light on the "prion hypothesis" conundrum. The HET-s protein from *P. anserina* is a prion involved in a cell death reaction, termed "heterokaryon incompatibility". When two genetically distinct strains interact, one that harbors a HET-s prion (in the form of amyloid aggregates) and the other that expresses a soluble HET-S protein (96% identical to HET-s), a cell death reaction occurs at the point where the interaction occurs. It is still unknown how the HET-s prion association with HET-S initiates cell death. However, recent evidence suggests that HET-s induces HeLo (the prion-forming domain of HET-S), to unfold and adopt the β-solenoid fold previously observed in HET-s. This new partially unfolded HeLo domain exposes a buried ~34 residue N-terminal transmembrane segment. Eventually, this segment targets HET-S to the membrane where it further oligomerizes, leading to a loss of membrane integrity [69]. These cascades of events are reminiscent of the mechanisms associated with mammalian prions. Hence, the HET-s prion from *P. anserina* has provided additional genetic and biochemical data that has shed light on nature, self-propagating mechanisms, toxicity, and structural complexity of mammalian prions.

1.2.1.2. The yeast prions [URE3] and [PSI+]. Discovery and characterization of two yeast prion proteins, Ure2 and Sup35, have provided a model for understanding disease-associated mammalian prions. In 1994, Reed Wickner expanded the prion concept to explain that the previously known yeast non-chromosomal genetic elements [URE3] [70,71] and [PSI+] [74,80] in *S. cerevisiae*, were respectively prion forms of the Ure2 and Sup35 proteins [71].

Prion	Prion protein function	Normal protein	Protein normal function	Refs.
[β]ᵃ*	Active vacuolar protease B, poor sporulation and poor survival in stationary phase.	Prb1p	Vacuolar protease PrB zymogen (made as an inactive precursor). Prion form is active PrB. Not amyloid.	[74]
[GAR+]ᵃ	Designated for "resistant to glucose-associated repression". Makes cells resistant to the glucose-associated repression of alternative carbon sources.	Pma1p/ Std1p	Plasma membrane proton pump; glucose signaling.	[75]
[ISP+]ᵃ	Accumulates in the nucleus and results in larger cell size. Increased drug resistance.	Sfp1	Transcription factor that regulates ribosomal protein and ribosome biogenesis gene expression.	[76]
[MOD+]ᵃ	Increased level of membrane lipid ergosterol and acquired resistance to antifungal agents.	Mod5	tRNA isopentenyl transferase.	[74,77]
[MOT3+]ᵃ	Produces diverse lineage-specific multicellular phenotypes in response to nutrient deprivation; and transcription repressor of genes derepressed under anaerobiosis.	Mot3p	Transcription regulator; derepression of anaerobic genes.[72]	[78]
[OCT+]ᵃ	Cause slow growth, defects in sporulation and mating.	Cyc8p	Transcription co-repressor subunit.	[74,77]
[PIN+]ᵃ	Increased frequency of generation of [PSI+] and [URE3] prions.	Rnq1	Not determined.	[72]
[PSI+]ᵃ	Increased readthrough of translation termination codons. It is detrimental for its host.	Sup35p	Translation termination factor, mRNA turnover. Causes nonsense suppression.	[79]
[RNQ+]ᵃ	Controls the ability of a cell to acquire other prions.	Rnq1	Not determined.	[72]
[SWI+]ᵃ	Abolishes flocculin (*FLO*) gene expression and leads to a complete loss of multicellularity. Poor growth on raffinose, galactose or glycerol.	Swi1p	Subunit of SWI-SNF chromatin remodeling complex.	[80]
[URE3]ᵃ	Altered form of Ure2p, leads to inappropriate derepression of enzymes and transporters for the utilization of poor N sources (detrimental for its host).	Ure2p	Nitrogen catabolism repressor. In the presence of a rich N source, Urep2 binds the positive transcription factor Gln3p, keeping it in the cytoplasm.	[71,75]
[C]ᵇ*	Designated for "crippled growth".	MAP kinases	Mitogen-activated protein kinase kinase kinase.	[74,77]
[Het-s]ᵇ	Causes "heterokaryon incompatibility" with genetically distinct matting partners.	HET-s	Not known function.	[74,77]

Table 1. Yeast and filamentous fungal prions, and their normal protein counterparts. All prions found in *S. cerevisiae*ᵃ and *P. anserina*ᵇ, induce the formation of amyloid folds, except for [β] and [GAR+]. Only [Het-s] and [β] have normal functions. *Prions having an enzymatic role, whose precursor activation requires their active form (prion) (Table adapted from [74] and reprinted with permission from John Wiley &Sons).

The prion isoform [URE3] permitted yeast to grow on poor nitrogen sources, specifically ureidosuccinate, the catabolism of which Ure2 represses. Similarly, the prion isoform [PSI+] repressed Sup35 function, a translation terminator, and allows read-through stop codons. Generation of both [URE3] and [PSI+] elements seems to be the last strategy for stressed yeasts to survive under harsh environmental conditions without resorting to a genetic mutation. Both elements are inherited by offspring yeasts as non-Mendelian dominant traits [19,81].

Three lines of evidence led to the proposal that both [URE3] and [PSI+] are proteins analogous to the prion agent causative of TSEs in mammals [71]. First, both [URE3] and [PSI+] are reversible curable, i.e., they can arise, again spontaneously, in a cured yeast previously grown in the presence of 5 mM guanidine hydrochloride [82]. Second, propagation of [URE3] and [PSI+] require Ure2 and Sup35, respectively, i.e., the gene encoding the normal form of the prion protein is essential for prion propagation as it can only propagate by converting the normal isoform into the prion form. Third, transient Ure2 and Sup35 overproduction increases the frequency of de novo appearance of [URE3] or [PSI+] respectively, due to the fact that a prion conversion rises as the amount of the counterpart molecules increase [71,83]. Other non-genetic elements involved in cell maintenance have been identified in *S. cerevisiae* (Table 1). Hence, yeast prions are often lethal, although some variants only slightly impair growth. There are three properties that are characteristic for a non-chromosomal genetic element to be a prion, and not for a nucleic acid replicon: 1) Reversible curability, 2) prion appearance is induced by overproduction of the prion, and 3) prion phenotype mimics prion protein gene mutation [84].

Results from yeast prion research have provided crucial information supporting the "prion protein-only" hypothesis. Early studies have demonstrated that both isoforms can exist in two alternate conformational states, with one state capable of imprinting its conformation onto the other via cytoplasmic mixing or mating [72]. Furthermore, yeast prions have also provided valuable insights into the mechanisms associated with their misfolding, aggregation, and protein-based heredity. The diversity of fungal prions and their ubiquitous presence found thus far, suggest that they are a natural biological phenomenon. As one of the simplest eukaryotic organisms, sharing

many essential cellular processes with animal cells, and feasibility for biological manipulation, yeast will continue to be a powerful model organism to understand the mechanisms underlying the disease-forming mammalian prions.

1.2.2. Animal prion diseases. Prion diseases comprise a wide-ranging group of neurodegenerative diseases, that affects animals, including humans. The major animal prion disease phenotypes includes: chronic wasting disease (CWD) in cervids [85]; BSE in cattle [86]; exotic ungulate encephalopathy (EUE) in a number of ungulate species in zoos [87–89]; scrapie in sheep, mouflons [90], and goats [91]; transmissible mink encephalopathy (TME) in ranch-reared mink[92]; and feline spongiform encephalopathy (FSE) in domestic and big cats [87,88,93]. Scrapie was the first TSE identified in 1732 [35,94]; the name derived from one of the clinical symptoms of the condition, wherein affected animals will compulsively scrape off their fleeces against rocks, trees, or fences [95]. In 1936, scrapie was experimentally transmitted to goats, providing evidence of the infectious nature of the agent and eventually fulfilling Koch's postulates [96].

Bovine spongiform encephalopathy (BSE) was first described in 1986 [97] and has since linked with emerging TSEs in other species, including and humans [98]. In the 1990s, the BSE outbreak reached epidemic dimensions in the UK, resulting in a devastating loss of livestock and significant economic, social, and political impact [99]. In the early 2000s, BSE cases were also reported in some European countries leading to mandatory BSE testing for any slaughtered cattle older than 24 (Germany) or 30 (European Union) months. Whether BSE originated from scrapie-infected sheep [57,100], or was a spontaneous event in cattle [101] is yet unclear. Although both theories implicate that the infectious agent was distributed by feeding contaminated meat and bone meal (neo-cannibalism). Indeed, the sterilization method for processing meat and bone meal was significantly changed in England in the late 1970s due to economy measures. However, it might have resulted in an insufficient inactivation of prions, and thus the emergence of BSE [57]. Nevertheless, closely following the BSE epidemic in cattle a new variant form of CJD became evident in human populations exposed to BSE; suggesting that BSE had crossed the species barrier and created a new variety of human prion disease, termed variant CJD (vCJD) [31,99]. Hence, BSE is considered a public health risk due to its ability to cross species transmissibility and particularly its zoonotic potential,

therefore extensive measures have been established to detect and eliminate the disease. Table 2 summarizes some animal prion diseases, their etiology and mechanisms of transmission.

Prion strain	Host	Etiology / Mechanism of transmission	Reported date / References
Scrapie	Sheep and goats	Infection with prions of unknown origin/ Vertical and horizontal transmission; oral transmission sporadic	1732 [102,103]
TME (Transmissible Mink Encephalopathy)	Mink	Infection with prions of either sheep or cattle origin / Apparently ingestion of contaminated food (produced from sheep and cow)	1947 [104]
CWD	Cervids	Infection with prions of unknown origin / Vertical and horizontal transmission; oral transmission; sporadic?	1967[105]
BSE , mad cow disease	Cattle	Infection with prions of unknown origin / Ingestion of contaminated bone meal; sporadic?	1986 [57]
EUE (exotic ungulate encephalopathy)	Nyala, Oryx, Greater Kudu	Infection with prions of BSE origin / Ingestion of BSE contaminated food	1986 [106]
FSE (Feline Spongiform Encephalopathy)	Cats	Infection with prions of BSE origin / Ingestion of BSE contaminated food	1990 [87]
NHP (Non-Human Primate)	Lemurs and Rhesus macaques	Infection with prions of BSE origin / Experimental transmission studies	1996 [57]
Camel Spongiform Encephalopathy	Camel	Infection with prions of unknown origin / Ingestion of BSE contaminated food?	2018 [57]

Table 2. Animal prion diseases. (Table adapted from [54-104] and reprinted with permission from BMJ Publishing Group Ltd.) .

1.2.3. Human prion diseases. Prion diseases occur worldwide and affect both genders equally. They can be classified according to their: 1) etiology, 2) clinicopathological phenotype, 3) mutations and polymorphisms of the prion gene (*PRNP),* and 4) immunoblot characteristics of PrP^{Sc}, into three different subtypes:

1. Sporadic, arising spontaneously without any known risk factors or gene mutations, although hypotheses include somatic prion gene (*PRNP*) mutation or the spontaneous conversion of PrP^C into PrP^{Sc} as a rare stochastic event [108]. It accounts for approximately 80% of the total

human prion diagnoses, at a rate of 1-2 cases per million populations per year across the world [28].

2. Inherited, with autosomal dominant pathogenic mutations in the *PRNP* gene. This form accounts for approximately 8% of all diagnosed cases of human prion disease. There are three main subtypes in this category: GSS, CJD, and FFI. All differ slightly with regards to typical signs, symptoms and duration of illness [109].

3. Acquired, caused by exposure to the abnormal prion protein whether by medical procedures or by exposure to contaminated food with BSE. This form accounts for less than 2% of total cases in human prion diseases. Acquired human prion disease can be further subdivided into: 1) *iatrogenic*, transmitted through medical procedures, 2) *kuru*, transmitted by cannibalism among the South Fore tribe of the Eastern Highlands in Papua New Guinea during funeral rites, and 3) *variant CJD (vCJD)*, transmitted by consuming prion-contaminated meat and blood transfusion. The appearance of this variant in the United Kingdom (1995) and its impact on the human population as an epizootic event has led to a widespread concern as a threat to public health worldwide [110].

The Canadian CJD Surveillance System (CJDSS), operated by the Public Health Agency of Canada (PHAC), conducts prospective national surveillance for all types of human prion diseases in Canada since 1994 [111]. According to CJDSS, as of January 2019, 971 deaths have been attributed to definite and probable CJD, from which 898 cases corresponds to sCJD cases (92.4%), 5 cases to iCJD (0.5%), 66 cases (6.7%) to genetic prion disease (includes fCJD, GSS, and FFI) and 2 cases of vCJD (0.25%). Hence, the threat to public health has intensified the research efforts to understand the molecular basis of these diseases, to improve methods of diagnosis, and to develop therapeutic strategies for treatment and prevention of these diseases. Table 3 depicts human prion diseases etiology when they were first reported.

Disease	Etiology	Reported date / Ref.
Kuru	Ritual cannibalism	1900s [18]
sCJD	Spontaneous conversion of PrP^C to PrP^{Sc} or somatic mutation	1920 [22]
fCJD	Mutations in *PRNP*	1924 [112]
GSS	Mutations in *PRNP*	1936 [26]
iCJD	Accidental transmission with prions of human origin, during or after organ transplants, electroencephalogram (EEG) electrode implantation, and other surgeries	1974 [29]
FFI	*PRNP* haplotype 178N-129M	1986 [52]
vCJD	Infection with prions of BSE origin	1996 [31]
sFI	Spontaneous conversion of PrP^C to PrP^{Sc} or somatic mutation	1999 [52]
VPSPr	Spontaneous conversion of PrP^C to PrP^{Sc} or somatic mutation	2008 [113]

Table 3. Human prion diseases and their etiology.

The classical histopathological features of prion diseases include spongiform change, neuronal loss, amyloid plaques deposition, astrocytosis, and microgliosis. In general, CJD is characterized by the formation of focally clustered, occasional confluent vacuoles in the neuropil, also called spongiform encephalopathy. It is distinguished from non-specific spongiosis of the brain parenchyma seen in brain edema, metabolic encephalopathies, artifacts, from perineuronal vacuolation in acute/hypoxic damage, and spongiosis of the superficial layers of cortex in other neurodegenerative disorders [114]. vCJD is characterized by abundant amyloid plaques surrounded by vacuoles, designated as "florid plaques" [115]. Amyloid plaques are seen only in a less common molecular subtype of sCJD. Familial insomnia (FI) histopathology is present predominantly as a thalamic degeneration with a relatively characteristic clinical syndrome either lacking or associated with a specific mutation in the *PRNP* gene (i.e., D178N associated with methionine on polymorphism at codon 129 of *PRNP*). GSS is classified as an encephalo(myelo)pathy with multicentric amyloid plaques, although morphologically different from the amyloid plaques seeing

in kuru and vCJD (112). Figure 1 summarizes human prion disease forms, their major neuropathological features and etiology [116].

1.2.4. Functional amyloids: the brighter side of the prion story. Conformational diseases (or amyloidosis), a general term comprising more than 40 disorders, are characterized by the aggregation and deposition of unfolded or improperly folded (misfolded) proteins. Improper protein folding, as well as unfolded proteins, can lead to the formation of disordered (amorphous) or ordered (amyloid fibril) aggregates, which can lead to cell death in specific organs. The amyloid state is an inherent characteristic of polypeptide molecules under denaturing conditions, independent of the native structure or primary structure. For example, it is well known the heat-denatured amyloid fibrils formation (gelation) of β-lactoglobulin from milk and lysozyme from egg white [117]. However, not all amyloid fibrils cause a disease in the organism that harbors them. Recent studies have indicated that amyloid fibrils are ubiquitously expressed in living organisms, from prokaryotes to eukaryotes, that have evolved as native proteins and perform physiological functions in the host. These amyloids are known as "functional amyloids". The term amyloid is used here for clarity, when a cross-β core structure is formed and present a typical X-ray fiber diffraction pattern of a meridional reflection at ~4.7 Å and an equatorial reflection at ~6–11 Å. Figure 2 depicts the fundamental structure of amyloid fibrils [118].
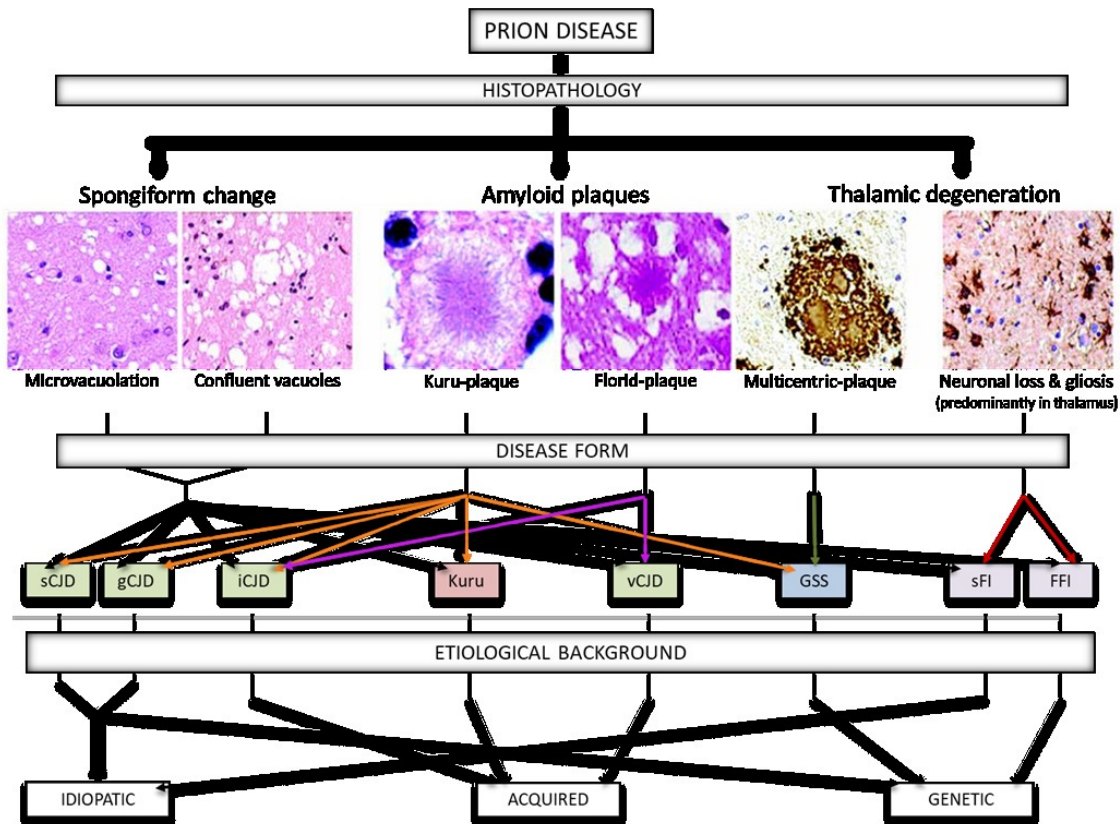
Figure 1. Overview of the broad spectrum of human prion diseases. (Figure adapted from [116])

The fibrous structure of these fibrils facilitates their use as scaffolds for structural and biochemical processes, whereas the compact nature of the amyloid fold is ideal for the storage of proteins and peptides [119]. For example, "Curli" are extracellular amyloid fibers produced by *Escherichia coli* to colonize and bind to host surfaces [120,121]. The [URE3] and [PSI+] amyloid prions derived from Ure2 and Sup35 yeast proteins, respectively, confer a selective advantage to the host under harsh environmental conditions [71,122]. Another unexpected member of this group is spider silk, which has been reported to form an amyloid-like cross-β-structure [123].
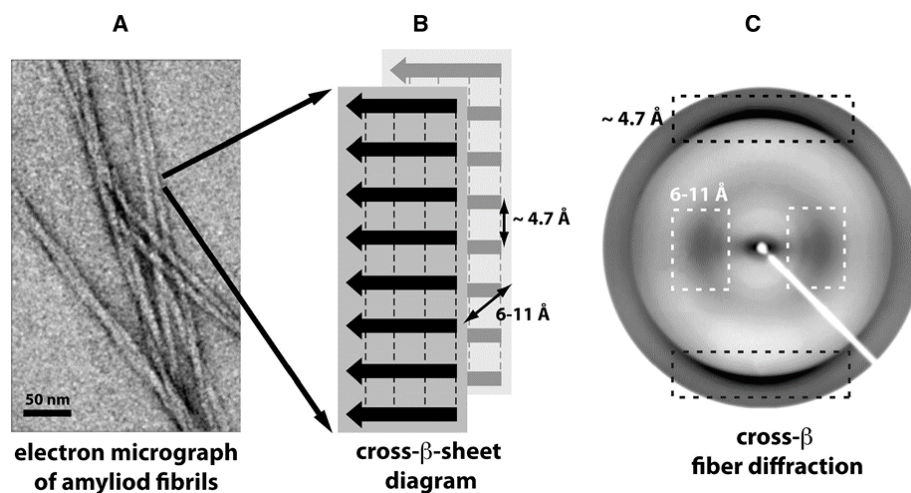
Figure 2. Fundamental structure of amyloid fibrils. A) Amyloid fibrils are composed of long filaments that are visible in negatively stained transmission electron micrographs. B) The schematic diagram of the cross-β sheets in a fibril, with the backbone hydrogen bonds represented by dashed lines, indicates the repetitive spacing distance that give rise to C) the typical fiber diffraction pattern with a meridional reflection at ~4.7 Å (black dashed box) and an equatorial reflection at ~6–11 Å (white dashed box). (Figure taken from [118]).

Formation of functional amyloids has also been reported in mammals. For instance, in humans, several different peptides and proteins have shown to self-assemble into amyloid fibrils and perform physiological functions. As an example, the pigment cell-specific pre-melanosomal protein (PMEL, also known as Pmel17), which acts as a template (scaffold) for melanin polymerization, and perform a physiological amyloid-like fibers role in the lumen of melanosomes (a specialized organelle localized in skin and eyes that acts as the site for the synthesis of the pigment melanin) [119,121,124]. Another example of functional aggregated protein is MAVS (mitochondrial antiviral-signaling), which mediates the activation of Type-I interferons (like interferon –α (IFN-α) and –β (IFN-β)) in response to viral infection. Aggregated MAVS forms a protease-resistant prion-like aggregate that activates interferon-regulatory factor 3 (IRF3) dimerization, which plays an essential role in the innate immune system's response by inhibiting viral infection [125]. Other functional human amyloids are shown in Table 4. Due to their physicochemical and robust mechanical properties amyloids are considered potential candidates in the development of new nanomaterials with prospective applications in nanotechnology and biomedicine [121].

19

Protein, Peptide or Cellular Structure	Proposed functions	Experimental evidence for amyloid fibrils
Amyloid-bodies (A-bodies)	Stores of proteins in stressed cells	A-bodies are stained by Congo red and thioflavin-S. Proteins that accumulate in A-bodies can form fibrils with a cross-β, X-ray fiber diffraction pattern.
Acrosomes	The acrosome reaction during fertilization of oocytes	Acrosomes in sperm are stained by thioflavin-S and are recognized by amyloid-specific antibodies. Purified acrosomal matrix has a cross-β, X-ray fiber diffraction pattern.
Cathelicidin peptide LL-37	Antimicrobial	Fibrils exhibit green birefringence with Congo red.
Peptide hormone	Storage of the hormone in secretory granules	Purified granules from endocrine cells have a cross-β, X-ray fiber diffraction pattern and exhibit green birefringence with Congo red. The fibrils bind Congo red and have a cross-β, X-ray fiber diffraction pattern.
Pigment cell-specific pre-melanosomal protein (PMEL)	Pigmentation	Purified melanosomes are stained by thioflavin-S and Congo red. The fibrils have a cross-β, X-ray fiber diffraction pattern, bind Congo red and thioflavin-T and have a far ultraviolet circular dichroism spectrum consistent with β-sheet content.
Prostatic acid phosphatase peptides	Removal of damaged sperm	The fibrils have a cross-β, X-ray fiber diffraction pattern, bind thioflavin-T and exhibit green birefringence with Congo red.
Protegrin-1	Antimicrobial	The fibrils bind thioflavin-T.
Receptor-interacting protein 1 (R1P1)/RIP3	Regulated necrosis	The fibril has a cross-β, X-ray fiber diffraction pattern, a ssNMR spectra consistent with a β-sheet core and bind thioflavin-T and Congo red.
Semenogelin proteins (SEM1 and SEM2)	Removal of damaged sperm	The fibrils bind thioflavin-T and Congo red and an amyloid-specific antibody-specific antibody pulls down SEM1 and SEM2 from seminal fluid.

Table 4. Synopsis of the experimental evidence for the formation of functional amyloid fibrils in humans. (Table adapted from [119]).

1.3. PrP and its role in neurodegenerative diseases

Extensive research has been done to elucidate the physiological role of PrP^C, yet the pathological mechanisms related to PrP^C in TSEs remain abstruse. However, it is widely accepted that PrP^C plays a neuroprotective role in cells under environmental stress. Data obtained from previous studies using transgenic animal models, such as PrP^C knockout mice and PrP^C overexpressing mice, have provided insights in the role of PrP^C and some of its physiological function [126]. Numerous studies have confirmed different signal pathways involved in the neuroprotective function of PrP^C, including Fyn, cAMP/PKA [127], and phosphorylation of extracellular signal-regulated kinase (ERK1/2) [128] and Akt [129]. In addition, caspase-3 [130] and STAT-1 [131], have been also demonstrated to be essential modulators between PrP^C and cell survival. It is well known that PrP^C is a copper-binding protein. The histidine-containing octapeptide repeats specifically bind up to four copper ions (Cu 2+) in a pH-dependent and negatively cooperative manner with an affinity that may be as high as 0.1 nM (depending on the binding site occupancy). Hence, the expression level of PrP^C seems to correlate with the activities of Cu/Zn superoxide dismutase or glutathione reductase [132]. Identifying other cellular proteins to which PrP^C might interact is a powerful strategy to elucidate its physiological role [130], including protection against apoptotic and oxidative stress [133], cellular uptake of copper ions [134], transmembrane signaling [135], formation and maintenance of synapses [101], and adhesion to the extracellular matrix [136].

1.4. Cell biology of PrP^C

PrP protein can exist in multiple isoforms: 1) the normal PrP^C, 2) the pathogenic protease-resistant PrPres (PrP^{Sc}), or 3) the isoform located in brain mitochondria, with the C-terminus facing the mitochondrial matrix and the N-terminus facing the intermembrane space [137]. PrP^C is expressed early in embryogenesis, at highest levels in neurons of the brain and spinal cord in adults [138]; but can also be found at basal levels in glial cells of the central nervous system (CNS)[139]. Most PrP^C

molecules are normally localized on the cell surface, where they are attached to the lipid bilayer via a C-terminal, glycosylphosphatidylinositol (GPI) anchor.

During its biogenesis, PrP^C is co-translationally translocated into the lumen of the endoplasmic reticulum (ER), where the N-terminal signal sequence is removed. Then, a series of post-translational modifications (PTMs) occurs, which play a role in the transformation of PrP^C to PrP^{Sc}. Human PrP contains two consensus sites for N-linked glycosylation, at Asn181 and Asn197. These glycosylation sites affect the conformation of PrP^C and PrP^{Sc} stability and the rate of its clearance. Other two PTMs include the formation of an intramolecular disulfide bridge and the attachment of a GPI-anchor promoted by a C-terminal signal peptide. Once PrP^C is properly folded, it exits the Golgi apparatus, and finally incorporates into the outer leaflet of the plasma membrane via its GPI anchor moiety [140]. PrP^C associates with cholesterol- and glycosphingolipid- rich lipid raft domains through its GPI anchor. Expression of PrP^C has also been reported in important sites for signal transduction, suggesting that PrP^C might play a physiological role in these processes. PrP^C has been demonstrated to be a copper-binding protein, and increasing evidence has shown a correlation between the level of PrP expression and tolerance to oxidative stress [130, 138].

PrP^C can interact with ionotropic glutamate receptors such as α-amino-3-hydroxy-5-methyl-4-isoxazolepropionic acid (AMPA) receptor subunits GluA1 and GluA2. This interaction may be relevant to the PrP^C-mediated cellular uptake of zinc through AMPA receptors [142]. PrP^C can interact with metabotropic glutamate receptors as well (glutamate receptors of group I, mGluR1 and mGluR5). Metabotropic glutamate receptors are members of the G protein-coupled receptor (GPCR) superfamily, a group of seven transmembrane-domain proteins that are activated by glutamate and transduce intracellular signals via G proteins. PrP^C binds to and signals through mGluR5 in disease-related conditions [143]. Previous studies have found that Aβ-oligomers, the neurotoxic protein species involved in AD, can interact with PrP^C and activate the Fyn kinase through mGluR5. It has been suggested that Aβ- PrP^C –mGluR5 complexes are responsible for the facilitation of long-term depression (LTD) in vivo [144], and dendritic spine loss in cultured neurons [143]. Although the function of PrP^C remains unknown, there is now growing evidence that indicates

that PrP^C has a neuroprotective role [145,146], and that it exerts its function in concert with additional membrane proteins.

The mechanism by which PrP^C is internalized is controversial. It may be either endocytosed via lipid rafts [147] or depending on clathrin-[148] or caveolin-mediated pathways [149], potentially in concert with some lipoprotein receptor-related [150,151]. PrP^C containing endosomes can recycle back to the plasma membrane [147] or fuse with lysosomes for degradation [152]. PrP^C can regulate the cellular transport and localization of its binding partners, as well as modulate their functions (i.e., glutamate receptors). For instance, it has been suggested that PrP^C appears to scavenge amyloid aggregates of Aβ, posing the question of whether PrP^C can recognize other pathological aggregates. Mouse models have provided evidence that PrP^C plays a role in several physiological functions in the central and peripheral nervous systems. However, genetic impurity (allogenicity) can arise from different sources, like: incomplete inbreeding, mutation, inadvertent outcrossing, mislabeling, and epistatic and heterozygote selection; consequently, hampering the interpretation of the results. PrP^C-deficient mouse studies have generated several validated pathological phenotypes, suggesting that PrP^C is involved in very few numbers of cellular functions. The emergence of new, rigorously controlled animal models will be advantageous for the critical assessment of phenotypes and shed light on the role of PrP^C [153].

1.5. The prion conversion process

It has been hypothesized that the conformational conversion of PrP^C into the abnormal PrP^{Sc} isoform involves a physical interaction between the two isoforms, that occurs at the cell surface, either in lipid rafts or caveolae-like domains (CLDs) and/or along the early endocytotic pathway [154]. The 37/67 kDa laminin receptor (LR), a non-integrin protein [155] or polyanions like glycosaminoglycans [156] have been suggested as potential co-factors for prion generation. PrP^{Sc} is mainly located in the endosomal-lysosomal system (ELS) [157], and it has also been found near the plasma membrane [158]. Additionally, a small portion of PrP^{Sc} was shown to accumulate in cytosolic aggresomes under certain experimental conditions where it appears to impair proteasomal function

[159]. The spread of prions from cell to cell could be imparted through exosomes or via cell-to-cell contact [160]. An ample variety of mechanisms and permutations of them have been proposed to explain the conformational change of PrP^C into PrP^{Sc} [161]. Two conceptually mechanisms that are most commonly accepted are the heterodimer model, also known as the template assistance model [43,162], and the nucleation [seed]-dependent polymerization model [43,163]. Figure 3 illustrates the proposed models of PrP^C conversion to PrP^{Sc}[164].
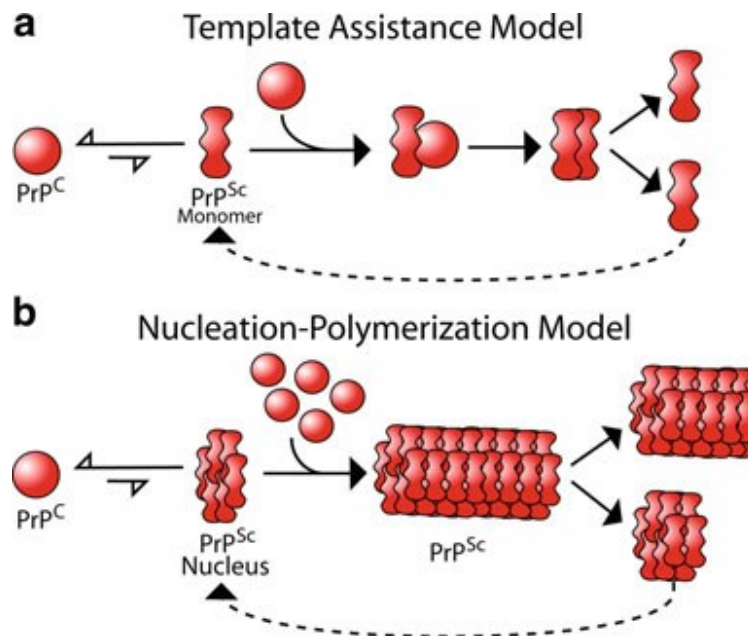
Figure 3. Models of prion formation. (a) In the template assistance model, PrP^{Sc} monomer is more stable than PrP^C, but is kinetically inaccessible. Spontaneously created (or provided exogenously) PrP^{Sc} monomer, can act as a template for the conversion of PrP^C into PrP^{Sc}, by direct interaction. The dashed line shows that the newly synthesize PrP^{Sc} monomer can act as another seed to formation of PrP^{Sc}. (b) In the nucleation polymerization model, the formation of a nucleus in which the protein adopts a PrP^{Sc}-like structure is the barrier for prion conversion. The formation of such a low order aggregate is not favored; however, once it has formed, polymerization from a pool of PrP^C molecules can take place efficiently. Fragmentation of the polymer increases the number of ends for the recruitment of PrP^C monomers. (Figure taken from [164] and reprinted with permission from Springer Nature).

The heterodimer model suggests that PrP^{Sc} exists in a monomeric state that is kinetically inaccessible, although more thermodynamically stable than PrP^C [165]. Hence, by forming a heterodimer between PrP^{Sc} and PrP^C, or a partially destabilized folding intermediate of PrP^C with

PrP^{Sc} (acting as a monomeric template), the conformational change in PrP^C occurs, and a homodimer is formed. The resultant PrP^{Sc} homodimer then splits apart to give two PrP^{Sc} monomers. The rationale behind this model is that, although PrP^{Sc} is more stable thermodynamically than PrP^C, conversion of PrP^C to PrP^{Sc} is rare unless catalyzed by a preexisting PrP^{Sc} template, and that PrP^{Sc} homodimer can dissociate into monomers. While such a mechanism is plausible, there is no experimental evidence for the existence of a stable PrP^{Sc} monomer. By contrast, available data indicate that prion protein conversion is intimately associated with the aggregation process, and the infectious entity is oligomeric [164].

A model consistent with the oligomeric nature of PrP^{Sc} is the so-called nucleated polymerization mechanism. The fundamental basis for this model is that the conversion between PrP^C and PrP^{Sc} is reversible, although the PrP^{Sc} monomer is much less stable than PrP^C (i.e., the equilibrium is strongly displaced toward PrP^C) [164]. Hence, oligomerization /polymerization of PrP is necessary to stabilize PrP^{Sc} and sufficient to allow its accumulation to biologically relevant levels. Stabilization of PrP^{Sc} occurs only upon the formation of a stable oligomeric nucleus, which is thermodynamically not favorable. Spontaneous formation of a core of PrP^{Sc} is an unusual event due to the weakness of monovalent interactions between PrP^C molecules and/or the rarity of the conformers that polymerize. However, once the PrP^{Sc} nucleus has formed, monomeric PrP^C could efficiently add to it, adopting the conformation of PrP^{Sc} contributing to the formation of oligomeric or polymeric seeds that are stabilized by multivalent interactions [166]. The rate-limiting step in this mechanism is not the conformational conversion itself but the nucleation step. This step, responsible for the lag phase in the spontaneous conversion, can be bypassed by addition of preformed PrP^{Sc} seeds. Therefore, to stabilize PrP^{Sc} propagation, the rate of its template-mediated aggregate growth must exceed the rate of its biological clearance [164].

In their various permutations, the two types of models can overlap. Nevertheless, in either type of model, a metastable PrP^C folding intermediate might interact with PrP^{Sc} during the conversion reaction. A critical question from a biological standpoint is what physical state(s) of PrP^{Sc} is active in TSE disease processes in vivo. The nucleated polymerization model predicts that active PrP^{Sc} seeds could range in size from the minimum stable oligomeric nucleus to large

polymers. In agreement with this prediction are the recurrent observations that self-converting and -replicating activities, as well as infectivity, are associated with a wide size range of PrP^{Sc} aggregates, but not monomers [167–169]. In contrast, the heterodimer-type models propose that discrete monomers (or in related permutations, small discrete oligomers) are the active autocatalytic units. Aggregation of PrP^{Sc} would then be a side issue. A theoretical consideration of the kinetic consequences and likelihood of the two models [170] concluded that a strict non-cooperative heterodimer model is highly unlikely. However, if a small oligomer (e.g., trimer or tetramer) served as a template in a highly cooperative autocatalytic reaction, then the model becomes more plausible. In any case, it was suggested that aggregation of PrP^{Sc} is likely to be an important "prerequisite of infection." Mathematical modeling of the nucleated polymerization mechanism by Masel and coworkers [171] revealed that systems of short polymers would grow the fastest.

Conversion of PrP^{C} to PrP^{Sc} has been attempted to be explained in terms of the "energy landscapes concept" and "folding funneling". According to the "folding funnel hypothesis", proteins fold into their minimal-energy configuration due to the physicochemical properties of their amino acid sequence. Proteins fold rapidly because their amino acids interact locally, thus limiting the conformational space that the protein has to explore and forcing the protein to follow a funnel-like energy landscape that allows it to fold quickly. However, partially folded proteins can become "trapped" in what is called "non-native local minima", leading to the formation of off-pathway intermediates. The "folding funnel hypothesis" assumes that the driving forces for protein folding are hydrophobic interactions, the formation of intramolecular hydrogen bonds and van der Waals forces; where hydrophobic amino acid side chains are sequestered in the interior of the protein allowing the water solvent to maximize its entropy. Hence, the free energy of the protein is lowered by favorable energetic contacts: isolation of electrostatically charged side chains on the solvent-exposure protein surface and neutralization of salt bridges within the protein's core. Figure 4 illustrates the hypothetical energy landscape model for protein folding and aggregation [172].
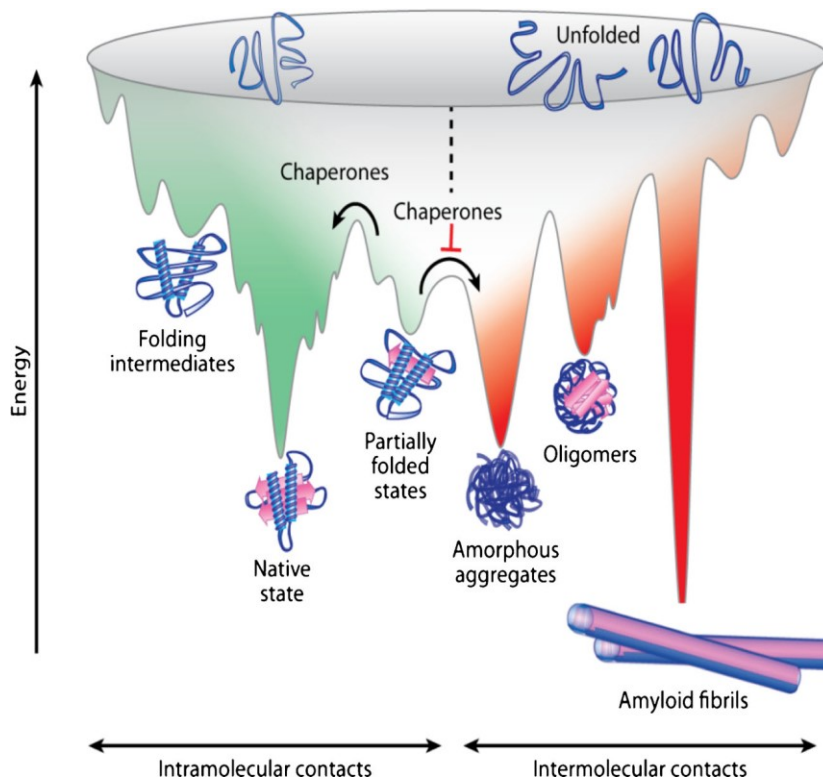
Figure 4. Hypothetical energy landscape for protein folding and aggregation. Although, the surface shows multiple conformations, intramolecular contact formations will drive conformations "funneling" to the native state (green); while intermolecular contacts will guide conformations "funneling" toward amorphous aggregates or amyloid fibrils (red). Both parts of the energy surface overlap. Accumulation of intermediates during the novo folding or destabilization of the native state into partially folded states can lead to formation of aggregates, normally prevented by molecular chaperones. Cell-toxic oligomers may occur as off-pathway intermediates of amyloid fibril formation. (Figure taken from [172] and reprinted with permission from John Wiley & Sons).

In familial and sporadic human prion diseases, specific PrP mutations can potentiate the formation of a seed or an initial template [162,166]. In TSE diseases of infectious origin, a transmission might be explained by the acquisition of preformed PrP^{Sc} templates/seeds. Nonetheless, until the TSE infectious agent is fully understood, it seems prudent to remain open to the possibility that other factors may enhance PrP^C conversion and stabilizes PrP^{Sc} propagation in the infected hosts.

1.6.   Prion strains, the species barrier phenomenon and prion strain mutations

Prion strains. Another piece in the puzzle of the "prion protein-only" hypothesis is the observation that prions derived from a given species can cause a myriad of patterns of the disease in the brain, such as different incubation times and lesion profiles [173]. Hence, the term "prion strain" was coined to explain this phenomenon within the intellectual framework of the "protein-only" hypothesis. Prion strains are associated with different biological and biochemical features (Figure 5), characteristics of each PrP^{Sc} strain, such as partially resistant to PK digestion, particular glycoforms profiles, and clinical and neuropathological phenotype like incubation time, clinical symptoms and neuropathological changes [60,173,174]. Current evidence suggests that prion strains also have different three-dimensional conformational arrangements, that drive the molecular changes leading to varying folds of PrP^{Sc} [175]. They can be faithfully propagated in inbred mouse lines and, in the case of BSE, even across a variety of species [60,176]. In humans, for example, different prion strains are responsible for the various phenotypes of CJD [177].

Species barrier. Prions can be efficiently transmitted intra-species (within species), but less efficient inter-species (between species), a phenomenon known as "species barrier". Previous studies have shown a longer incubation time of the disease upon the first transmission to a new host compared to a shortened incubation time upon subsequent passages within the same host[40,178]. These findings demonstrate that inter-species transmission of a single PrP^{Sc} strain resulted in adaptation and stabilization of at least two strain-associated PrP^{Sc} conformations, that underwent selection until one type of PrP^{Sc} conformation and strain phenotype became predominant. Although these findings have demonstrated the importance of PrP amino acid sequence for prion transmission, subsequent experiments have shed some doubts on this premise
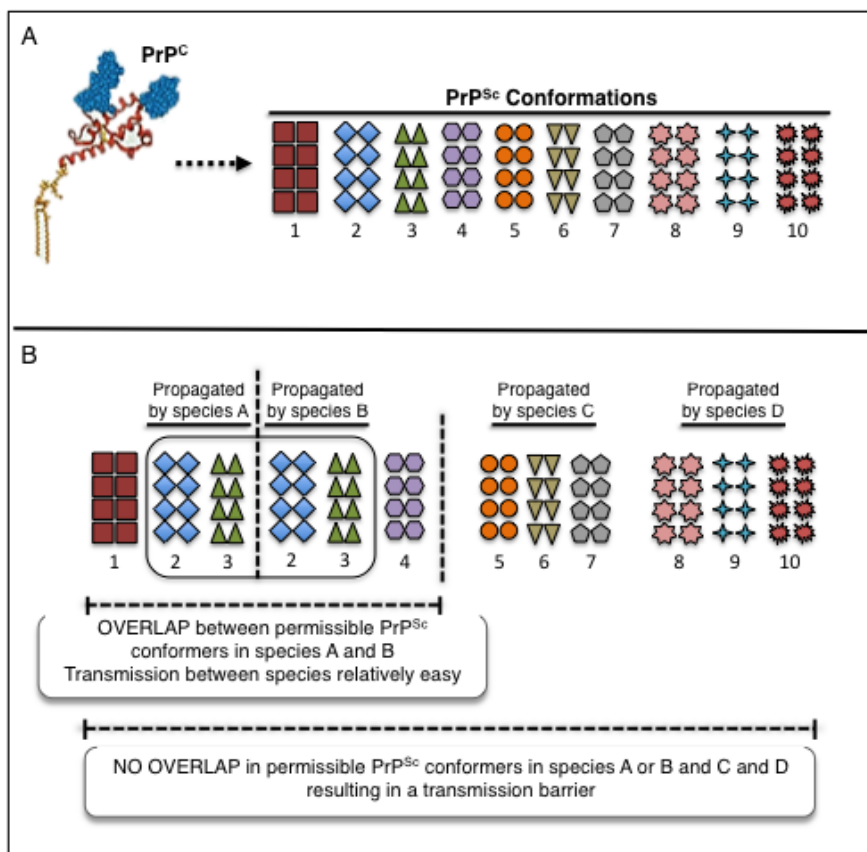
Figure 5. Conformational selection and transmission barriers. A) A large number of different PrP^{Sc} conformations are possible among a full range of mammalian PrP sequences. B) However, only a subset of these would be compatible with each individual PrP primary structure. The strength of transmission barrier relates to overlap of permissible PrP^{Sc} conformations between PrP primary structures from the two different species: the larger they overlap, the lower the species barrier, i.e., a relatively easy transmission of the disease. Although the resulting phenotype always displays clonal properties, prion strains may consist of an ensemble of molecules and transmission barriers that correlate to the overlapping regions of these populations. (Figure adapted from [179]).

Previous studies have shown that the "species barrier" varies with different prion strains, regardless that they were originated from the same donor species. These results suggested that the type of PrP^{Sc} strain influence the outcome of interspecies transmission [98,180]. Furthermore, the transmission of prion strains from different unrelated donors, has given a remarkably uniform disease characteristic in transgenic mice expressing PrP [180]. Barron and coworkers demonstrated

that the structurally "flexible" amino-terminus region of PrP plays a critical role during the replication and targeting of PrP^{Sc} pathology.

Transmission of prions from different species to transgenic mice expressing PrP with the single amino acid mutation proline to leucine, at amino acid position 101 (P101L), was shown to alter the incubation time when compared to wild-type mice in a strain-dependent manner, which cannot be explained simply by differences in their sequences [181]. Moreover, transgenic mice expressing bovine PrP (Tg(BoPrP)) were found to be susceptible to prions from humans with vCJD, which on the second passage in Tg(BoPrP) mice, the incubation times shortened by 30 to 40 days. However, these mice were resistant to sporadic, familiar, or iatrogenic forms of CJD, which prompted S.B. Prusiner and colleagues to introduce the denotation "strain barrier" for this phenomenon [182]. Surprisingly, wild-type mice have shown to be more susceptible to vCJD than transgenic mice over-expressing human PrP [108], providing evidence that some factors other than PrP sequence similarity between host and donor PrP may play a role in PrP^{Sc} transmission and suggesting that the term "transmission barrier" might be more appropriate than "species barrier". Recent work showed that some CJD isolates could be primarily transmitted to bank voles in the absence of any obvious species barrier, although the sequence of man and vole shows various amino acid exchanges [183].

Anfinsen's paradigm asserts that the structure of a protein is governed by its amino acid sequence. However, this principle is contradicted to some extent by the observation that the two isoforms of the PrP protein, the cellular PrP^{C}, and the misfolded PrP^{Sc}, share the same amino acid sequence. Furthermore, it was difficult to accept that a biological agent could replicate in the absence of nucleic acids. In particular, the existence of distinct strains of prions seemed implausible without invoking a mutation in a nucleic acid genome [184]. According to the conformational selection model, particles with different conformational stabilities and aggregated sizes frequently co-exist, which leads to a competitive selection of those with lower initial conformational stability [185]. Hence, the dominant PrP^{Sc} conformers are subject to further evolution by natural selection of the subpopulation with the highest replication rate due to its lowest stability. In line with this theory,

a lack of overlap in PrP^{Sc} conformers of different species may be the basis of the transmission barrier [179].

Prion strain mutations. This theory laid the groundwork to explain a further phenomenon "the prion strain mutations". Typically, referring to viruses or bacteria, a strain mutation corresponds to a modification of the genetic information. However, as has been previously mentioned, the genetic content of PrP isoforms, PrP^{C} and PrP^{Sc}, is the same. Hence, the term "prion strain mutation" refers to the conformational changes of PrP^{C} during its conversion to PrP^{Sc}, following its propagation in the host [186]. In other words, strain mutations arise when a propagated strain does not maintain the same biochemical and pathogenic characteristics of the inoculum, thereby resulting in the propagation of a new strain [186]. This phenomenon has been demonstrated through different approaches for strain typing. For example, 1) their assembly can be characterized by techniques like sedimentation [173], light scattering [187], transmission electron microscopy and atomic force microscopy [188]; 2) their conformational structural changes can be analyzed through circular dichroism [174], limited proteolysis [189], and dye-binding [190–192], and 3) their conformational stability can be assessed by SDS solubility [177].

Previous studies have shown that some strains, like BSE, can maintain their strain-specific characteristics while being highly transmissible across a wide variety of species [68], i.e., the conformation of a particular strain is compatible with a range of different PrP^{C} conformers. Other strains do not ´breed true` upon transmission into a new host, resulting in the occurrence of a new strain in the infected species [179]. Strains may constitute an ensemble of PrP^{Sc} molecules, and the new host preferentially propagates a non-prevalent conformer (Figure 6). Alternatively, when strains are composed of a single PrP^{Sc} conformer, only a direct conformational mutation enables its successful transmission to a host due to a previous PrP sequence incompatibility for this particular strain. Of note, some studies revealed that background genes other than the *PRNP* gene might also influence strain selection [186,193,194].
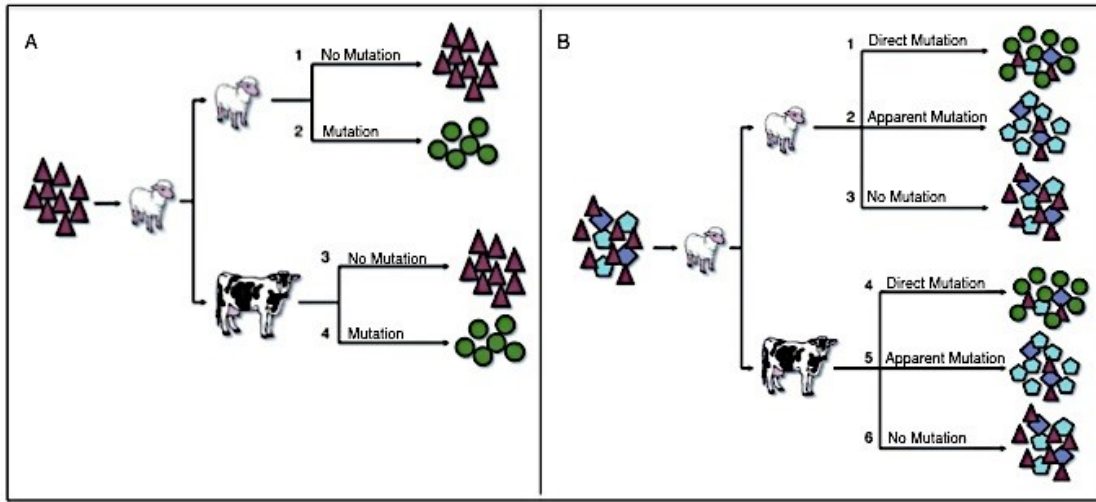
Figure 6. Hypothesis of prion selection during propagation. (A) PrP^Sc strains in a pool of a single clone. The strain can remain the same as the inoculum (1 and 3) when both PrP sequences (donor and recipient) are compatible. However, the strains can also undergo an adaptation process due to the presence of different cofactors, diverse cellular environment, or direct mutations (transmission within the same species) (2). When the inoculation occurs into a host expressing PrP with a sequence incompatible with this PrP^Sc conformation, transmission would only result by a direct strain mutation (transmission between different species) (4). These alternatives are not mutually exclusive. It is possible that mutations and strain selection may occur in different tissues of the same host as well as between different hosts as a result of heterogeneity in cellular mechanisms affecting prion propagation and clearance kinetics [179,186]. (B) Prions infect as an ensemble of PrP^Sc molecules of different conformations. Transmission of PrP^Sc within the same species can generate a new PrP^Sc type as a result of a direct mutation (1), a minor type can emerge becoming the major one due to an apparent mutation (2), or the pool of PrP^Sc can remain the same as the inoculum ("breed true"), where the dominant PrP^Sc type is preferentially propagated (3). Similarly, when the transmission is between different species, a cross-species transmission can occur, where the pool of different conformations of PrP^Sc must adapt to the new host, resulting in the propagation of a different pool of PrP^Sc from which a new PrP^Sc type can be generated (4), or in the selection of a minor strain from the pool, that becomes the major one, resulting in an apparent mutation (5). It is also likely that the propagated pool of PrP^Sc remain identical to the original infecting unit (6). (Figure taken from [179,186]).

In addition to clinical signs, neuropathological features, and etiology, other approaches have been implemented to distinguish and assert different prion strains. These approaches are based on the neuropathological characteristics they generate in the host or the particular biochemical properties of each prion variant. The most widely used approaches to characterize and distinguish

prion strains are summarized in Figure 7. However, identifying prion strains in a natural host is cumbersome and less reliable; along with the limitation of current techniques in determining the conformational structure of PrP^{Sc} variants [68].

Other factors involved in transmissibility of prions. Correlation analyses have been used to examine the relationship of a diverse set of physical, genetic, and immunological characteristics and the incubation period of prion disease. For example, it is well known that polymorphisms in the *PRNP* region affect disease susceptibility and incubation periods in the host. However, significant differences in incubation times are still present even with the same amino acid sequence, suggesting that other genes are also involved. Lloyd and coworkers analyzed quantitative trait loci (QTLs) that affect prion disease incubation times in a broad set of mice strains, that encoded identical PrP molecules but with different incubation periods. Interval mapping identified eight QTLs on three chromosomes (mouse chromosomes 2, 11, and 12). Based on these results, they caution against the validity of epidemiological predictions of vCJD that are based on genetic models of current patients who have shown a short incubation period[194].

Based on a set of previously published data collected, Bae and coworkers analyzed the correlation between incubation period and physical properties of the brain and cells, such as brain weight (BW), mean corpuscular volume (MCV) and cell size (CS). They found that given the same inoculation dose of prion, animals with smaller BW, MCV, and CS may have a more virulent disease and shorter latent periods when compared to larger animals; this is possibly due to the largest capacity of the brain and cells when compared with smaller size, effectively decreases the concentration of PrP^{Sc} which in turn determine the rate of interactions to the existing aggregates. These results suggested that the physical magnitude of prion-infected organs or individual cells is important in determining the length of the latent period of the disease. In other words, the mechanism underlying prion disease pathology may be physical, indicating that the incubation process is governed by simple chemical stoichiometric principles [195].
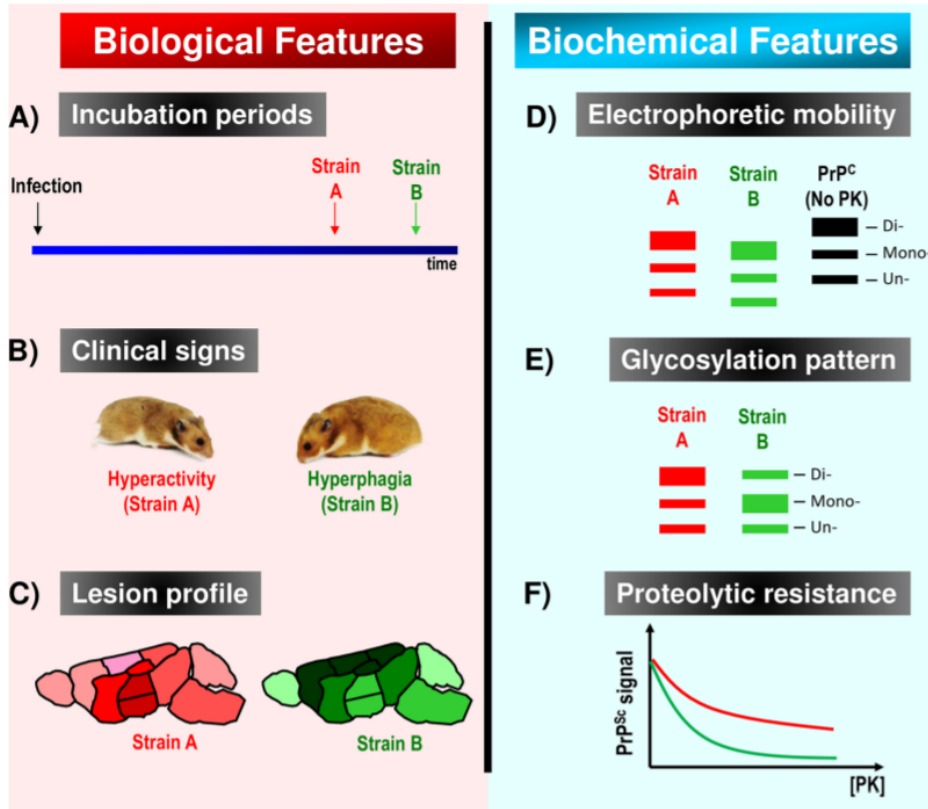
Figure 7. Biological and biochemical approaches used to differentiate between prion strains. The unique biology of prions can help in distinguish among different variants. (A) In experimental and controlled settings, incubation periods contribute to identify between prion strains, the time will depend also on the route of administration. (B) Clinical signs have been very useful to distinguish prion strains in some species (like goats and hamsters), but inefficient in others (such as mice). (C) Brain tropism of prion strains can help in the diagnosis, as it has been seen that prions accumulate in the brain in a strain-specific manner with distinct pathological brain-lesion profile. A molecular approach is also useful in the analysis of prion variants. (D) Prion strain-specific conformational folding is thought to protect different regions of the polypeptide chain from proteases, leading to different electrophoretic mobilities. Likewise, its C-terminal region has a partial proteolytic resistance that may help in distinguishing its variants. Although this approach has some limitations, as it has been shown that different prion strains can have same electrophoretic mobility. (E) The glycosylation profile can facilitate the characterization of prion variants, as they have two putative glycosylation sites, allowing it to exist in di-, mono- or un-glycosylated forms; with each variant favoring a specific proportion of PrP glycoforms. (F) Increasing the concentration of proteases or denaturing agents, can help to differentiate among prion strains, as they have been shown to have a partial resistance to proteolytic digestion or denaturation by chaotropic agents in a strain-specific manner. (Figure taken from [68]).

Several determinants seem to play a role in the transmissibility of the disease and consequently, act as species barrier; factors like the amino acid sequence content in the *PRNP* gene, the degree of homology of the amino acid sequences between donor and host, and the position of these sequences where the interaction and exchange occur [196–199]. This effect has been previously demonstrated for the human *PRNP* gene, where a polymorphism at residue 129 has a critical role for the susceptibility to vCJD [200].

1.7. Structure of the human prion gene (*Prnp*)

The human *PRNP* gene (NC_000020.11), which encodes the cellular prion protein PrP^C, is 16 kb long and it is located on the short (p) arm of chromosome 20 between the end of the arm and position 12 (p12-pter) (4686151-4701588). The structure of the *PRNP* gene for all species of mammals studied to date contains two exons. Exon 1, which is a noncoding exon, may serve as a transcriptional initiation site and it has in its 5' untranslated region (5' UTR) a highly GC-rich region, features commonly seen in housekeeping genes [201]. The promoter region of *PRNP* is highly GC-rich, lacks a canonical TATA box, contains a CCAAT box, and has several of putative binding sites for transcription factors, such as SP1, AP1, and AP2 [202]. To date, there are no reported prion disease-associated mutations in exon 1 or within any of the introns. The open reading frame (ORF), which encodes the 253 amino acid long prion protein [203], lies entirely within exon 2 [106] and transcribes an mRNA of 2.1–2.5 kb in length [100,204], with approximately 50 copies/cell in neurons [205]. Figure 8 depicts a schematic representation of the human PrP protein.

Genetic prion diseases (CJD, GSS, and FFI) have a pattern of autosomal dominant inheritance and are linked to point mutations or insertions/deletions in the *PRNP* gene [206,207]. Mutations in the *PRNP* gene can be classified as (1) point mutations (single nucleotide substitutions), can cause an amino change (missense mutation), can be silent (do not cause alteration in the amino acid sequence), or cause the coding to terminate prematurely (stop or nonsense mutation); and (2) insertions and deletions, which are associated with prion diseases. At the N-terminal region of PrP (amino acid residues 23-90), the nucleotide sequence from codons 51

to 91 of the *PRNP* gene encode a nonapeptide followed by four octapeptide repeats, which are almost identical to the nonapeptide except for the omission of a glycine and the presence of a histidine instead of a glutamine at the second position (P(H/Q)GGGWGQ [50,208].

A variety of insertions have been found only in the octapeptide repeat region. These insertions so far comprise one to nine extra octapeptide repeats [50]. Raman spectroscopy studies have demonstrated that binding of copper ions (Cu^{2+}) to the octapeptide repeats in PrP is coordinated by histidine residues, suggesting that this region may be involved in the transport of extracellular Cu^{2+} ions to an endosomal compartment [209]. At the C-terminal region of PrP (amino acid residues 91-231), more than 20-point mutations have been identified in clusters. Previous studies have revealed that the human PrP core structure is stabilized by extensive hydrophobic, aromatic, and salt bridge interactions between the β2-α2-α3 secondary elements and α3-α1 helices. These stabilizing networks are responsible for the proper folding of the C-terminal domain. Hence, the point mutations in this region contribute to destabilizing the native HuPrP conformational structure [210–213].
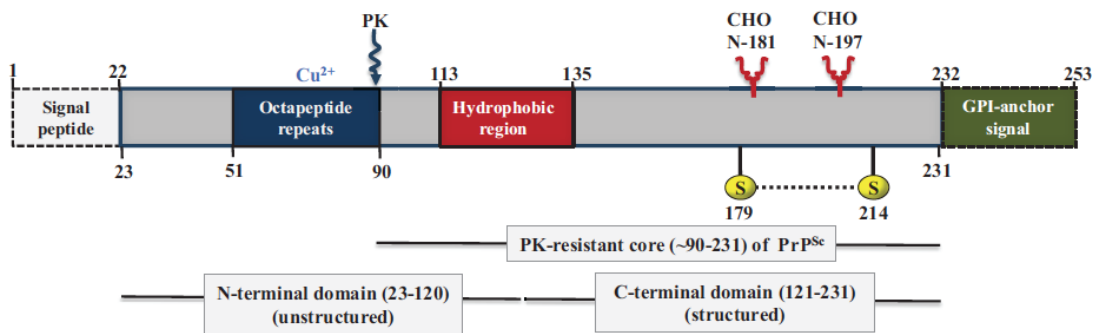
Figure 8. Organization of human PrP. The unprocessed PrP is 253 amino acid residues in length and includes a signal peptide (1–22), four OR, a hydrophobic region (113–135), one disulphide bond between cysteine residues (179–214), two **N**-linked glycosylation sites (at residues 181 and 197), and a GPI-anchor attached to the **C**-terminus of PrP replacing the GPI-anchor signal (residues 232 to 254). The four OR in the **N**-terminal domain have a high affinity for copper ions (Cu^{2+}), while a preceding nonapeptide (PQGGGGWGQ) lacks the histidine that is necessary to bind a Cu^{2+} ion. Mutated forms of PrP can contain insertions of one to nine additional OR or a deletion of one

OR. A palindromic region, AGAAAAGA (113–120), lies in the hydrophobic region (113–135) and is thought to be important in the conversion of PrP^C to PrP^{Sc}. OR: Octapeptide repeat; GPI: glycophosphatidylinositol; PK: proteinase K; CHO: carbohydrates. (Figure taken from [214]).

1.7.1. Evolutionary origins of the *PRNP* gene.

The emergence of the prion protein founder gene has been proposed occurred based on two genomic rearrangements that occurred hundreds of millions of years ago [215]. The first event occurred within the N-terminal ectodomain of a ZIP (Zrt, lrt-like protein) predecessor gene when metazoans first emerged on the planet. As a consequence of this rearrangement, a cysteine-flanked core (CFC) region was generated within this ectodomain. The second event, which allowed the creation of the prion protein founder gene to be traced back, occurred approximately a half-billion years ago (around the Cambrian explosion). This later event resulted in the apparent genomic retro-insertion of a spliced and C-terminally truncated ZIP gene transcript, indicating that the prion protein founder gene is equivalent to a retrogene [216]. An earlier investigation using a quantitative interactome analysis identified ZIP6 and ZIP10 as potential molecular interactors of PrP at the cell surface, revealing that the known prion proteins are structurally related to an extracellular domain of ZIP6 and ZIP10 [215]. Similarly, other authors using interactome analyses have identified multiple interactions between PrP^C and other molecules, like the neural cell adhesion molecule (NCAM) [136], the laminin receptor precursor [217], Na/K ATPase's [218], and protein disulfide isomerases (PDI)[219]. Together, these findings suggest that PrP^C organizes its molecular environment by binding adhesion molecules, which in turn recognize oligomannose-bearing membrane proteins.

1.7.2. Polymorphisms and mutations in the *PRNP* gene open reading frame (ORF).

Inherited prion diseases, including CJD, GSS, and FFI, are linked to more than 30 mutations identified so far, in the *PRNP* gene (Figure 9 depicts a schematic representation of the human PrP protein and its associated mutations and polymorphisms) [66]. Mutations can lead to changes in a single amino acid in PrP, insert additional residues, or cause an abnormally short version of PrP to be expressed. These mutations affect the primary structure of PrP, may lead to changes in the secondary and tertiary structure and could result in the emergence of PrP^{Sc} conformers [66]. Furthermore, several common polymorphisms (variations) have been identified in the *PRNP* gene as well (Figure 9). Polymorphisms do not cause prion disease but may affect the susceptibility or influence a person's

risk of developing the disease, the incubation period, the pathology and phenotype. Hence, as these features define strains, polymorphisms may also lead to the preferential propagation or generation of certain variants [220].
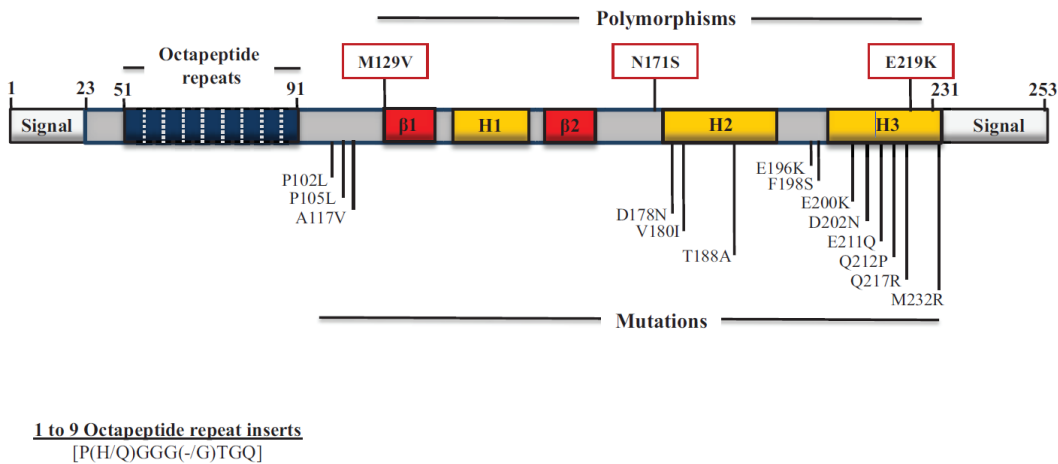
Figure 9. Schematic representation of the human PrP protein and its associated mutations and polymorphisms. The 0.76 kb ORF of the *PRNP* gene encodes a 253 amino acid protein, PrP^C. Human PrP consists of a cleaved signal peptide (1–22), an octapeptide repeat-containing unfolded domain (OR, 51–91), three α-helices (H1, H2, and H3), one small, antiparallel β-sheet (β1 and β2), and a GPI-anchor signal (232–253). The N-terminal octapeptide repeat motif is comprised of eight residues: P(H/Q)GGG(-/G)WGQ. Normal PrP contains five copies of this motif; a single OR deletion is considered a non-pathogenic polymorphism. However, insertional mutations consisting of one to nine additional OR are pathogenic. Polymorphisms and pathogenic mutations of the *PRNP* gene are represented above and below the schematic, respectively (Figure taken from [214]).

The most common and best-studied polymorphism in human PrP occurs at codon 129 and acts as a predisposing factor for sporadic, iatrogenic, and variant CJD [221,222]. Either methionine (M) or valine (V) is encoded at this position. M/M homozygosity at this position appears to be associated with an earlier age of onset and rapidly progressive dementia; whereas a more prolonged course with an ataxic onset is most often related to the V/V allele. It is important to highlight that the allele frequencies at codon 129 differ across populations [223]. For example, compared with Caucasian frequencies of M(0.66):V(0.34), the allelic frequencies reported in Japan are

M(0.96):V(0.04). Although the incidence of the disease has not been reported to be higher in Japan, it may predispose an individual to develop a particular clinical phenotype [223].

While M or V homozygosity at codon 129 in human PrP results in a predisposition to acquire sporadic or iatrogenic CJD, glutamate (E) to lysine (K) substitution at codon 219 appears to have a protective effect against sCJD. The E219K polymorphism has been reported to occur in the Japanese population, with an allelic frequency of 6% [224]. This polymorphism was also reported on the same allele as the P102L mutation (see below) in a Japanese family in which dementia rather than ataxia was prominent and cerebellar plaque pathology was less noticeable compared with cases of the P102L mutation alone [225]. Recent studies in knock-in mice have shown that a heterozygous state at codon 219 confers reduced susceptibility to prion infection [226].

1.8.   Conformational diversity of amyloid structures: from fungus to humans

Amyloid and amyloid-like aggregates are elongated unbranched fibrils, formed by normally soluble proteins, which assemble to form insoluble fibers that are resistant to degradation. The term "amylon" was coined for the first time, in 1834, by German botanist Matthias Schleiden, when he used the iodine-sulphuric acid test on plants to demonstrate what he considered to be a transformation of the plant material into a waxy starch [227]. In 1854, Rudolph Virchow used the word "amyloid" to describe macroscopic tissue deposits that exhibited a positive iodine staining reaction [228].

In 1959, electron microscopy examination of ultrathin sections of amyloidogenic tissues revealed the presence of fibrils, undefined in length and width ranging from 80 to 100 Å. Subsequent advances in light microscopic studies using polarizing optics, showed the particular features of amyloid deposits when using the Congo red stain (Congophilia): they look pink under normal lighting but show apple-green birefringence under polarized light. Hence, Congophilia was the first criterion used for amyloids [228]. Further analysis of more than 20 biologically and

biochemically forms of amyloids from distinct origin throughout the animal kingdom have shown common features of amyloid fibrils: they have similar fibrillar morphology and tinctorial properties (Congophilia), and width ranging from 80 to 100 Å. X-ray diffraction analysis also revealed the ordered structure in a β-sheet conformation, with their polypeptide backbone running perpendicular to the fibril axis (cross-β structure) [228,229]. Hence, although structurally unrelated peptides and proteins can form amyloid fibrils, they share a common denominator: the secondary structure of the native protein suffers a conformational change to a β-sheet rich fold, with a characteristic cross-β core conformation.

Amyloids can be set apart from other biopolymers such as DNA and polysaccharides, in that their cross-β core is formed by monomers, which are relatively large polypeptides arranged in a stack of β-strands running perpendicular to the fibrils; showing a characteristic X-ray diffraction pattern of 4.8 Å separation and with an intersheet spacing in the order of 9-11Å. A dense network of hydrogen bonds stabilizes the elongated stack. The sequence-specific side chains tend to affect the propensity to form fibrils [117,230,231]. The formation of amyloid fibrils might lead to the development of a disease, with specific pathophysiology. Well-known examples of amyloid diseases include Alzheimer's disease, Diabetes type 2, and spongiform encephalopathies. A model of a fibril from GPI-anchorless PrP 27-30 expressed in transgenic mice is shown in Figure 10. The views along the entire fibril axis in this model reveal the dense stacking of a four-rung β-solenoid structure with four β-strands from two individual PrP^{Sc} monomers per layer with a height about ~17.7 Å. Each fibril contains two distinct protofilaments. This β-solenoid of parallel β-sheets is one of the prominent characteristics of amyloids. A view perpendicular to the fibril axis (Figure 10) illustrates the 4.8 Å spacing between individual β-strands of parallel β-sheets and their perpendicular orientation to the fibril axis. The cross-section images of the reconstructed fibrils show two protofibrils that usually twist together to form unbranched, elongated mature amyloid fibrils, which look like twisted rope-like structures (Figure 10).

The high degree of structural order within the fibrils leads to strong interactions between the protofibrils forming a mature amyloid fibril. For instance, 310 k_BT/um for insulin [232], that results in the inherent mechanical stability of amyloid fibrils. Regarding, the PrP^{Sc} 27-30 fragment, 3D-

reconstructions revealed two 50 x 29 Å oval-shaped protofilaments with a molecular volume of 18,990 Å^3, a maximum width of 9.1 nm, and a crossover distance of 95 nm. Based on these findings, a height of ~19.1 Å has been predicted for each PrP 27-30 molecule, in agreement with the previous Fourier transform analysis of averaged fibril segments [233]. These results indicate a four-rung β-solenoid structure as a key feature for the architecture of infectious mammalian prions.
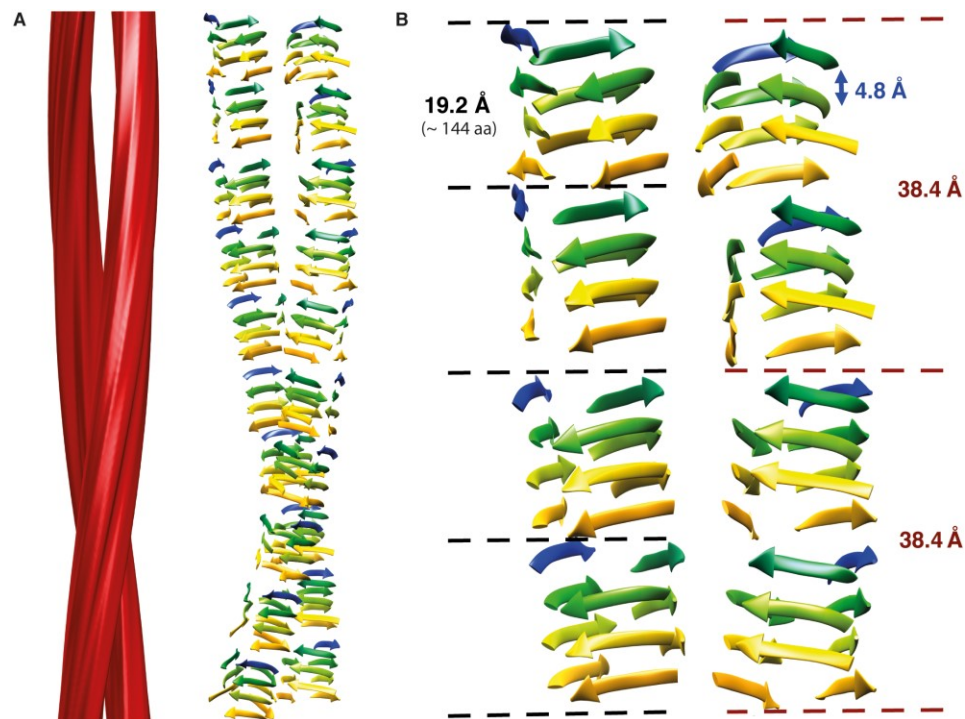
Figure 10. Structural conformation model of a GPI-anchorless PrP 27-30 fibril. (A) cartoon representation of a 3D reconstruction for an individual GPI-anchorless PrP 27-30 fibril formed by two protofilaments (left side), and the potential organization of the polypeptide chains in the PrP 27-30 monomers (right side). (B) Close up view for the proposed β-sheet stacking organization in a four-rung β-solenoid structure. (Figure taken from [233]).

The amyloid pathway to form protein fibrils have drawn considerable attention in materials science, owing to their potential to be used as artificial materials. Amyloid fibrils can self-assemble from natural proteins (such as β-lactoglobulin), but they can also be pharmaceutically designed (like insulin) [117]. The unique molecular organization of these fibrils endows them with remarkable

mechanical properties, such as stiffness with a Young's modulus on the order of 3-20 GPa [234], and with a surprising high strength (resistance to break) on the order of 0.6 GPa (comparable to the strength of silk and steel) [235]. Recent experimental and theoretical studies have demonstrated that the exceptional rigidity of amyloid fibrils originates from the regular network of intermolecular non-covalent interactions (hydrogen bonds) in the cross-β core [236]. These interactions between the variable side-chains (hydrophobic or hydrogen-bonding), further stabilize the fibril and enhance Young's modulus [117,236]. However, despite the advances in characterization techniques to elucidate protein aggregation mechanisms and analysis of amyloid fibrils, a detailed understanding of the relation between the molecular properties of amyloids (like the role of the amino acid side chains content) and their material properties (like stiffness and mechanical strength), has remained challenging. The lag in our fundamental understanding of the relation between the conformational structure of amyloids and their mechanical properties rely on the limited development of structural and physicochemical techniques that can provide information on the molecular interactions underlying the assembly and material properties of protein fibrils [117].

1.8.1.   Structure of the filamentous fungal HET-s prion. Analysis by high-resolution solid-state NMR (ssNMR) requires homogeneous and diamagnetic samples (magnetized in a direction at 180° to the applied magnetic field), to generate sharp signals. Amyloid fibrils of the HET-s prion of *P. anserina* are a particular case, as they present a single and homogeneous conformation, they are suitable for ssNMR analysis, as judged by sharp (~0.25 to 1 ppm) lines obtained from a two-dimensional solid-state NMR [237]. By using a broad set of ssNMR measurements, Meier and coworkers have provided an accurate β-helical model for HET-s fibrils[84,238]. This model, also known as β-solenoid, is a structural motif in which short parallel β-strands segments bend and associate in a helical pattern, alternating to create multiple coils in a solenoid-like rod. The β-strand segments run perpendicular to the axis of the rod. A single polypeptide chain contributes many coils to the β-helix.

In HET-s fibrils, each protein molecule is a two-turn β-helix, so the hydrogen bonds between β-strand segments are both intramolecular and intermolecular [239] (Figure 11). MPL measurements have supported this model. MPL peak values were determined by fitting the histograms to one or

more Gaussian functions for HET-s fibrils, generating a single peak at 8.3 kDa/nm, predicting a β-helix-like molecular structure in agreement with the previous results based on ssNMR analysis [240,241].
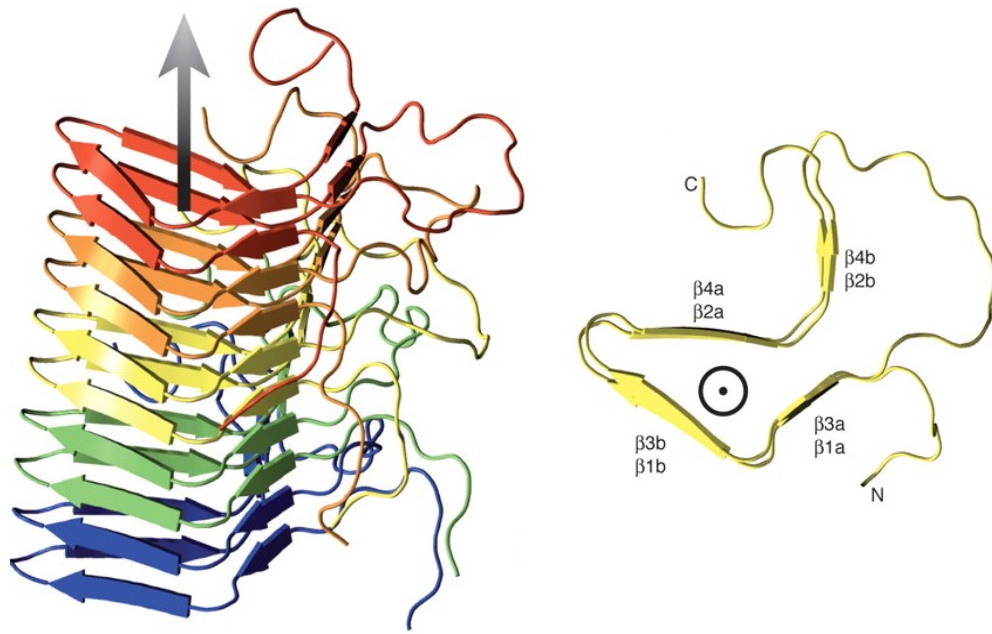
Figure 11. Structure of the HET-s (residues 218 to 289) fibrils from the filamentous fungus *Podospora anserina*. The overall organization of a HET-s (218 289) fibril is a left-handed β-solenoid with two windings per molecule. The core of the fibril is defined by three β-strands per winding (six β-strands per molecule) that form continuous in-register parallel β-sheets. (A) Side view of the structural model of HET-s (218-289), based on 134 intra- and intermolecular experimental distance restraints, obtained by ssNMR. This model proposed a left-handed β-solenoid conformational structure, with each molecule forming two helical windings, a compact hydrophobic core, at least 23 hydrogen bonds, three salt bridges, and two asparagine ladders. (B) Top view of the central molecule from (A). β3 and β4 lie on top of β1 and β2. The fibril axis runs perpendicular as indicated by the arrow. RCSB PDB ID: 2RNM. (Figure taken from [238] and reprinted with permission from Science).

1.8.2. Structure of the yeast prions [URE3] and [PSI+].

The parallel-in-register (PIRIBS) architecture was hypothesized to explain the ability of Sup35p and Urep2 (with their prion isoforms [PSI+] and [URE3], respectively), to shuffling their prion domain sequences without impairing their ability to form prions [242]. In this structure, the backbone amide and carbonyl groups of residue n of one peptide chain are hydrogen-bonded to carbonyl and amide groups of residues n-1 and n+1

of a neighboring chain, respectively. The Q/N domains form the fibril core in the parallel-in-register β-sheet structure [239]. Several follow-up studies, using solid-state NMR confirmed this structural conformation for these proteins, including the Rnq1 protein, a transferable epigenetic modifier which forms a prion responsible for the non-Mendelian trait [PIN+] [243,244]. These findings establish that it is the composition of the prion domain, not the sequence, the critical factor in determining the prion-forming ability. Scrambling experiments demonstrated that the ability of Ure2 and Sup35 to form prions is mainly dependent on the amino acid sequence, also known as prion-forming domains (PFDs) [245]. Both proteins contain remarkably high glutamine/asparagine (Q/N) rich prion domains, as well, as highly hydrophobic residues content.

Their prion domains also contain relatively few charged residues and prolines, which inhibit prion formation (Figure 12). As previously mentioned, previous studies have also shown the effect of sequence content in transmission barriers [84]. Differences in amino acid sequence content between donor and receptor, in even a single amino acid, can act as a barrier [246–248]. Another study suggested that the sequence identity required for propagation interacts positively between amino acid side chains, i.e., identical residues paired, which are not affected by the shuffling, in agreement with an in-register parallel β-sheet conformation, but not with an antiparallel or β-helix structure [242].

Mass-per-length (MPL) peak values were also determined by fitting the histograms to one or more Gaussian functions for Sup35NM fibrils, generating a single peak at 60.8 kDa/nm, consistent with a parallel-in-register β-sheet structure in agreement with previous results based on ssNMR measurements [241]. Much of the N-terminal domain of PrP encompasses proline and glycine-rich repeats and pseudo-repeats. This region is an evolutionarily conserved motif, though the number of octapeptides can vary between species. In human PrP, there are four perfect sequential repeats of the sequence PHGGGWGQ (residues 60-91) and one pseudo-repeat in which a glycine is omitted and a histidine is substituted with glutamine.
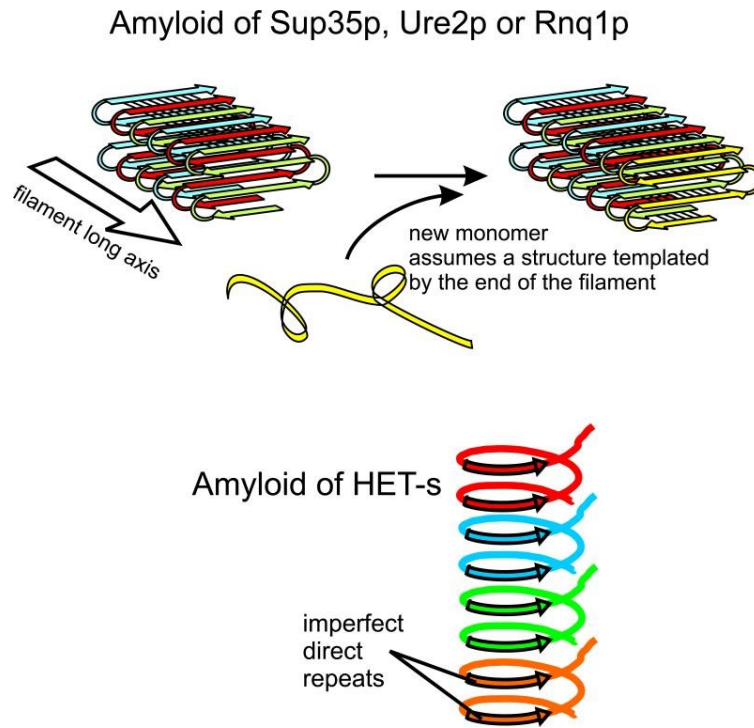
Figure 12. Models of yeast and filamentous fungal prions. The parallel in-register β-sheet model of yeast prions [URE3], [PSI+] and [PIN+] is shown on the top. In this model, the main chain hydrogen bonds run parallel to the filament axis, while the main chains themselves are perpendicular to the filament axis; with each molecule forming a single β-strand layer of the fiber. In contrast, as depicted below, in the β-helix model of the fungal [Het-s] prion of *Podospora anserina*, each molecule contributes two strands (as shown by the colors). (Figure adapted from [244] and reprinted with permission from John Wiley and Sons).

Under specific conditions (e.g., when bound to certain ligands), these repeats gain a level of order that has allowed for atomic-level insights into their structure [164]. Pseudo-repeats also participate in the structural complexity of prion proteins. Favorable alternation of positive and negative charges in ladders along the fibril axis can be possible only because of the pseudo-repeats, leading to a structure in which one molecule forms two turns of the solenoid as in the case of HET-s prion. These interactions lead to the formation of three salt-bridges that stabilize the structure. In contrast, the presence of pseudo-repeats in yeast prion protein Sup35NM is probably more related to structural variability and the existence of prion strains [238].

1.8.3. Structure of the human amyloid-β (Aβ) protein: implications in Alzheimer's disease.

Alzheimer's disease (AD) is a chronic, progressive neurodegenerative disease with a gradual decline in cognitive function. Neuropathologically, it is characterized by the presence of neuropil threads, specific neuron loss, and synapse loss [249]. Hallmarks of AD include 1) formation of paired helical filaments (PHF) in neurofibrillary tangles (NFTs) inside the brain's cells, which consist primarily of a neuronal microtubule-associated protein, tau (tubulin-associated unit). In AD, tau is hyperphosphorylated (p-tau), which renders the protein insoluble and twisted, and as a consequence to be aggregated and deposited [250]. 2) Accumulation of amyloid plaques, extracellular fibrils between nerve cells (neurons) is another hallmark of AD. These fibrils are now known to be composed of an amyloid-β peptide, with the length of the fibrils ranging from 39 to 43 residues, and generated from the proteolytic cleavage of the amyloid precursor protein (APP) by β- and γ-secretases. Hence, different species can be generated, with two alloforms being the most abundant species generated from this cleavage: Aβ40 and Aβ42, composed of 40 and 42 amino acids, respectively. Aβ42 has being identified as the more toxic species, with a higher propensity to aggregate and facilitate the nucleation of fibrils formation. Although Aβ40 has been widely studied and its structure has been already elucidated [251–253], little is known about the Aβ42 structure.

Data obtained by ssNMR, have suggested that the fibril core consists of a dimer of Aβ42 molecules, each containing four β-strands in an S-shaped amyloid fold. The conformation is arranged in a manner that two hydrophobic cores are capped at the end of the chain by a salt bridge (Figure 13 depicts a ribbon representation of the structure of Aβ42 protein, PDB ID: 5KK3). The hydrophilic side chains are present on the outer surface of the monomers and are exposed to the solvent. Internuclear distances at the interface between monomers and intermolecular constraints demonstrated that the amyloid fibrils are organized in a parallel in-register structure [252]. These findings are in agreement with previous works, where MPL measurements were determined by scanning electron microscopy (STEM) [241,254], which also showed a highly heterogeneous population of molecules in the same sample. Aβ40 fibrils present two-fold symmetric (2f-Aβ40) or three-fold symmetric (3f-Aβ40) structures predominantly, depending on growth conditions [240,241]. MPL values were estimated from the Gaussian peak position for 2f-Aβ40 of 17.4 kDa/nm and for3f-Aβ40 of 27.7 kDa/nm; while MPL value for Aβ42 fibrils was 23.5 kDa/nm. These

findings are in agreement with previous MPL values determined by STEM, suggesting that these fibrils form a cross-β structure that contains a parallel-in-register β-sheet conformation [254,255].

1.9. Biochemistry and structure of human prion proteins: PrP[C] vs. PrP[Sc]: overview

Since the discovery of prions, there have been multiple attempts to elucidate the mechanisms involved in the pathogenic conversion from PrP[C] to PrP[Sc] and their structural differences. However, these efforts have failed due to the limitations of the biophysical and biochemical techniques that have been used. PrP[C] and PrP[Sc] have identical molecular weights (33 to 35 kDa), the same amino acid sequence, similar N-linked carbohydrate side chains, and glycophosphatidylinositol (GPI) anchors [218,219].
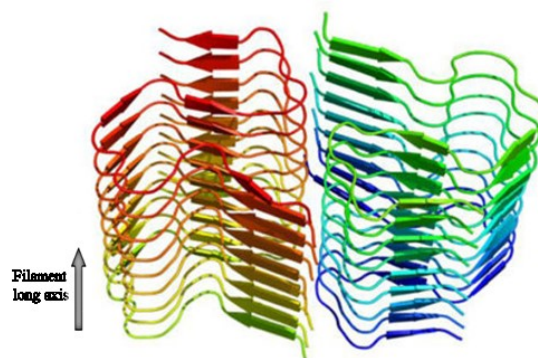
Figure 13. Ribbon representation of the structure of Aβ42. Side view showing the alignment of the dimers along the fibril axis. The structure (PDB ID: 5KK3) shows that the fibril core consists of a dimer of Aβ42 molecules, each containing four β-strands in an S-shaped amyloid fold, and arranged in a manner that generates two hydrophobic cores that are capped at the end of the chain by a salt bridge. The outer surface of the monomers presents hydrophilic side chains to the solvent. The interface between the monomers of the dimer shows clear contacts between M35 of one molecule and L17 and Q15 of the second. Intermolecular 13C and 15N constraints demonstrate that the amyloid fibrils are parallel in register. (Figure taken from [252]).

In spite of these similarities, PrP[C] and PrP[Sc] differ regarding their solubility, fibril formation tendency, and PK resistance. PrP[C] is a soluble protein with a high susceptibility to proteolytic

digestion, whereas PrP^{Sc} is characterized by its insolubility in detergents and partially digested to a 27 to 30- kDa protein designated PrP 27-30 (approximately 142 amino acids) which is associated with infectivity and resistance to proteolysis in its aggregated form [66,221,222]. These differences appear to be based on their structural conformations.
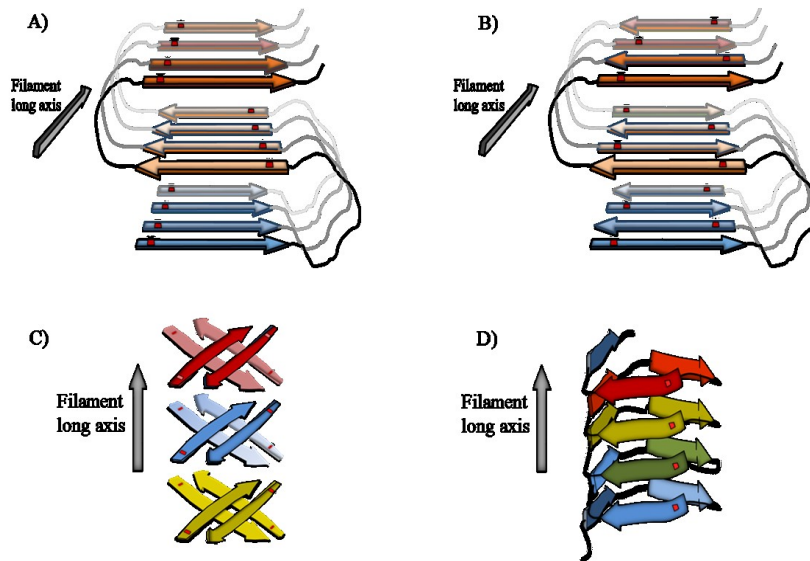
Figure 14. Four types of cross-β structures are present during and/or after the formation of amyloid fibrils. Small dark dots represent a single 13C-labeled atom in each protein molecule. Smaller space distance between labeled atoms (measured by ssNMR), such as ~0.5 nm, represent parallel-in-register conformation, while greater spacing is present in other structures [84,256]. A) parallel in-register (present in some amyloid fibrils, like Amyloid-β (Aβ) involved in Alzheimer's' disease) [252]; B) antiparallel (present in the majority of proteins and nucleic acids); C) parallel out-of-register (present in metabolite intermediates during the amyloid pathway formation [257]; and D) β-helix (β-solenoid) (present in virulence factors, toxins, allergens, and some amyloid fibrils [257]. Small dark dots represent a single 13C-labeled atom in each protein molecule. (Figure adapted from [84] and reprinted with permission from ACS Publications).

Early studies based on circular dichroism and infrared spectroscopy have shown that PrP^C is dominated by α-helices (~43%) and has only a small fraction of β-sheet content (less than 3%)[222], whereas PrP^{Sc} contains predominantly β-sheets (>43%), a characteristic of amyloids, and no detectable α-helices [222,223]. The N-terminally truncated PrP 27-30 has higher β-sheet content (>54%) and no detectable α-helices. In contrast to PrP 27-30, which polymerizes into rod-shaped amyloids, PrP^C does not form aggregates detectable by electron microscopy [222–224]. Figure 15 depicts four types of cross-β structures present in amyloid fibrils.

1.9.1. Structure of PrP^C. PrP protein exists in multiple conformations, and its cellular isoform PrP^C is found in healthy organisms. In spite of being among the most extensively studied proteins, the physiological function of PrP^C and its role in the molecular pathways that lead to degeneration of the brain in patients suffering from TSEs is still elusive. In humans, the newly synthesized and unprocessed PrP^C is approximately 253 amino acids in length and has a molecular weight of 35-36 kDa (Figure 16 illustrates a schematic representation of the structure of PrP^C). The low yield of PrP^C during the purification process confers one of the most cumbersome limitations for its analysis by conventional biophysical methods [258,259]. By using recombinant PrP (recPrP) as a surrogate for PrP^C, these limitations were overcome, as NMR studies have shown that recPrP appears to have the same molecular architecture as PrP^C [260–262].

These studies have helped to determine different regions in the sequence of this protein. It consists of an amino-terminal signal peptide (residues 1-23), a flexible N-terminal domain (residues 23-120), a folded C-terminal domain (residues 121-231), and a signal peptide (residues 232-254) for a GPI anchor to extracellular membrane attachment via lipid rafts [260,261]. The structure of recPrP is composed of three α-helices (amino acids 144-154, 175-193 and 200-219) and a small antiparallel β-sheet (amino acids 128-131 and 161-164) [160,164]. The N-terminal domain contains a repetitive motif (P(H//Q)GGG(-/G)WGQ), which has a high affinity for metal-ion binding, i.e., copper ions (Cu^{2+}), suggesting that PrP^C might be involved in copper metabolism [264–266]. PrP^C also contains a single disulfide bond linking the cysteine residues at positions 179 and 214, connecting the helices 2 and 3, and two N-linked glycosylation sites at asparagine residues 181 and 197 [259,267]. After ~5 h at the cell surface (its average half-life), PrP is internalized through a caveolae-dependent mechanism and is degraded in the endolysosome compartment. It has been speculated that the PrP^C conversion to PrP^Sc may occur in caveolae-like domains [147].
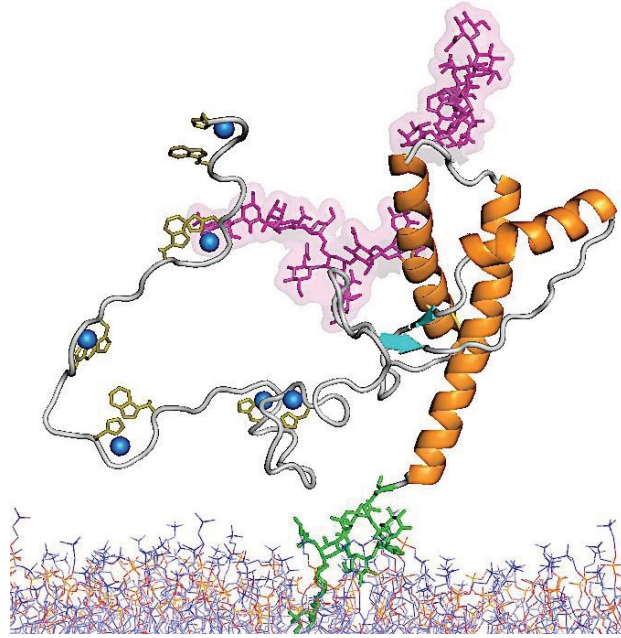
Figure 15. Schematic diagram of the structure of PrP^C. The carbohydrate moieties that are linked to Asn 181 (down) and Asn 197 (up) are shown in pink. The *C*-terminal GPI-anchor is shown in green and is extending into the cell membrane in blue and red. OR residues in the *N*-terminal domain are known to bind copper ions (shown in blue). This graphic was kindly provided by Professor Glenn Millhauser, Department of Chemistry and Biochemistry, University of California, Santa Cruz, and based on a figure from Liu *et al*., 2011 [263]. Coordinates for the PrP^C-terminal domain, along with carbohydrates, GPI anchor, and membrane, were kindly provided by Professor Valerie Daggett, University of Washington. (Figure taken from [263] and reprinted with permission from American Society for Microbiology).

1.9.2. Structures of PrP^{Sc} and PrP 27-30. Numerous attempts have been made to determine the structure of PrP^{Sc} and its proteolytically truncated variant PrP 27-30 (which retains full infectivity and about 65% of the prion protein). However, details underlying their conformational structure remain unknown. Their high-resolution structures have evaded experimental determination due to their insolubility and propensity to aggregate. However, it is widely accepted that 1) during the conversion of PrP^C to PrP^{Sc} the β-strand content increases substantially [154,258,268]; 2) fibrillar assemblies of PrP^{Sc} display a typical cross-β sheet architecture, which is characteristic for amyloid [269]; and 3) conversion of PrP^C to PrP^{Sc} increases its proteinase-K (PK)-resistance [162], although this feature is not obligatory [174]. Table 5 summarizes the structural and biochemical properties of PrP^C and PrP^{Sc}.

Cellular prion protein (PrP^C)	Pathogenic isoform of PrP (PrP^{Sc})
Non-infectious	Infectious
Conformational structure: mainly α-helical	Conformational structure: β-sheet rich
Detergent soluble	Detergent insoluble
Proteinase K (PK) sensitive	Partially PK resistant (PrP 27-30 fragment)

Table 5. Structural and biochemical properties of PrP^C and PrP^{Sc}. (Table taken from [259]**).**

1.10. Techniques for structural analysis of prions: overview

Several techniques have been used to assess the conformation of prions. Data generated by biochemical and biophysical methods, such as spectroscopy analysis, electron microscopy, X-ray fiber diffraction, small-angle X-ray scattering, limited proteolysis, hydrogen/deuterium (H/D) exchange, and surface reactivity measurements, have led to proposed various 3D structural models of PrP^{Sc}. However, there are still several discrepancies between the experimental data and the proposed models, indicating that these models fail to accommodate the research findings[270].

Limited proteolysis as a biochemical tool in the analysis of proteins. Limited proteolysis enables the delineation of a proteome-wide profile of a conformational structure for a protein. The method is based on short controlled exposures of the protein to a proteolytic enzyme. The first cleavage occurs in the outermost regions of the protein, exposed on the surface, i.e., the areas that are more accessible to the active site of the proteolytic enzyme. Because most enzymes are globular proteins with a molecular weight of at least 15-20 kDa, the location of the cleavage sites will reflect their accessibility to a nearly spherical probe, whose diameter corresponds to the size of the enzyme used [271].

Proteinase K is a serine protease, enzymes that cleave peptide bonds in proteins, in which serine serves as the nucleophilic amino acid at the enzyme's active site. The predominant site cleavage of PK (molecular weight 28.9 kDa) is the peptide bond adjacent to the carboxyl group of aliphatic and aromatic amino acids with blocked alpha amino groups [272]. Limited proteolysis of PrP^Sc by PK has proven to be a convenient tool in the detection of this protein in samples, as it often produces a smaller, protease-resistant core of approximately 142 amino acids, referred to as 27-30 fragment, which consists of the carboxy-terminal two-thirds of the protein. The PK-labile amino terminus has been suggested to be solvent-accessible and largely unstructured [273]. Under the same conditions, PrP^C and some other forms of PrP^Sc are completely hydrolyzed; although, not all PrP^Sc is resistant to protease digestion [274].

Techniques for structural analysis of prions. X-ray fiber diffraction data obtained from brain-derived prions showed a repeating unit of 19.2 Å per molecule, with the characteristics meridional diffraction signals at 4.8, 6.4, and 9.6 Å. The underlying structure was previously identified as a four-stranded ß-sheet core in a cross-ß arrangement [55]. Based on these findings, several models have been proposed to accommodate the subunits in PrP^Sc conformation; however, these models contradict the experimental observations that have indicated that the C-terminal domain of PrP^Sc appears not to contain any residual α-helical structure [275,276]. Contributing to the PrP^Sc structure puzzle are the findings that amyloid fibrils are highly polymorphic, as it has been shown by TEM, cryo-electron microscopy (cryo-EM) and atomic force microscopy (AFM) analyses [277–279]. These studies have shown that relatively short amyloid-forming polypeptides self-assemble into protofilament strands that in turn aggregate to form the amyloid fibrils. The resulting fibrils can have from two to six protofilaments arranged either coiled in cable-like structures or packed side-by-side in ribbon-like-structures [277]. The morphology of amyloid fibrils depends on their internal structure, and two features have essential implications on this organization: 1) the periodic narrowing observed in many TEM analyses suggesting that fibrils twist around their long axis and 2) the number of filaments forming the fibril, as it has been previously determined by tilted-beam (TB)-TEM mass-per-length (MPL) analysis [241,280]. The greatest advantage of EM over other structural approaches is that: 1) it requires a small amount of sample, compared to other techniques like NMR or X-ray crystallography, 2) it does not require crystalline forms for the

samples, 3) it allows the analysis of transient quaternary structural intermediates, 4) it allows the study of heterogeneous samples and 5) it can reach powerful magnifications (~500,000X) and a high resolution (~0.1 nm) [281]. Recent advances in cryo-EM and image processing techniques have allowed structural studies of large macromolecules, including protofibrils and amyloid fibrils [281–284]. Hence, several EM approaches enable: 1) to characterize the heterogeneity of fibrils polymorphs, 2) to determine the relationship between these polymorphic variants that co-exist in the same fibril population and 3) to test the current proposed structural models for PrP^{Sc}. Elucidating the three-dimensional structure of PrP^{Sc} is central to understand the molecular mechanism of prion diseases and hence provide a platform for the development of structure-based drugs and strategies against mechanisms of propagation of prions and prion-like diseases.

1.11. Mass-per-length (MPL) analysis: introduction

As it was already mentioned, numerous attempts to elucidate the structural conformation of PrP^{Sc} have been performed over the past 20 years, but none has been conclusive due to the poor correlation with experimental data. Therefore, complementary experimental data can restrain the number of solutions that are ambiguous or similar. One possibility is mass measurements of biomolecules by TEM [285]. MPL data impose a stringent constraint on viable fibril models when the subunit mass is known. By calibrating the image intensity of the target helix, in this case, PrP^{Sc}, to an internal reference standard, the MPL in kDa/nm of the PrP^{Sc} fibrils can be obtained[285]. These measurements limit the number of possible indexing schemes and provide independent experimental validation to the proposed structural models [285]. The HET-s prion protein of the filamentous fungus *Podospora anserina* and the TMV rods have been widely studied, and their structures, as well as their MPLs, have been well characterized. Hence, HET-s fibrils or TMV rods can be used as an internal standard for absolute mass quantification (the choice of HET-s or TMV rods will be determined experimentally).

Previous MPL measurements on HET-s fibrils have yielded 1.02±0.26 subunits per 0.94 nm, which is the half the packing density of ~1 subunit per 0.47 nm previously obtained for Ure2p and

Sup35p yeast prion fibrils, and hence applying a critical constraint that helped to determine that these amyloid architectures are different [243]. In another study, in preparation of seeded protein fibrils, morphological variations of amyloid-β fibrils were examined by dark-field imaging and TEM. The number of filaments comprising these fibrils frequently changed from two to six along their length, and these changes only became apparent when the MPL was determined [286].

1.11.1. MPL analysis: expected outcomes. Evidence obtained by site-directed spin labeling, electron paramagnetic resonance (EPR) spectroscopy, and solid-state NMR (ssNMR) spectroscopy, have suggested a parallel, in-register β-sheet (PIRIBS)-like conformation model for recombinant PrP amyloid fibrils [287,288]. For this model, it is expected to have an MPL = ~60-70 kDa/ nm, this value corresponding to two protofilaments, where each PrP^{Sc} molecule contributes with 0.48 nm to the length of the fibril. However, this model fails to accommodate the repeating unit size of 19.2 Å (= 4 β-strands high) determined by X-ray fiber diffraction analysis on PrP^{Sc} and PrP 27–30 [55]. Another proposed model, based on electron micrographs of 2D crystals of PrP 27-30 and the fibrillogenic miniprion PrP^{Sc} 106, suggested a parallel left-handed β-helical model for the core of the infectious conformer [289,290]. This model has been supported by subsequent X-ray diffraction studies on PrP 27-30 [55], which showed meridional reflections at 4.8, 6.4 and 9.6 Å, suggesting a four-rung β-solenoid structure, where each PrP 27-30 molecule constitute four-rungs of β-structure and spans 19.2 Å along the axis of the fibril. For this model, it is expected an MPL= ~30 kDa /nm, this value corresponding to two protofilaments, where each PrP^{Sc} molecule is expanding 1.92 nm, this value corresponding to fibrils containing one protofilament only. Although X-ray diffraction data strongly support the β-solenoid model for PrP^{Sc} fibrils, there is still not enough evidence whether it can be applying to the infectious conformer.
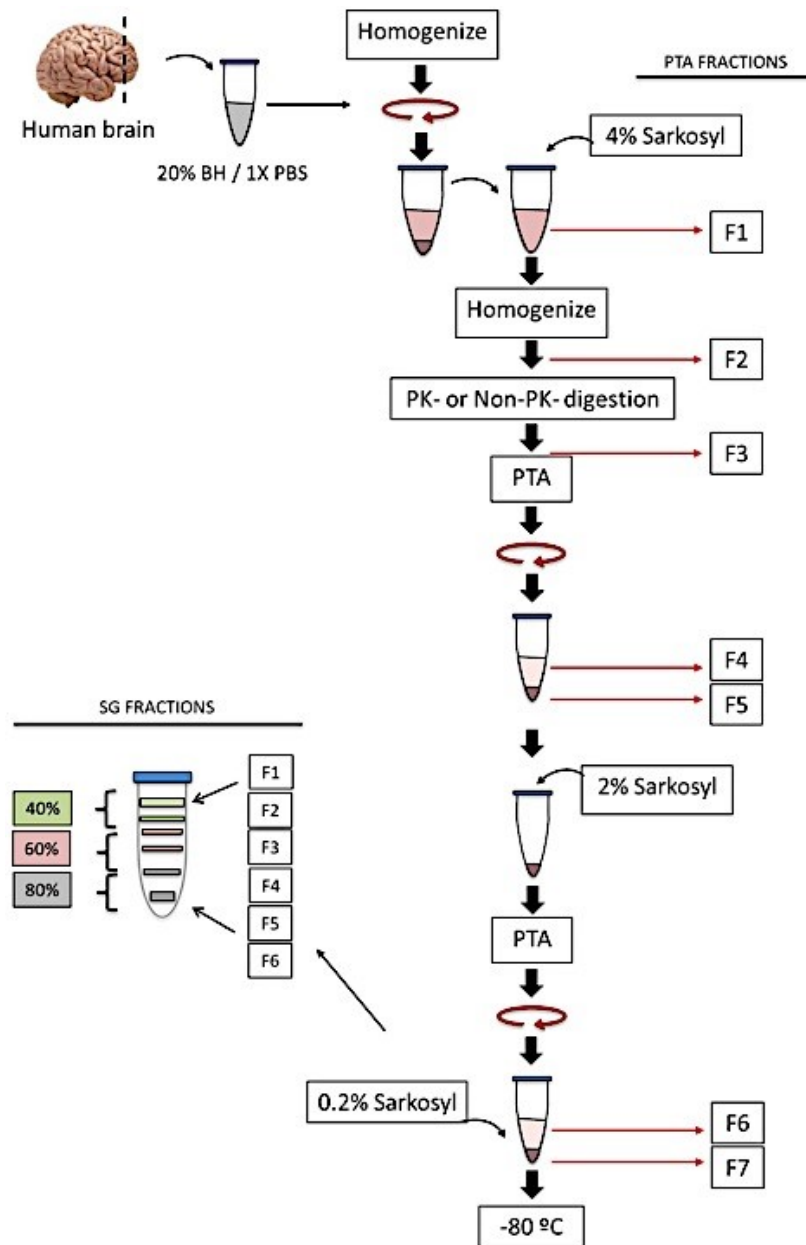
Figure 16. Overview of the purification method. Samples of frozen brain tissues obtained from patients were homogenized at 20% (w/v) in sterile 1X PBS. Followed a mild centrifugation, supernatants were collected to which a similar volume of 4% sarkosyl was added to a final concentration of 10% brain homogenate (BH). Following another round of homogenization, the resulting homogenates were split in two sets: 1) samples enzymatically digested with PK, and 2) samples non-digested with PK (negative control for the enzymatic digestion). Next, an overnight PTA precipitation was carried out, following centrifugation to collect the pellet. A second round of PTA precipitation/centrifugation was followed. Small aliquots were taken at each step of this purification, to evaluate the integrity, purity and concentration of the resulting products (PTA

fractions F1 to F7). The resulting pellets were pass through a sucrose gradient cushion (40%, 60%, and 80% sucrose), to obtain a highly purified PrP^{Sc} product.

2.1. Protein purification

Brain homogenates (BHs) were prepared from frozen human brain samples at a final concentration of 20% (w/v) in sterile Ca^{2+}/Mg^{2+}-free 1X PBS. Brain samples were homogenized (blended) three times during 15 s, with intervals of resting in ice between each homogenization. Followed mild centrifugation at 500g for 5 min at 4 °C, the supernatants were collected, and the pellets were discarded to remove cell debris from the samples. A volume of 4% sarkosyl was added to each supernatant at a final concentration of 10% (w/v). A second round of homogenization was carried out to assure a complete homogenization. The sample was split into two groups: 1) a sample to which a final concentration of 50 µg/ml PK solution was added, and 2) a non-digested sample (used as a negative control for the enzymatic digestion). PK-digestion hydrolyzes the N-terminal 67-amino acid residues. PrP^{Sc} is a membrane-bound protein which polymerizes upon detergent extraction [291]. The enzymatic digestions were incubated at 37°C with shaking at ~700 rpm during 1 h. Next, the enzymatic reactions were stopped by adding 1mM phenylmethylsulfonyl fluoride (PMSF) at a final concentration of 1mM. To both groups of samples (digested and non-digested), 10% phosphotungstic acid (PTA) solution, pH 7.2, was added to a final 2% (w/v) and incubated overnight 37 °C. Followed centrifugation at 16,000xg during 30 min, the supernatants were discharged, and the pellets were resuspended in 50 µl of 0.2% sarkosyl. Aliquots (~50 µl) for sampling were taken at each step during the whole purification to evaluate the quality and integrity of the samples.

2.2. SDS-PAGE and western blot analysis

SDS-PAGE electrophoresis was performed on Mini-Protean TGX^{TM} precast protein gels, 12% polyacrylamide gels (BioRad). The gels were transferred onto polyvinylidene difluoride (PVDF) membranes (BioRad), using Tris-glycine transfer buffer with 20% methanol in the Mini-

Protean Tetra Cell transfer-blot chamber (BioRad). The PVDF membranes were previously rinsed in methanol for ~30 min. After transferring the gel, the membranes were saturated with blocking buffer (2.5% fish gelatin (Truin Science) in 1X TBST (10 mM Tris HCl pH 8.0, 150 mM NaCl, 0.05% (v/v) Tween 20)), for 2 hours, at gentle shaking and RT. The membranes were incubated overnight at 4 °C with monoclonal antibody D15.15 (internal lab code) at a 1:5000 dilution (antibody kindly provided by Dr. Xinli Tang, Centre for Prion and Protein Folding Diseases, University of Alberta). This antibody was expressed in hybridoma cells at a concentration of 1.9 mg/ml, and it recognizes the epitope region between the residues 175-186 in PrP derived from mouse, hamster, deer, elk, bovine, rat, and human. The primary antibody was detected by using an alkaline-phosphatase-conjugated anti-mouse IgG secondary antibody (Sigma). Precision Protein StrepTactin-AP conjugate (BioRad) was used for detection of the molecular weight marker (BioRad). Immun-Star AP substrate was used for detection (BioRad). Molecular weight marker used Precision Plus Protein Standard (BioRad).

2.3. Equilibrium sedimentation in sucrose density gradient

About 150-μl to 300-μl (depending on the availability of the sample) of PrP^{Sc} samples that have been PTA –purified and concentrated were loaded on a sucrose gradient cushion prepared by adding 1 ml of 80%, 60%, and 40% sucrose solutions from bottom to top in SW55Ti rotor tubes (Beckman, Brea, CA, USA). Sucrose solutions were prepared in TNS buffer (10 mM Tris, 150 mM NaCl, 1% Sarkosyl). The gradients were loaded in an SW41Ti swinging bucket rotor (Beckman-Coulter) and centrifuged at 37,000 rpm for 24h at 4 °C. From each sample loaded, six fractions were collected (as shown in Figure 17), labeled from F1 to F6: F1: corresponding to the top fraction (upper layer on the 40% layer); F2: the 40% layer; F3: the interface between 40%-60% layers; F4: the 60% layer; F5: the interface between 60%-80% layers; F6: the bottom 80% layer. The resulting fractions were analyzed by Western blot.
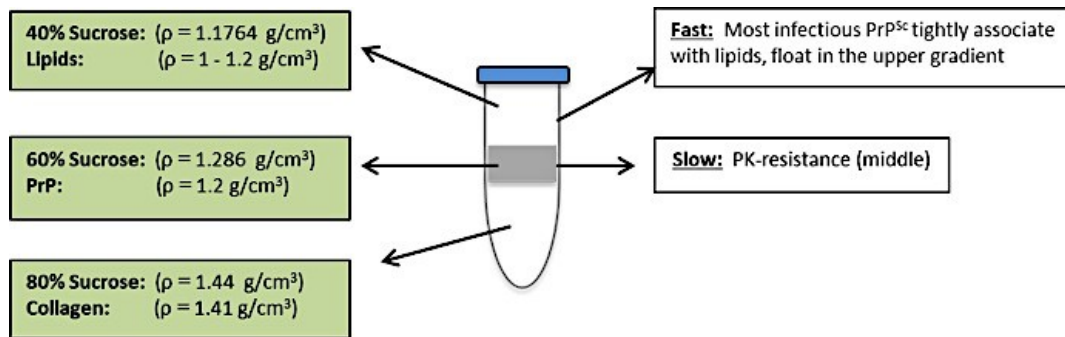
Figure 17. Separation of PrP protein in a sucrose gradient rate-zonal ultracentrifugation. Before centrifugation the sample is loaded on the top of the gradient in a thin band. After centrifugation, the PrP particles separate based on their density (shape and mass). Higher density particles migrate faster to the higher density portion of the gradient (bottom), while lower density particles stay in the lower density portion of the gradient (top) [292].

2.4. Quantification of PrP^{Sc} species by ELISA

Relative PrP^{Sc} levels obtained as a final PTA-purified product were determined by sandwich ELISA. Samples (including the standards, positive and negative controls, and PrP^{Sc} samples) were pelleted by centrifugation at 16,000xg for 30 min at 4 °C, and the pellet was dissolved in 20 μl 8M guanidine hydrochloride. Each sample was prepared in triplicate. Costar 96-well microplates were coated overnight at 4 °C with the capture antibody D15.15 (internal lab code) at a concentration of 0.25 μg/ml. Following blocking for 2h with 1% BSA prepared in 0.1% TBST (Tris-buffered saline containing 0.1% Tween 20). After three washes with 0.1% TBST, 5 min each, 100 μl reaction buffer (1% BSA diluted in 1X PBS) was added on each well. Next, 5-μl samples, i.e., standards and samples, were loaded in triplicate. As standards, denatured recombinant PrP mice (recPrP, 23-231) were used. Wild type FVB mice (*Prnp +/+*) and PrP^{C}-null FVB mice (*Prnp -/-*) were used as positive and negative controls, respectively. Samples derived from fCJD, sCJD, and GSS were examined for PrP^{Sc} quantification as a final purified product. The plate was incubated at RT during 1.5 h with gentle shaking. Afterward, the solutions were discarded, and the wells were washed with 0.1% TBST, three times, five min each. The detection antibody (HRP-labeled 38C12 antibody-

diluted in blocking buffer) was added and the plate incubated for 1h at room temperature. The plate was washed five times with 0.1% TBST and then developed by adding 100 μl TMB and incubated at room temperature for about 15 min. The reaction was then stopped by the addition of 2 N sulfuric acid and then read at 450 nm using a multilabel plate reader (Victor³V, Perkin Elmer). ELISA results were expressed as normalized concentrations against albumin (Figure S1).

2.5. Characterization of GSS samples by limited proteolysis

Brain homogenates (BHs) were prepared from GSS-human brain samples at a concentration of 10% (w/v) in Ca^{2+} /Mg^{2+} -free 1X PBS, as described before. Three enzymatic digestions were developed using 50 μg of protein, as follows: 1) using 25 μg/ml proteinase K (PK) (Sigma), incubated at 37 °C for 1 h; 2) using 5 μg/ml pronase E (PE) (Sigma), incubated at 37 °C for 1 h; and 3) using 5 μg/ml thermolysin (Sigma), incubated at 70 °C for 1 h. All digestions were carried out in a total volume of 250 μl. For sequential digests, two sets of samples were run: one group was methanol-precipitated, another group was PTA- precipitated. After the first round of enzymatic digestions, the reaction was stopped with 5 mM PMSF (for PK digestion) or 5 mM EDTA pH 8 (for pronase and thermolysin digestions). The samples were centrifuged at 16000 xg for 1 h at 4°C. Pellets were resuspended in sample buffer containing 50 mM DTT. Molecular weight marker used Precision Plus Protein Standard (BioRad, 161-0374). The resultant enzymatic products were examined on a 12% SDS-PAGE and transferred to PVDF membranes as previously described. PrP immunodetection was performed using monoclonal antibody Sha31 (YEDRYYRE, epitope (amino acids 145 to 152)) at a 1:30000 dilution (in 1X TBST 0.5%) (kindly provided by Dr. David Westaway lab), incubated overnight at 4 °C. The secondary antibody used was horseradish peroxidase-conjugated goat-anti mouse diluted 1:10000 (BioRad). For the detection system, the Pierce ECL Western blotting substrate (Thermo Scientific #32106). Molecular weight marker used Precision Plus Protein Standard (BioRad, 161-0374).

2.6. Negative staining

Negative staining was carried out onto freshly glow-discharged carbon film-coated on 200-mesh copper grids. For each purified PrP^{Sc} sample, 5 µl aliquot was loaded onto the grids and allowed to adsorb for up to 1 min. The excess sample was removed by quickly touching the grid edge with filter paper. Right after the excess sample was removed, each grid was washed in two serial passages: In the first passage, by using three drops (50 µl each drop) of 100 mM ammonium acetate atop a Parafilm sheet, and quickly touching the grid sequentially with each drop. In the second passage, the same procedure was developed but this time using 10 mM ammonium acetate. Following the negative staining was done by sequentially immersing the grid in two drops (50 µl each drop) of 2% (w/v) aqueous solution of uranyl acetate (UrAc) for ~20 seconds. The UrAc was freshly filtered through a cellulose acetate filter (0.2 µm) to remove small precipitates. Immediately after the staining was done the grids were blotted with filter paper to remove the excess of solutions, and allowed to air dry. Images were acquired at 200 kV acceleration voltage, electron dose: 1.41 – 1.89 e/Å^2 s in a FEI Tecnai G^2 electron microscope, using the following settings: condenser aperture (No. 4): 150 µm, objective aperture (No. 4): 70 µm, and selected aperture (SA) (No. 2): 40 µm.

2.7. Mass-per-length analysis (MPL)

Preparation of unstained samples. Samples were allowed to adsorb to freshly glow-discharged carbon film-coated on 200-mesh copper grids. A 5 µl aliquot of PrP^{Sc} purified sample and a 1 µl aliquot of tobacco mosaic virus (TMV) rods' solution (0.085 mg/ml) were applied simultaneously to the grid. TMV rods were used as the standard for internal mass calibration. After a 5 min adsorption period, solutions were blotted, and the grids were rinsed with six drops of ultrapure water atop a Parafilm sheet (by quickly touching the grid sequentially with each drop), blotted, and dried in air.

Image acquisition. Bright-field images were acquired at different magnifications from 10X to 50X using an acceleration voltage of 200 kV. Dark field TB-TEM images were acquired at different magnifications using an acceleration voltage of 80kV, with an electron dose beam of 0.03-0.70 e$^-$/Å^2 s., and using the following settings: integration time: 32 s, binning: 1 (gain value), image size: 4096 x 4096. The FEI Tecnai G2 EM is equipped with an on-axis TEM bottom-mounted, 2.5 Mpix/seconds read-out-speed, Eagle CCD (charge-coupled device) camera.

Dark-field TB-TEM images were acquired at a beam tilt angle of 1.008°, a 70-μm diameter objective aperture, and a 150-μm condenser aperture. Smaller or higher tilt angles did not produce adequate blocking of the unscattered electron beam. Other microscope settings included spot size 5, binning 1, and filament current in the 10-20 μA range. Before recording TB-TEM images, the microscope was aligned to be used at 80 kV. Alignments such as gun tilt/shift, beam tilt pivot point X/Y, beam shift, and rotation center were adjusted accordingly. The condenser stigmators were also carefully calibrated to give a circular beam profile when the beam was viewed on the carbon film in TB-TEM mode (at lower magnification), and the beam was carefully centered and spread to produce uniform illumination over the field of view, as indicated by uniform background intensity from the carbon film in the final images. Initially, the sample grid was scanned manually to find promising areas, using the search mode of the Eagle camera software with a camera gain value of 8, at lower magnification and lower beam intensities. Once an area that contained both TMV rods and amyloid fibrils was identified, the magnification and beam intensity were increased, the focus was quickly adjusted to maximize the clarity of the TMV rods, and final TB-TEM images were recorded. Each image was the average of 6 to 8 acquisitions, each with a 16s exposure time and a camera gain value of 1. Images were stored as raw 16-bit tiff files. Electron doses were estimated from our calibration of the camera grayscale in images of an empty sample grid with no beam tilt against direct measurements of current from the TEM viewing screen.

Image processing and analysis. TB-TEM images were analyzed by using the image processing software ImageJ. To calculate the MPL and the full-width at half-maximum (FWHM) values, only images that were sharp and clean for both the amyloid fibrils and TMV rods, and free of contaminants in the background, were selected for MPL measurements. For MPL measurements

on TMV rods, rectangular areas were chosen for intensities measurements. For this, non-overlapping rectangular boxes were drawn inside the TMV rod (I_{TMV}) and on equal areas of background on either side of the TMV rod segment (I_{B1} and I_{B2}). The length of each box was 60 nm and its width 18 nm, that is the wide size of these rods. The total signal image intensities on the rectangular areas inside these boxes were then integrated. For each image, the quantity of the integrated intensities I_{TMV} was calculated as the averages of the quantities of I_{TMV} within the image subtracting the background on either side of the TMV rod, as follows:

$$\text{Averages of the quantities of } I_{TMV} = I_{TMV} - \left(\frac{I_{B1} + I_{B2}}{2} \right) \qquad 241$$

For MPL measurements on amyloid fibrils, similar to TMV rods, non-overlapping rectangular boxes were drawn inside the amyloid fibril (I_F) and over areas of background (I_{B3} and I_{B4}) on either side of the amyloid fibrils. Once the total signal image intensities were integrated into the rectangular areas, the MPL of each amyloid fibril segment was calculated as follows:

$$MPL = \frac{131 \, kDa \, / \, nm \quad x \left[I_F - \frac{(I_{B3} + I_{B4})}{2} \right]}{I_{TMV}}$$

The MPL values were plotted in a histogram, and the bin size was selected accordingly. Each peak was fitted to a Gaussian function to determine the MPL and the FWHM values. To improve the signal-to-noise ratio and uneven illumination on the EM micrographs, EM images were processed by applying the inverse Fourier transform filtering, using the following settings: 1) radial filter (which modifies the amplitudes and phases of Fourier components with values that depend on the radius in reciprocal space), 2) R distribution = 0.491/Angstrom (which plots the radial distribution function estimated from the Fourier transform of the image), and 3) high pass filter.

2.8. Transmission studies in transgenic mice

Animal studies were conducted following the Canadian Council on Animal Care Guidelines and Policies with approval from the Health Sciences Care and Use Committee of the University of Alberta. Transgenic mice expressing the human prion protein gene (TgHuPrP) were kindly provided by Dr. Debbie McKenzie, Center for Prions and Protein Folding Diseases, University of Alberta. Mice were crossed to generate homozygous human PrP^C (+/+), and genotyped by tail DNA analysis using the PCR protocol described in Chesebro *et al*.,1985 [53]. Bioassays were performed with Tg(HuPrP) mice expressing the human prion protein. Weanling pups were inoculated intracerebrally (IC) in the right temporal lobe, with 30 µl of a dilution 1/10 (v/v) prepared in 1X filtered PBS with 10% (w/v) BH or with PrP^{Sc} purified. Animals were monitored for onset of disease and euthanized when the appearance of clinical signs and scored positive for prion disease, i.e., at least three signs of neurologic dysfunction and progressive deterioration were observed [293]. Once the clinical symptoms were detected, the mice were euthanized, their brains were removed, rinsed in 1X PBS and immediately stored at -80 C for further analysis. A parallel cohort of TgHuPrP mice was used as a negative control (non-inoculation). This group, to serve as negative control tissue, was euthanized at the same time when the clinical signs developed in the treatment group. Individual incubation periods are expressed as the number of days-post-inoculation (dpi) and were calculated from the day when mice were inoculated until the time signs consistent with prion disease was established.

2.9. Human PrP^{Sc} inocula

All human prion-infected tissues were obtained from neuropathologically confirmed cases. Immunoblot for all cases confirmed the presence of the PrP 27-30 kDa fragment. Samples were obtained from Spain, Netherlands, and Germany. Samples from each case are described in the subsequent chapters.

CHAPTER 3

CHARACTERIZATION OF FAMILIAL CREUTZFELDT-JAKOB DISEASE (fCJD) WITH A MUTATION AT CODON E200K AND A POLYMORPHISMS AT CODON M129V OF PRION PROTEIN GENE

Claudia Y. Acevedo-Morantes[1,2], Xiongyao Wang[1], Brian Tancowny[1], Susana Teijeira[3], Beatriz San Millán[3], and Holger Wille [1,2]

[1]Centre for Prions and Protein Folding Diseases and [2]Department of Biochemistry, University of Alberta, Edmonton, AB, Canada, [3]Galicia Sur Health Research Institute, IIS Galicia Sur, SERGAS-UVIGO, Vigo, Spain, [4]Pathology Department, Complexo Hospitalario Universitario de Vigo (CHUVI), IIS Galicia Sur, SERGAS, Vigo, Spain

Summary

Inherited prion diseases include familial Creutzfeldt-Jakob disease (fCJD). Regardless of etiology, these diseases share the pathogenic mechanism whereby the cellular prion protein (PrPC) converts into its pathogenic isoform (PrP^{Sc}). In fCJD, this conversion is dependent on the congenital presence of mutations in the prion gene, *PRNP*. In this study, PrP species derived from brain tissue of a patient diagnosed with fCJD and with a mutation of glutamic acid (E) for Lysine (K) at codon 200 and heterozygosity of the methionine/valine (M/V) polymorphic codon 129 is analyzed by limited proteolysis and via mass-per-length (MPL) measurements. Immunoblot analysis of fCJD species showed the typical ladder-like pattern of PK-resistant fragments, PrP27-30, cleaved at residues ~82 and ~97, with the three characteristic patterns of glycosylation, and electrophoretic mobility profile between ~16-27 kDa. Further examination of this sample by transmission electron microscopy (TEM) showed the typical fibrillar like- structures of these particles and MPL measurements of ~60 kDa/nm, indicated a β-helix structural-like conformation suggesting the presence of more than one protofilament. Evaluation of the infectivity of these particles in Tg(HuPrP) mice, revealed that in fact, these particles kept their infectious nature, a hallmark of prion particles.

3.1. Introduction

The first familial case of CJD was reported in 1924 by W.R. Kirschbaum [112]. However, it was F. Meggendorfer who recognized in 1930, that the individual affected by fCJD was a member of a large kindred that became known as the "Backer" family [294]. Subsequently, studies proved that this family carried an inherited form of CJD [295], and demonstrated the unique properties of prion diseases as being both inherited and infectious.

Familial CJD (fCJD) is the most common inherited form of prion disease. It is transmitted in an autosomal dominant pattern, i.e., first-degree relatives of an affected individual have a 50% chance to have inherited the pathogenic variant and be at risk of developing the disease. At least 30 pathogenic variants that cause genetic prion disease have been identified. For some pathogenic variants, the genotype-phenotype correlation favors a particular variant, hence allowing the expression of the corresponding phenotype. Most variants have displayed an almost complete penetrance, with nearly 100% of individuals developing the symptoms. Nevertheless, a considerable variable expressivity of the disorder has been reported. For instance, despite that the same pathogenic variant affects members within the same family, it displays different onset age and symptomatology between individuals [296].

A large number of mutations and polymorphisms have been reported in the *PRNP* gene. These variations include 24 missense point mutations, 27 octapeptide repeat mutations (with insertions of 1-9 additional repeats), two octapeptide repeat mutations with deletion of two repeats and two nonsense mutations. Three missense polymorphisms located at codons 129(M/V), 171(N/S) and 219(E/K), and the deletion of one 24-bp octapeptide repeat is known, along with 12 silent polymorphisms [52]. The most frequent point mutation associated with fCJD is E200K. At least four founders of this mutation exist, with the two largest groups being of Sephardic Jewish origin (often Libyan-Tunisian background) and Slovakians [222]. According to the Canadian CJD Surveillance System (CJDSS), operated by the Public Health Agency of Canada (PHAC) [111], since 1998 up to February 2019, 974 deaths have been attributed to definite and probable CJD, from

which 66 cases (6.7%) corresponds to genetic prion disease (including fCJD, GSS, and FFI). The typical clinical presentation of fCJD is similar to sCJD, rapidly progressive dementia with myoclonus, and pyramidal, cerebellar or extrapyramidal signs. Other clinical features include ataxia, visual disturbances, and motor dysfunction. The onset of the disease is usually between the ages of 30 and 55 years [297].

3.2. Diagnosis of fCJD

Patients with fCJD due to E200K mutation displays a typically MRI showing symmetric prominent striatal T2-diffusion-weighted imaging (DWI) hyperintensities, often with less noticeable ribbon-like signal intensities of cerebral cortical gyri (cortical ribboning). EEG also varies, with periodic sharp-wave complexes appearing late. The CSF biomarkers, like protein 14-3-3, NSE, and t-tau are usually elevated in fCJD, but less common in sCJD [298].

3.3. Case: Presentation

Here a case of fCJD from BioBanco Complexo Hospitalario Universitario de Vigo (Vigo, Spain) was examined. The patient presented rapidly progressive cognitive dysfunction, accompanied by akinetic mutism and tetraparesis. No spontaneous myoclonus was reported. Classical EEG changes and typical abnormal MRI features were observed. The patient passed away within three months, between his admission to the hospital until the *exitus*.

3.4. Case

A 52-year-old woman diagnosed with fCJD and with the *PRNP* mutation E200K, which in June 2007 is admitted to the hospital due to right basal pneumonia, urinary infection, fecaloma, and cutaneous *Candidiasis*. In July 2007, the patient suffered a fever that does not respond to the

antibiotics treatment, oliguria, and dyspnea. The patient rapidly developed akinetic mutism (AK) and kept her eyes open. Oculocephalic reflex abolished and flaccid tetraparesis with hyporeflexia. EEG was compatible with DWI in the cortical region. A brain MRI showed cortical and subcortical atrophy in the brain parenchyma, affecting supra- and infratentorial brain. Periventricular white matter hyperintensities in the frontal lobes, as well as in both cerebellar peduncles. The presence of PrP^{Sc} was confirmed by Western blot analysis. Her clinical history, together with physical signs, molecular analysis, and typical MRI findings were consistent with the diagnosis of fCJD.

Comments: Mutation E200K / polymorphism MV129 reported in the sample. The sample was derived from cortical and cerebellar brain tissue.

3.5. Results

3.5.1. Analysis of PrP species in fractions obtained during PrP^{Sc} purification. To determine if the PrP 27-30 fragment (a well-characterized PK-resistant PrP fragment hallmark for most prion diseases) was present and to remove other proteins that can cause cross-contamination, brain samples derived from cortex and cerebellum from a patient who suffered fCJD were initially subjected to limited proteolysis. Small portions of brain tissue, 1.5g, were enzymatically digested using 50 µg/ml of PK and incubated during 1h at 37 °C. This digestion hydrolyzes the N-terminal 67-amino acid residues [291]. The final PrP^{Sc}-PTA purified product was passed through a sucrose gradient density cushion at three different concentrations of sucrose (40%, 60%, and 80%), and subjected to ultracentrifugation during 24h (Materials and Methods). Each fraction was collected separately. To monitor the degree of PrP^{Sc} enrichment during the purification, small aliquots were taken along the procedure and analyzed by Western blot probed with the monoclonal antibody D15.15 antibody (PrP epitope 175-186). In both samples (derived from cortex and cerebellum), the PK treatment yielded the characteristic PK-PrP^{Sc} truncated fragment (core), referred to as PrP 27-30.

However, in samples derived from cortex (Figure 20), three bands with a molecular weight ranging between 16-27 kDa fragments were detected. These bands were found between the fifth

and sixth fractions of the sucrose gradient (corresponding to 60% and 80% sucrose), as this fraction has a similar sucrose density as the prion protein (~1.2 g/cm^3) (Figures 20, E, F: F5-F6, sucrose gradient fractions) [299]. These fractions contain low-lipid-content. The three characteristic patterns correspond to the glycosylation states (di-, mono- and nonglycosylated), as has been previously reported. The equivalent ~16 kDa band is equivalent to the classic PrP 27-30 PK-resistant fragment seen in brain-derived samples, which migrates between 27-30 kDa. In samples derived from cerebellum (Figures 20, F), bands with similar molecular weight as described for cortex samples, were identified. However, in this case, strong signals of PrP PK-resistant fragment were obtained in the top fraction of the sucrose gradient, corresponding to ~40% sucrose concentration (with a 1.1764 g/cm^3 density) (Figures 20, F1 sucrose gradient fraction). This fraction contained abundant lipids (with a ~1.2 g/cm^3 density), with PrP^{Sc} particles attaching to them. These findings are in agreement with early studies that have shown that PrP^{Sc} is tightly associated with lipid membranes. In this case, PrP^{Sc} derived from cerebellum samples was highly associated with lipids in comparison to cortex. Previous studies have shown that PrP^{Sc} is tightly associated with lipid membranes, in contrast to PrP^C, suggesting that conversion from PrP^C to PrP^{Sc} might take place on the cell surface or endocytic pathway, and involves interactions between PrP and lipid membranes [300]. In both samples (derived from cortex and cerebellum), the bottom of the sucrose gradient (80%) was enriched predominantly with collagen fibrils as they have similar densities (~1.44 g/cm^3). Antibody D15.15 (which recognizes the epitope 175-186) detected, as expected, the 16-27 kDa PK-resistant fragments in both samples (derived from cortex and cerebellum), hence no significant differences were observed between the samples regarding their molecular weight, although there is a variation in their content in both samples.

Silver-stained SDS-PAGE of PrP^{Sc} preparations was also developed to evaluate the quality of the purifications. Although PrP^{Sc} was not detected in the final product, no contaminants were found either. Silver staining has a detection limit of 100 pg protein, whereas the detection limit for our Western blot is 10 pg protein. Hence, it is not surprising that PrP^{Sc} was detected by Western blot, but not in the silver-stained gels. The electrophoretic mobility for the PrP 27-30 band of fCJD (E200K; MV129) sample analyzed here, showed a typical pattern of type 1B, with a relative abundance of diglycosylated PrP 27-30 bands. While type 1B has the same electrophoretic mobility

as type 1A, they differ in the glycosylation pattern, with a predominantly content of diglycosylated bands (type 1B), determined by the presence of the polymorphic residue in position 129 of PrP.

3.5.2. Quantification of PrP^{Sc} concentration in the final purified product. To assess the concentration of PrP^{Sc} in the final PTA-precipitated pellet, a colorimetric ELISA was developed using the anti-prion monoclonal antibody D15.15 (epitope 175-186) (Figure 19). Samples that showed an intense band in Western blots were selected for quantification. Eight-standards with concentrations ranging from 0 to 2.5 μg/ml, were used to normalize the concentration of the samples. Each sample was run in triplicate. For PrP^{Sc} samples derived from fCJD, the concentration was 2.04 μg/ml and 2.06 μg/ml for cortex and cerebellum, respectively.

3.5.3. Examination of the structural integrity of the PrP^{Sc} fibrils by TEM. Negative stain revealed the presence of ordered filamentous structures, as well as highly aggregated oligomeric amorphous deposits in these samples (Figure 21). As lipids have a similar density as the upper fraction of the sucrose gradient (40%, ρ=1.17 g/ml) [301], this fraction was enriched with lipid droplets and PrP^{Sc} amorphous oligomeric aggregates bound to them. These aggregates were found in all sucrose fractions. While the following layer, down on the sucrose gradient, (60%, ρ=1.2 g/ml) was enriched with PrP^{Sc} fibrillar and amorphous aggregates (Figure 21), collagen fibrils were found in the bottom layer (80%, ρ=1.44 g/ml) of the gradient.

3.5.4. Characterization of PrP^{Sc} fibrils derived from fCJD –affected brain by MPL analysis. Figure 22, A, B shows bright-field TEM images of negatively stained PrP^{Sc} fibrils obtained from fCJD-human cortex and cerebellum, respectively, and mixed with TMV rods. PrP^{Sc} fibrils are predominantly aggregated, irregular in length and size, and binding to what it has been suggested to be ferritin, an iron storage protein that becomes, aggregated, and detergent-insoluble during some protein purifications [302]. These PrP^{Sc} fibrils were PK-digested, PTA-precipitated, and negatively stained with uranyl acetate. Hence, it is assumed that the final product obtained from the purification is the PrP^{Sc} PK- resistant fragment core. While PrP^{Sc} fibrils have an irregular and heterogeneous appearance, TMV has a well-defined and bigger rod-like shape (volume= 7.6x10^4

nm^3) [303]. Bright-field images of unstained PrP^{Sc} fibrils alone were also taken to distinguish PrP^{Sc} fibrils from TMV rods (Figure 22, C) or mixed with TMV rods (Figures 22, D, E).

MPL values were extracted from unstained PrP^{Sc} fibrils, taken under dark-field conditions using a TB-TEM at 80 kV acceleration voltage, as previously described by Chen and coworkers[241]. Rectangle boxes were drawn over the PrP^{Sc} fibrils, over the TMV rods and around their respective backgrounds, where the areas were selected for intensity measurement. All rectangle boxes were 60 nm in length (Figure 24). Rectangle widths were adjusted to include the fibrils or the TMV rod width in each image. All intensities used to calculate a given MPL value were taken from the same image, as intensities from different images were not necessarily directly comparable due to variations in incident beam intensity.

In summary the procedure was as follows: 1) image intensities were measured inside the selected rectangular areas centered on fibril segments (I_F) and over equal areas of background on either side of each fibril segment (I_{B1} and I_{B2}); 2) similarly, image intensities were measured inside the selected rectangular areas centered on TMV segments (I_{TMV}) and over equal areas of background on either side of each TMV segment (I_{B3} and I_{B4}); 3) For each image, the quantity I_{TMV} was calculated as the average of the quantities $I_{TMV}-(I_{B3}+I_{B4})/2$ within the image; 4) MPL values were calculated as MPL=131x[$I_F-(I_{B1} + I_{B2})/2$]/ (I_{TMV}), as it is well known that TMV has an MPL of 131 kDa/nm [304]. Figure 23 shows the histogram extracted from 32 TB-TEM images of PrP^{Sc} –fCJD fibrils derived from cortex and cerebellum. MPL peak positions were determined by fitting the histograms to one or more Gaussian functions. The histogram in Figure 24 shows a predominant peak between 60-70 kDa/nm, in agreement with a predicted value for a β-solenoid-like molecular structural model, where an MPL= ~30 kDa / 1.92 nm (1 subunit per 1.92 nm) is expected. This value corresponds to fibrils containing one protofilament only. Although the present X-ray diffraction data strongly support the β-solenoid model for PrP^{Sc} fibrils, there is still not enough evidence whether it can be applied to the infectious conformer [289,290].

3.5.5 Assessment of prion infectivity in Tg(HuPrP) mice. Previous studies have shown that infectivity of brain samples derived from patients affected by prion diseases is determined by the animal model that is used. Inoculation of WT mice, which express mouse PrP, with prion species related to humans, which are composed of human PrP^{Sc}, leads to inefficient disease transmission due to so-called species or transmission barrier effects. However, utilizing Tg mice that express human PrP can mitigate these effects. Hence, Tg mice that express human PrP are susceptible to develop human prion disease. Another factor that influences the outcomes from transmissions studies is the presence of methionine or valine at residue 129, in both the inoculum and the mice.

In order to evaluate the level of PrP^{Sc} infectivity present in the final purified fCJD sample (expressing the mutation E200K and polymorphism M129V), transgenic mice homozygous for human PrP (*Prnp* +/+) (Tg(HuPrP) mice) were inoculated with 30 µl, 20% (v/v) (dilution 1/10) BH or PrP purified. The Tg(HuPrP) mice succumbed to the disease, showing symptoms, i.e., hunched, ataxic, scruffy coat and weight loss at 234+36 and 229+74 dpi for mice inoculated with BH or purified PrP, respectively (Table 6). A cohort group of Tg(HuPrP) mice was maintained as negative controls for infectivity (non-inoculated). These results demonstrated that PrP^{Sc}-derived from fCJD samples kept their infectious capacity. Immunoblot analysis of these PrP^{Sc} PK-resistant species present in Tg(HuPrP) mice brain, revealed the presence of the characteristic ladder-like pattern of the three di-, mono-, and nonglycosylated isoforms (Figure 25). A further examination of these PrP species by negative stain and bright-field TEM imaging showed well-defined fibrillar structures, similar to previously reported amyloid fibrils (Figure 26) [305].

3.6. Discussion

3.6.1. Characterization of fCJD PrP^{Sc} PK-resistant fragment by limited proteolysis. The human brain, both non-CJD and CJD -infected, encompasses PrP truncated fragments, in addition to the full-length protein. In a non-infected CJD brain, two well established truncated species exist the 18-kDa C-terminal fragment known as C1 (which is generated by the cleavage of full-length PrP^C between residues 111 and 112) and a minor ~20-kDa C-terminal fragment (CTF).

INOCULUM	BH DOSE (%)	No. OF MICE POSITIVE /TOTAL No. OF MICE TESTED	INCUBATION PERIOD $\pm$ SD (dpi)
sCJD	2	3 / 5	453 ± 50
fCJD	2	6 / 11	234 ± 36
GSS	2	13 / 35	313 ± 91
INOCULUM	BH DOSE (%)	No. OF MICE POSITIVE /TOTAL No. OF MICE TESTED	INCUBATION PERIOD $\pm$ SD (dpi)
sCJD	2	2 / 8	414 ± 22
fCJD	2	9 / 9	229 ± 74
GSS	2	6 / 29	282 ± 87

Table 6. Tg(HuPrP) mice inoculated with PrP species derived from brain tissue from patients affected by prion diseases. BH: Brain homogenates; SD: standard deviation; dpi: days-post-inoculation.

A brain infected with CJD accumulates, besides the C1 and CTF fragments, variable amounts of PK-resistant and detergent-insoluble fragments of PrP^{Sc} (PrP 27-30, also known as C2), which are generated by the preferential cleavage of the protein at either residue 82 or 97 [305]. These PK-cleavage sites serve to distinguish between the two types of PrP^{Sc} on a Western blot, as they have different electrophoretic mobility: type 1 and type 2 PrP^{Sc}, characterized by the size of their PK-resistant core (21 and 19 kDa, respectively), correlating with differences in the PK-cleavage site (at residues 82 and 97, respectively). It has been proposed that different PK cleavage sites affect in the aggregation pattern of PrP^{Sc}, suggesting that type 2 PrP^{Sc} has a larger aggregation size than type 1 [306]. Furthermore, type 1 have shown to run with a slow migration pattern in Western blot, with three bands at 28, 26, and 19 kDa; while type 2 had bands at 27, 25, and 17 kDa, corresponding to the di-, mono-, and un-glycosylated forms, respectively, with type 1 coexisting in all type 2 sCJD cases [307].

In this study, small samples of brain tissue derived from a patient diagnosed with fCJD, and who presented the mutation E200K and polymorphism M129V in the *PRNP* gene were examined.

Three different approaches were used: 1) limited proteolysis profile (expected to generate the characteristic PK-resistant fragment PrP 27-30 of approximately 142 amino acids), 2) equilibrium sedimentation in a sucrose gradient, and 3) MPL measurement of PrP^{Sc} fibrils. The density of protein aggregates is a consequence of features such as their size, degree of packing, and hydration. These features are influenced by the proportion of β-sheet content in their structure. Immunoblot analysis revealed PrP^{Sc} species with different electrophoretic mobility profile based on their glycosylation pattern (di-, mono- and nonglycosylated isoforms). A prominent representation of diglycosylated PrP^{Sc} species and underrepresentation of nonglycosylated PrP^{Sc} species were detected, with the nonglycosylated band migrating at 21 kDa. This migrating pattern corresponds to PrP^{Sc} type 1. No insertions or deletions were reported in the 51-91 region. The glycotype analyses of PrP^{Sc} as well as the genotype variations in the *PRNP* gene, i.e., mutations/polymorphisms, have been considered when classifying CJD. In particular, for fCJD, previous studies have shown that the mutation E200K influences in the glycosylation pattern, while the polymorphic residue 129, the site of a methionine/valine polymorphism, has a leading role in determining the PK degradation site of PrP^{Sc} [113].

Our case had several differences from previously reported fCJD studies. Our patient initially presented multiple infections, followed by akinetic mutism. The patient did not develop myoclonus or reported periodic-sharp wave complexes (PSWCs) on EEG, which are in agreement with previously reported E200K-129M cases (myoclonus in 73% and PSWCs in 75%). DWI was compatible with EEG in this patient, showing high signal intensities in the cortical region, and typical regional distribution, characteristic of the clinical progression in fCJD with the mutation at codon 200 in the *PRNP* gene [308,309]. In our patient who was M129V heterozygotic, the effect of this polymorphism at the codon 129 was not investigated. Although these results do not account for the clinical-stage, nor brain tropism/toxicity, this data may suggest that there are no significant differences between PrP^{Sc} fibrils affecting cortex and cerebellum in this patient affected by fCD.

3.6.2. MPL analysis of fCJD PrP^{Sc} fibrils by TB-TEM. MPL histograms for PrP^{Sc} fibrils derived from cortex and cerebellum showed a broad peak centered between 60-70 kDa/nm for both samples, with an FWHM = ~25kDa/nm and ~30 kDa/nm, respectively (Figures 24, A, B). These

MPL values were determined from TB-TEM images over an MPL range from 10 kDa/nm to 60 kDa/nm. The slight differences in FWHM values might be due to background intensity fluctuations, which in turn generate MPL variations. Several factors can contribute to these fluctuations, i.e., the presence of extraneous material on the sample grids, structural nonuniformity of the fibrils, which encompass unresolved breaks in the fibrils, and non-fibrillar material to the fibrils. However, the most significant limitation on the precision of MPL determination is sample quality (at least for MPL values above 10 kDa/nm). These issues can also affect STEM measurements [241]. Chen and coworkers demonstrated that damage to the fibrils and TMV by the electron beam play no significant effect in the TB-TEM measurements [241]. A total electron dose of 100 e/Å^2 (10^4 e/nm^2) at 80 kV produces a mass loss of roughly 30% for typical protein assemblies (including TMV) in STEM and EF-TEM studies. Chen and coworkers estimate the electron dose for a single TMV TB-TEM image, acquired in a time frame of 10 s to 200 s, to be 60-250 e/Å^2 (0.6 – 2.5 x10^4 e/nm^2). Comparison of TMV images recorded at different beam exposure times showed no systematic changes in MPL values, i.e., no evidence for rapid loss [241]. In this study, the TB-TEM images were recorded with an electron dose of 0.70 e/Å^2 s at 80 kV acceleration voltage, and a beam exposure time of 32 s (integration time). Comparison of TB-TEM electron beam exposure at 2.5 s was developed, that showed no evidence for rapid mass loss as it was previously reported [241].

3.7. Figures
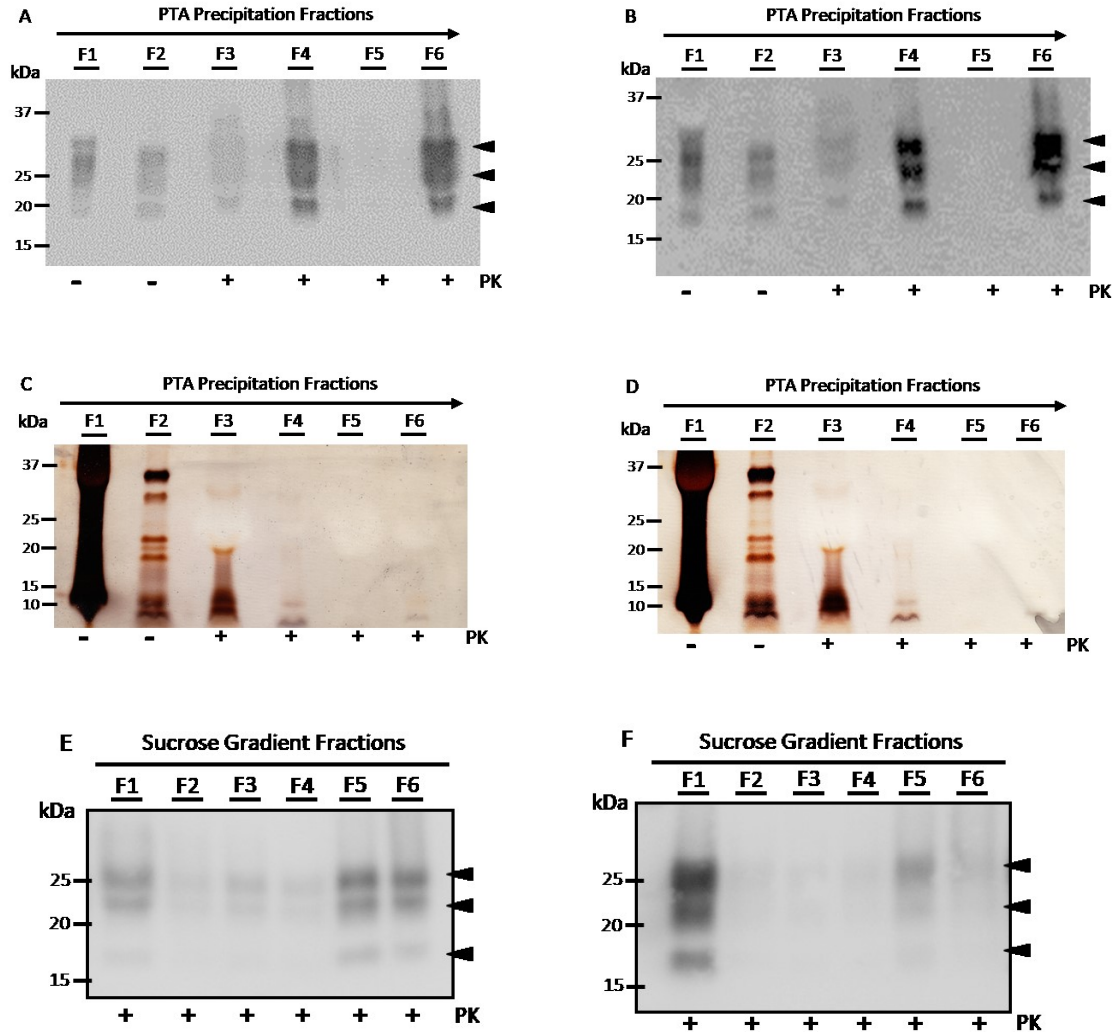
Figure 18. Western blot analysis of PrP^Sc PK-resistant from cerebral cortex (left panels A, C, E)-and cerebellum (right panels B, D, F) derived from a patient affected by fCJD. The final pellets from PTA-purification (A, B: F6) were passed through a cushion of sucrose gradient (40%, 60%, and 80%) and a density gradient ultracentrifugation was performed (E, F). Sampling was done along the purification and evaluated by Western blot. The three characteristic PrP^Sc bands corresponding to di-, mono-, and un- glycosylated isoforms, were detected in the final purified product (pointed by the black arrows). The equivalent 5 μl of samples was loaded per lane. (C D) SDS-PAGE stained by silver nitrate. F1: 20% BH, F2: 10% BH after first step of clarification; F3: after PK-digestion treatment; F4: first supernatant collected; F5: second supernatant collected; F6: final PrP^Sc pellet purified. +/- Symbols indicate whether the PK-digestion was carried out (+) or not (-) during the purification.
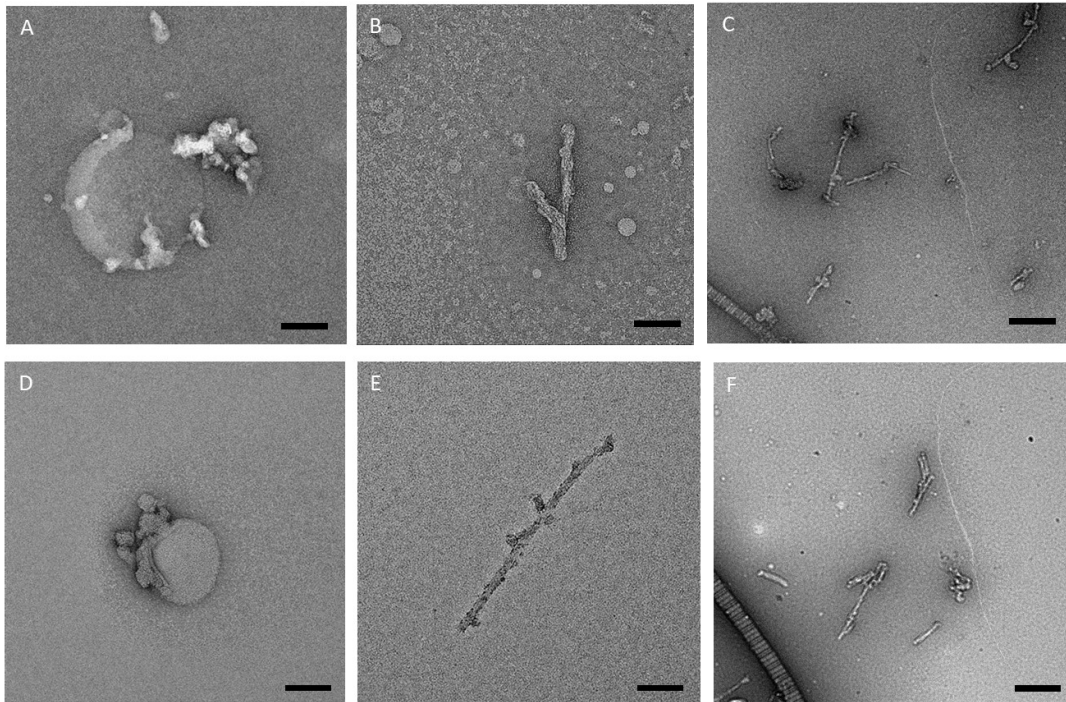
Figure 19. TEM images of negatively stained PrP^{Sc}-fCJD amyloid fibrils derived from human brain cortex (A-C) and cerebellum (D-F). Negative stain method was used to evaluate PrP^{Sc} morphology and structural integrity after its purification. Amorphous oligomeric aggregates bound to lipids were found in the 40% sucrose gradient fraction, as expected based on their similar buoyant density gradient (~1.006 mg/ml) (A, D). Fibrillar structures were found between the interface 60%-80% sucrose gradient, as it was expected since PrP^{Sc} has a similar buoyant density as this sucrose fraction (~1.21. g/ml) (B-C, E-F). No significant differences were found between cortex and cerebellum samples. Scale bars: A, B, D, E: 100 nm; C, F: 500 nm
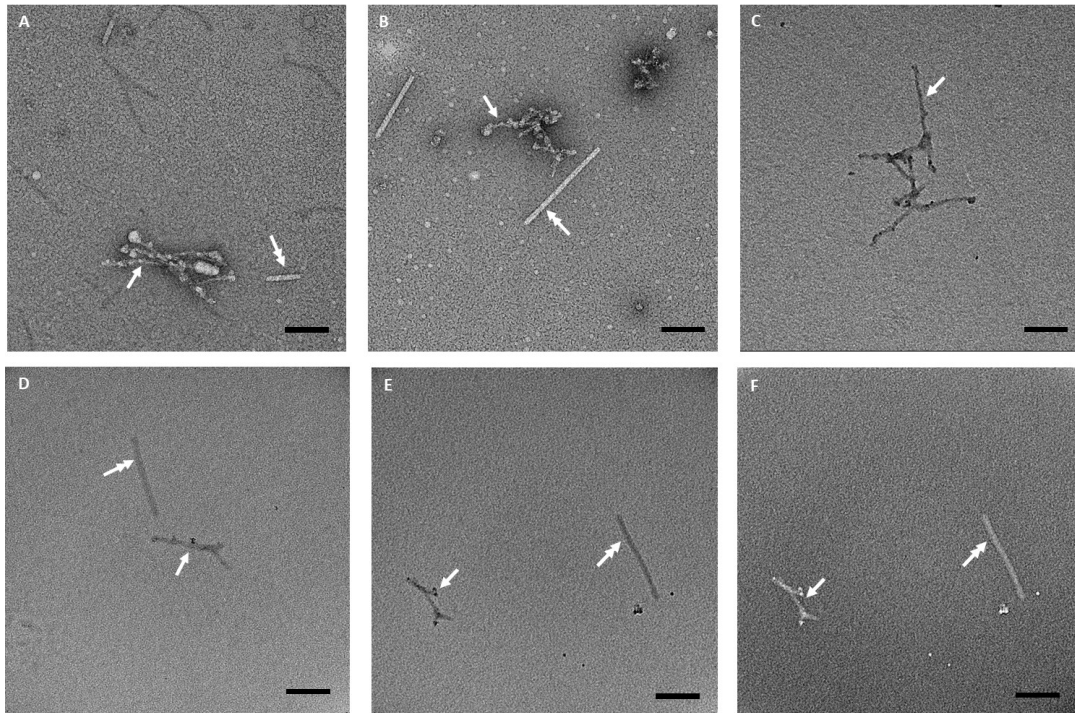
Figure 20. TEM images of PrP^Sc-fCJD fibrils derived from human brain cortex (A) and cerebellum (B) and mixed with TMV rods. Bright-field images of negatively PrP^Sc fibrils (derived from cortex and cerebellum) and TMV rods are shown (A, B). Bright-field images were taken of unstained PrP^Sc fibrils alone (C) or in a mixture with TMV rods (D, E). A sample of a dark-field image derived from cortex is shown in the bottom right corner (F). Single-headed arrows indicate the presence of PrP^Sc fibrils. Double-headed arrows indicate TMV rods (Scale bars: A, B, C: 200 nm; D, G, H: 500 nm).
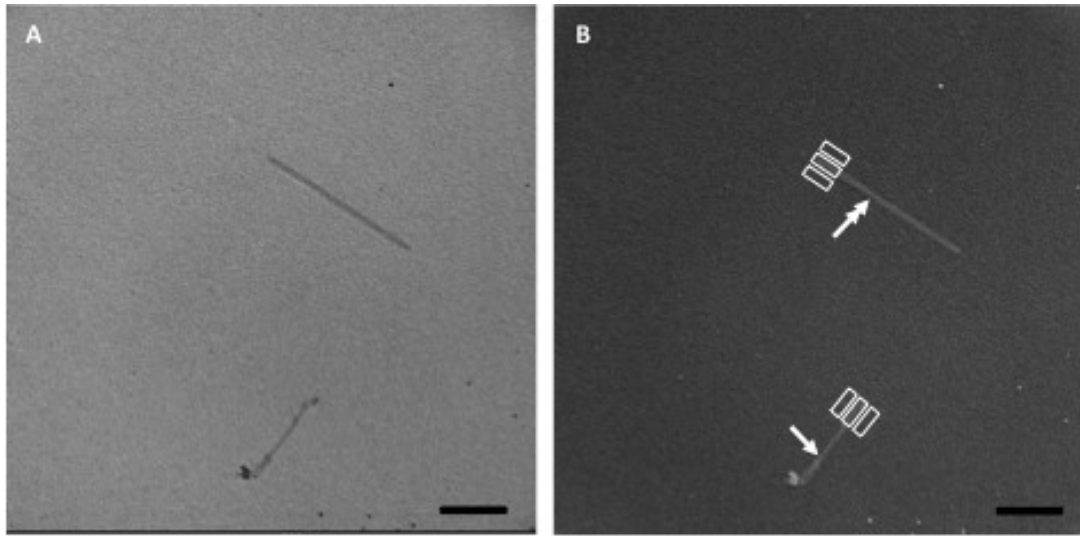
Figure 21. TB-TEM images of unstained PrP^{Sc}-fCJD fibrils derived from cerebellum and mixed with TMV rods. Unstained fibrils were analyzed on bright field (A) and dark-field (B) the later was used to assess the MPL of PrP^{Sc} fibrils (single-headed arrow) and TMV rods (double-headed arrow). The right panel shows examples of segments enclosed in rectangles, where the fibril (I_F) and background (I_B) intensities were taken. MPL values for PrP^{Sc} fibrils were calibrated with TMV (used as internal standard for mass calibration), assuming the average TMV MPL value to be 131 kDa/nm. (Scale bars, 500 nm).
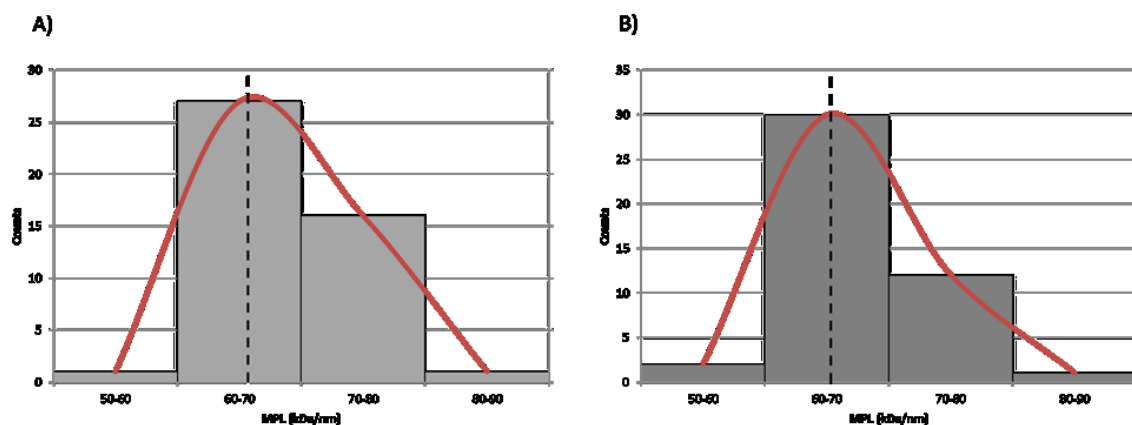
Figure 22. MPL histogram extracted from TB-TEM images of PrP^{Sc} unstained fibrils derived from cortex (A) and cerebellum (B) from a patient who suffered fCJD. The solid curve is fit to one Gaussian function. The vertical dashed line indicates the ideal MPL value predicted by experimentally based structural models. The preliminary MPL measurements from these samples give a ~60 kDa/nm value, with ~25 and ~30 kDa/nm FWHM for cortex and cerebellum, respectively. These values suggest a four-rung β-solenoid conformation for these fibrils.
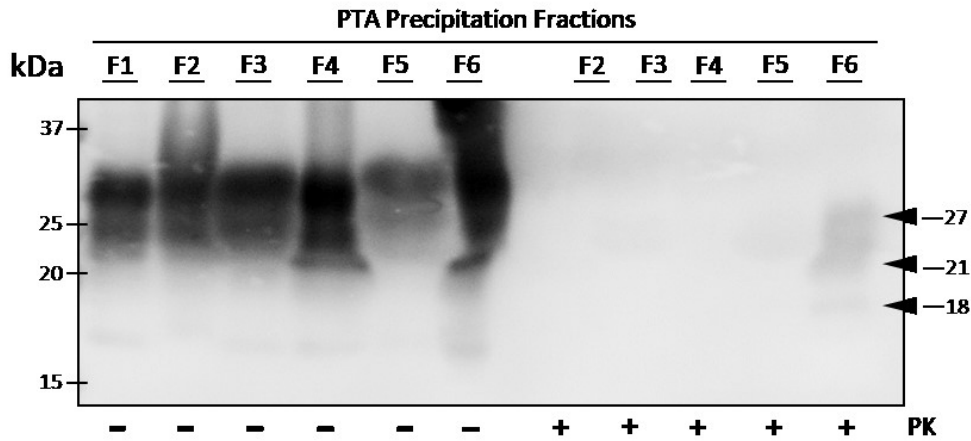
Figure 23. Immunoblot analysis of PrP species extracted from Tg(HuPrP) mice brain. Brains from Tg(HuPrP) mice that were intracerebrally inoculated with purified PrP[Sc] derived from brain cortex of a patient affected by fCJD. Mice brains were subjected to limited proteolysis, followed by PTA-precipitation and analyzed at each step during the purification. The three characteristic PrP[Sc] glycoform patterns (di-, mono-, and un-glycosylated) are revealed in the final purified product (F6) (pointed by the black arrows), with molecular weights between ~17-27 kDa. The equivalent 5 µl 10% (w/v) BH and 5 µl samples were loaded per lane. F1: 20% BH, F2: 10% BH after first step of clarification; F3: after PK-digestion treatment; F4: first supernatant collected (no first pellet sample was collected here); F5: second supernatant collected; and F6: final purified pellet. An alternative non-enzymatic digest control was carried out in parallel, where the samples were PTA-precipitated in a buffer containing protease inhibitors and maintained under non-PK enzymatic treatment (left fractions F1-F6). +/- Symbols indicate when the PK-digestion was applied during the purification.
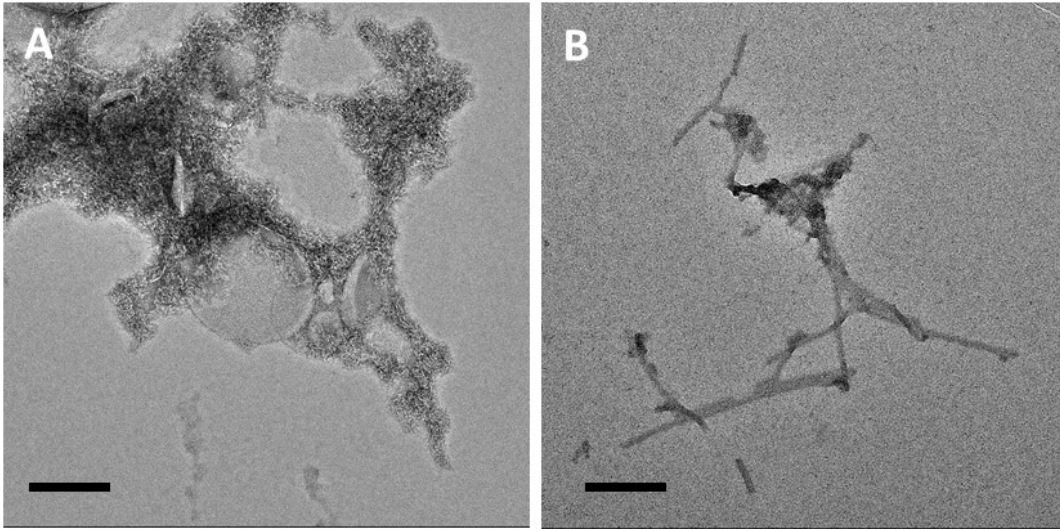
Figure 24. Bright-field TEM images of PrP^{Sc} PK-resistant species obtained from Tg(HuPrP) mice brain inoculated with PrP^{Sc} fCJD species derived from human cerebral cortex (A) and cerebellum (B).

CHAPTER 4

CHARACTERIZATION OF SPORADIC CREUTZFELDT-JAKOB DISEASE (sCJD) PRION SPECIES BY LIMITED PROTEOLYSIS AND VIA MPL MEASUREMENTS

Claudia Y. Acevedo-Morantes[1,2], Xiongyao Wang[1], Brian Tancowny[1], Susana Teijeira[3], Beatriz San Millán[3], and Holger Wille [1,2]

[1]Centre for Prions and Protein Folding Diseases and [2]Department of Biochemistry, University of Alberta, Edmonton, AB, Canada, [3]Galicia Sur Health Research Institute, IIS Galicia Sur, SERGAS-UVIGO, Vigo, Spain, [4]Pathology Department, Complexo Hospitalario Universitario de Vigo (CHUVI), IIS Galicia Sur, SERGAS, Vigo, Spain

Summary

Prion diseases are a group of progressive neurodegenerative disorders that affects a diverse group of animals, including humans. Sporadic Creutzfeldt-Jakob disease (sCJD) is the most common form of prion disease in humans and is clinically characterized by progressive dementia associated with a broad spectrum of neurological signs. In human sporadic Creutzfeldt-Jakob disease (sCJD), prion species separate as two main glycotypes: Type 1 and Type 2, with apparent electrophoretic mobility of the nonglycosylated isoform at 21 and 19 kDa, respectively. However, both types show similar glycosylation profile. In this study, PrP species obtained from brain tissue of four patients diagnosed with sCJD revealed similar electrophoretic mobility profile for all samples, but with different molecular weight. These findings provide evidence of the highly versatile nature of these particles. Further examination by TEM imaging revealed the characteristic fibrillar structures, as well as abundant amorphous oligomeric aggregates deposits. Fibrils that displayed a considerable amount of PrP[Sc] fibrils and presented a well-defined fibrillar structure were chosen for MPL measurements. MPL values of ~60 kDa/nm suggested that these fibrils are organized in a β-helix structural conformation. Evaluation of the infectivity of these particles in Tg(HuPrP) mice, also revealed that in fact these particles maintained their infectious characteristics, a hallmark of prion particles. However, as it was aforementioned, a higher resolution analysis would bring detailed information regarding the elusive nature of these particles.

4.1. Introduction

Sporadic CJD (sCJD) is a rapidly progressive, degenerative, multifocal dementia, usually presented with myoclonus (sudden, involuntary muscle twitching). Although distinctive clinical and pathological features in sCJD patients have been described, the most common clinical features include fatigue, insomnia, depression, weight loss, headaches, general malaise, and ill-defined pain sensations. Also, neurological features including extrapyramidal signs (such as tremor, slurred speech, anxiety, paranoia, and distress), cerebellar ataxia, pyramidal signs, cortical blindness, and psychiatric features are frequent; about 12% of sCJD patients are reported to epidemiological surveillance studies by psychiatrists [203]. The disease has a mean survival of about six months (median about five months), with 85% to 90% of patients dying within one year. The peak of onset is 55 to 75 years of age, with a median age of onset of about 67 years and mean of 64 years [298].

According to the Canadian CJD Surveillance System (CJDSS), operated by the Public Health Agency of Canada (PHAC) [111], since 1998 up to February 2019, 974 deaths have been attributed to definite and probable CJD, from which 899 cases correspond to sCJD (92.3%), and 2 cases to vCJD (0.25%). Hence, sCJD is the most common form of all human prion diseases [310].

4.2. Classification of sCJD

It has been hypothesized that possible causes of sCJD include spontaneous production of PrP^{Sc} via rare random events, somatic mutation of *PRNP* or unidentified environmental prion exposure. sCJD can be classified by 1) the neuropathological profile; 2) biochemical features of PrP^{Sc}, including their electrophoretic mobility based on their molecular mass after PK digestion (with PrP^{Sc} having a PK-resistant fragment of 21 kDa or 19 kDa, corresponding to type 1 and type 2, respectively); 3) the PrP glycosylation pattern ratios (di-, mono- and nonglycosylated isoforms); and 4) the amino acid residue in the *PRNP* gene at codon 129. Thus, sCJD can occur with six

genotype/PrP^{Sc} type permutations: MM1, MM2, MV1, MV2, VV1, and VV2. These types have been categorized in turn, in six well-recognized sCJD phenotypic subtypes: MM1/MV1, MM2 cortical, MM2 thalamic, MV2, VV1, and VV2. Molecular classification of sCJD has important implications for epidemiological studies when determining the etiology of sCJD since it is possible that apparent environmental variables and individual human prion strains are overlooked when epidemiological studies assess sCJD as a whole.

4.3. Diagnosis of sCJD

The histopathological examination has been a definite diagnosis of prion diseases. Specifically, to sCJD, prominent hallmarks for this disease include nerve cell loss, gliosis, vacuolation (formerly called spongiform change), and PrP^{Sc} deposition. Immunohistochemistry can be performed on formalin-fixed or frozen tissue sections to allows the detection of PrP^{Sc} protein *in situ*, and determine its distribution in the brain and lymphoid tissues [203]. Molecular analysis, i.e., Western blot, has also become a commonly used technique for the detection of PrP^{Sc} in samples. Clinical diagnosis of sCJD relies upon a variety of symptoms and ancillary test, including 1) cerebrospinal fluid (CSF) an increase in CSF protein concentration by approximately 10% is typical and attributed in part to the release of the normal neuronal 14-3-3 protein into the CSF following neuronal death; although this finding is not specific for prion disease; 2) EEG with periodic sharp wave complexes (PSWCs), consisting of triphasic or sharp wave bursts every 0.5 to 2.0 seconds, and perhaps most important 3) Brain imaging including magnetic resonance imaging (MRI), diffusion-weighted MRI (DWI), and positron emission tomography (PET). These analyses show atrophy or metabolic activities in the brain, depending on what technique is used. The classic clinical phenotype of sCJD is a rapidly progressive dementia with behavioral abnormalities, ataxia (usually gait), extrapyramidal features, and eventually myoclonus. Early symptoms include fatigue, headache, vertigo/dizziness, altered sleep and eating patterns, unexplained weight loss, and visual disturbances, to name a few. Because sCJD affects many areas of the brain, its presentations are protean, and it can mimic, at early stages, many other neurologic or psychiatric disorders, making its diagnosis difficult. Although these techniques are used for differential diagnosis, they help to

validate the determination of possible prion disease and evaluate for other conditions of the central nervous system [5].

4.4. Cases: Presentation

In this study, four patient cases with neuropathologically confirmed sCJD from BioBanco Complexo Hospitalario Universitario de Vigo (Vigo, Spain) are analyzed by limited proteolysis, sucrose gradient density and MPL measurements by TB-TEM (for those samples with a suitable concentration). All cases presented with rapidly progressive cognitive dysfunction, accompanied by spontaneous myoclonus. Classical EEG changes and typical abnormal MRI features were observed. All patients underwent brain biopsy. In some cases, comprehensive clinical data was not provided.

4.4.1. Case 1. A 70-year-old Spanish man presented with cephalic tremor noted by his family (Sept. 2003). In his clinical history, a cholecystectomy was identified (1978). In March 2006, he was admitted in the Neurology service, due to a lacunar infarct-right ganglia, and depressive syndrome. As he was discharged from the hospital and returned to his home, his condition continues to worsen, including difficulty in walking, cognitive impairment, rigidity, incontinence, and speaking alterations. Hence, he was admitted again to neurological services. Neuropathological diagnosis was confirmed for CJD based on histology examination. Western blot analysis showed the PrP^{Sc} resistant bands corresponding to sCJD. Brain MRI showed an apparent diffusion coefficient (ADC) map and left caudate nucleus and putamen hyperintensity, consistent with prion disease. His EEG showed periodic wave complexes. High signal intensity in the left of the caudate nucleus and the putamen were shown in fluid-attenuated inversion recovery (FLAIR) and diffusion-weighted (DW) imaging. His condition deteriorated rapidly, succumbing to the illness three years after its onset (July 2006). The patient was diagnosed as having possible sCJD [311].

Comments: No mutation / polymorphism were reported with the sample. The sample was derived from cortical brain tissue.

4.4.2. Case 2. A 59-year-old Spanish woman hospitalized in July due to cognitive impairment. Her family reported that in two months, the patient displayed difficulty in speaking, memory loss, asked incoherent questions, and had trouble recognizing people. She also developed rapid progressive difficulty in walking and maintaining balance. No cephalalgia (headache) or fever was reported. A neurological examination indicated dysarthria; the patient cannot remember dates, phone numbers.

Nevertheless, she can shower herself and get dressed. Ataxic episodes and difficulty to turn around were also described. She had myotatic reflexes. Her symptoms rapidly deteriorated with many spontaneous limb myoclonic jerks, as well as in her jaw, when opening her mouth. Brain MRI showed discrete cortical atrophy. EEG revealed slow waves with other theta rhythms. A full blood examination and cerebrospinal fluid (CSF) evaluation were performed. Genetic diagnosis negative for Huntington. After her admission to the hospital, the patient showed rapidly progressive neurological deterioration, with anarthria, myoclonic seizure increase, dysphagia, inability to walk, and ideomotor apraxia. During the last two days, the patient showed a progressive deterioration of consciousness and breathing capacity. She passed away on July 15, 2007. The post-Morten histopathological examination found neuronal loss, spongiosis in brain and PrP deposition in basal ganglia. Her clinical history, together with physical signs, typical EEG, and brain MRI findings were consistent with a diagnosis of probable CJD [311].

Comments: No mutation / polymorphism were reported with the sample. The sample was derived from cortical and cerebellar brain tissue.

4.4.3. Case 3. An 80-year-old Spanish woman admitted to the hospital due to a decreased level of consciousness and cognitive impairment. She had a history of alcoholism and primary biliary cirrhosis, invasive ductal carcinoma (she went under surgery for mastectomy and draining lymph node, in August 1999), and amputation of colorectal adenocarcinoma. She also suffered from chronic thrombocytopenia and iron deficiency anemia. She went under endoscopic polypectomy. She was hospitalized due to bleeding after a colostomy. In December 2006, after a year of progressive cognitive impairment, the patient was diagnosed with Alzheimer's disease. In June

2007, the patient started treatment with Prometax® (rivastigmine). However, five days after the treatment began, the patient developed social withdrawal, visual impairment, cry at nights, and auditory and visual hallucinations. Her family mentioned that these symptoms started a few days before the Prometax® treatment. On July 6, she became mute, with a gaze palsy and following the conversation occasionally. Two weeks later, she suffered a urinary infection, that was treated with Baycip[500]. On July 23, myoclonic limb jerks, generalized hypertonic, social withdraw, and verborrhea were observed. EEG revealed status epilepticus. Her clinical condition gradually deteriorated, and the patient entered a comatose state with no response to painful stimulation. A brain MRI study showed cortical and subcortical atrophy and chronic ischemic vascular disorders.

Comments: No mutation / polymorphism were reported with the sample. Sample was derived from cortical and cerebellar brain tissue.

4.4.4. Case 4. A 62-year-old woman diagnosed with rapidly progressive dementia. On July 2007, the patient was admitted to the hospital due to difficulty eating, vomiting, and diarrhea. Her condition became progressively worse, and eventually she became akinetic-rigid and mute. The patient did not follow simple commands, presented with dysarthria, with a, gaze limited to vertical movement and spontaneous movement of limbs. She exhibited diffuse osteo-tendon reflex (OTR). Positive protein 14-3-3 led to suspicion of CJD. Dyslipidemia (abnormal levels of lipids (e.g., triglycerides, cholesterol and/or fat phospholipids) were also reported. EEG revealed intermittent periodic generalized sharp wave complexes. Her symptoms rapidly deteriorated, presenting dyspnea and bronchospasm. Her clinical history, progression, and physical findings suggested a diagnosis of possible CJD, classic form.

Comments: No mutation was reported. Polymorphism M129V was reported in the sample. Sample was derived from cortical and cerebellar brain tissue.

4.5. Results

4.5.1. Molecular analysis of PrP^{Sc} species by limited proteolysis. Limited proteolysis was applied to brain samples derived from cortex and cerebellum from four different patients diagnosed with sCJD, to detect the presence of the PrP 27-30 PK-resistant fragment and other proteins that can cause cross-contamination. Small portions of brain tissue, 1.5 g, were enzymatically digested using 50 µg/ml of PK and incubated for 1h at 37 °C. This digestion hydrolyses the N-terminal 67-amino acid residues. The final PrP^{Sc}-PTA purified product was passed through a sucrose gradient density cushion at three different concentrations of sucrose (40%, 60%, and 80%), and subjected to ultracentrifugation for 24h. Each fraction was removed separately. Small aliquots were taken along the procedure, to monitor the degree of PrP^{Sc} enrichment during the purification and analyzed by Western blot probed with the monoclonal antibody D15.15 (PrP epitope 175-186). The electrophoretic mobility pattern was similar for all patient cases, although the concentration of purified protein from each case differed. Here, each case is examined as follows:

4.5.1.1. Case 1. Patient's EEG showed periodic wave complexes. High signal intensity in the left of the caudate nucleus and the putamen were shown in fluid-attenuated inversion recovery (FLAIR) and diffusion-weighted (DW) imaging, in agreement with previously reported studies for sCJD diagnostic [312]. PrP^{Sc} PK-resistant fragments were detected at high concentration in cortex-derived samples in the final PTA-purification fractions (Figure 27, A: F7). The characteristic three ladder-like electrophoretic profile was revealed, with molecular weights ranging from ~19-31 kDa, and slight predominance of the monoglycosylated pattern. Similar results were found in the fractions that were maintained under non-PK-digestion conditions (i.e., non-digested with PK), with an extra band at ~16 kDa in the final purified products (Figure 27, C: F7), which suggest that these PrP species correspond to type 1A (possibly MM1/MV1). Since the concentration of PrP^{Sc} final product was present at high concentration (determined by immunoblot intensity), the sample was selected for further examination by TEM.

4.5.1.2. Case 2. PK-resistant PrP fragments were detected at low concentration in cortex-derived samples, as seen in both fractions digested with PK (Figure 28, A) or non-digested (Figure 28, C). Since intensity of the signals in the immunoblots for the final purified PrP^{Sc} products were similarly weak in both PK-digested or non-PK-digested fractions, it can be inferred that PrP^{Sc} concentration might be below the detectable levels of the Western blot or it was present at higher concentration in adjacent tissues (that were not examined here), considering that only 1.5 g (~0.11%) of human brain tissue was analyzed and that a human brain weighs on average about 1.2-1.4 kg [313]. On the other hand, PrP^{Sc} content in the sample derived from cerebellum showed a different pattern. PK-resistant fragments were not detected in the fractions that were PK-digested (Figure28, B). However, the three characteristics bands were seen in the fractions that were maintained under non-PK-digestion conditions (non-digested with PK) (Figure 28, D: F5), suggesting this PrP^{Sc} sample might be sensitive to PK-digestion. For the non-digested samples, three bands can be seen with slightly higher molecular weights (~23-35 kDa) in comparison with sCJD samples that were subjected to limited proteolysis. A weak predominance of the diglycosylated pattern can be seen in the final product (Figure 28, D: F5). A pale band at ~16 kDa is also seen in the early fractions of the purification (Figure 28, D: F1-F2).

4.5.1.3. Case 3. PK-resistant PrP fragments were detected at low concentration in cortex-derived samples, as seen in both fractions digested with PK (Figure 29, A: F7) or non-PK-digested (Figure 29, C: F7). Band intensities for the final PrP^{Sc} purified products were similarly weak in both PK-digested or non-PK-digested fractions suggesting that PrP^{Sc} concentration might be below the detectable levels of the Western blot or it was present at higher concentration in adjacent tissues that were not examined here. As previously stated, only 1.5 g (~0.11%) out of the total human brain was analyzed (a human brain weighs 1.2-1.4 kg) [313]. On the other hand, PK-resistant fragments were detected at higher concentration in cerebellum-derived samples, as it is shown in the final PrP^{Sc} purified product, in both fractions, PK-digested (Figure 29, B: F7) or non-PK-digested (Figure 29, D: F7). The characteristic three ladder-like electrophoretic profile present molecular weights ranging from ~19-31 kDa, with a predominance of the monoglycosylated pattern, suggest type 2A [314]. These results indicated brain tissue tropism of PrP^{Sc} species in cerebellum, specifically

in this patient. Since the concentration of PrP^{Sc} final product was shown to be high, determined by a high-intensity band in the Western blot, the sample was selected for further examination by TEM.

4.5.1.4. Case 4. PK-resistant PrP fragments were detected in the final purification product of samples derived from cortex and cerebellum (Figures 30, A and B, respectively), as it is seen in both fractions digested with PK. For both samples, the band intensities for the final PrP^{Sc} purified product were similar, suggesting that PrP^{Sc} was homogeneously spread in these tissues. The characteristic three ladder-like electrophoretic profile displayed molecular weights ranging from ~19-31 kDa, with a predominance of the di- and mono- glycosylated pattern, suggest that these samples can be classified as Type 2 A/B. In this case, the patient was confirmed to be MV heterozygous at codon 129. These findings are in agreement with previous studies that suggested that 86% of the patients who are either VV homozygous or MV heterozygous have PrP^{Sc} type 2 [297]. These samples were selected for further examination by TEM, as the concentration of PrP^{Sc} in the final product was shown to be high (based on the intensity of the band in the Western blot. The PrP^{Sc} product was not detected by SDS-PAGE silver nitrate staining, maybe due to the lowest detection limit of this technique (100 pg protein), when compared with Western blot (10 pg).

Silver-stained SDS-PAGE of PrP^{Sc} preparations was also developed to evaluate the quality of the purifications. Although PrP^{Sc} was not detected in the final product, no contaminants were found either. Silver staining has a detection limit of 100 pg protein, whereas the detection limit for our Western blot is 10 pg protein. Hence it is not surprising that PrP^{Sc} was detected by Western blot, but not in the silver-stained gels.

4.5.2. Quantification of PrP^{Sc} concentration in the final purified product by ELISA. To assess the concentration of PrP^{Sc} in the final PTA-precipitated pellet, a colorimetric ELISA assay was developed using the anti-prion monoclonal antibody D15.15 (epitope 175-186). Samples that showed an intensity band in Western blots were selected for quantification. Eight-standards with concentrations ranging from 0 to 2.5 µg/ml, were used to normalize the concentration of the

samples. Each sample was run in triplicate. For PrP^{Sc} samples derived from sCJD, the concentration for these samples ranges from 1.36 to 2.02 µg/ml (Figure 18).

4.5.3. Examination of the structural integrity of the PrP^{Sc} species by TEM. Figure 31 shows examples of bright-field TEM and dark-field TB-TEM images of PrP^{Sc} fibrils obtained from sCJD –affected human brain-derived from cortex (case 1). Bright-field images of negatively stained PrP^{Sc} fibrils revealed the presence of ordered filamentous structures as well as PrP rods, the latest with a close resemblance to prion rods seen in preparations of purified hamster prions isolated by Prusiner and coworkers [162] (Figure 31, A). Initially, these rods were considered to be artifacts, generated as side products during the purification, due to both detergent and limited proteolysis of PrP^{Sc}. However, a later study using different exposure times of detergent (from 10 to more than 60 min) and a high concentration of PK (200 µg/ml), the research group was able to demonstrate that detergent serves to facilitate the observation of pre-existing PrP rods in brain homogenates rather than to catalyze their formation [315]. Figure 31, B shows a sample of a dark-field TB-TEM image of unstained PrP^{Sc} fibrils and TMV rods. PrP^{Sc} fibrils are predominantly aggregated and irregular in length, while TMV rods present a bigger size and straight-structure (volume= 7.6×10^4 nm^3) [303]. These PrP^{Sc} fibrils were PK-digested, PTA-precipitated, and negatively stained with uranyl acetate, hence what is shown is the core PrP^{Sc} PK-resistant of these fibrils. Figures 32, A and B show bright-field TEM images obtained from PrP^{Sc} fibrils derived from cerebellum of a patient diagnosed with sCJD, reported in case 3. As it is shown, highly dense packaged aggregates, as well as, fibrillar structures are clumping together. Due to the challenge in disaggregating these fibrils, they were not included for MPL evaluation, but they are still being processed for further assessment.

Figure 33, A, displays examples of bright-field TEM images of PrP^{Sc} obtained from a patient affected by sCJD, case 4. Negative stain revealed the presence of highly aggregated amorphous oligomeric deposits clumping together, as well as PrP^{Sc} fibrils, varying in length, some of them binding to collagen fibrils. Some fibrils seem to have an intertwined structure, while others have a straight appearance. The structure of the twisted assembly is difficult to discern in these EM images. Hence a higher resolution imaging might provide more detailed information regarding the

conformational structure of these fibrils. Figure 33, B shows a sample of a dark-field TB-TEM image of these PrP^{Sc} fibrils and TMV rods, both unstained and processed for MPL measurements.

4.5.4. MPL characterization of PrP^{Sc} fibrils derived from a brain sample affected by sCJD.

Dark-field TB-TEM images of unstained PrP^{Sc} fibrils derived from cortex (case 1) and cerebellum (case 4), mixed with TMV rods are shown in Figure 34 A and B, respectively. Those samples that displayed a high-intensity band (high concentration) in Western blots were selected for MPL assessment. MPL values were extracted from unstained PrP^{Sc} fibrils, taken under dark-field conditions using a TB-TEM at 80 kV acceleration voltage, as previously described by Chen *et al*., 2009 [241]. Rectangle boxes were drawn over the PrP^{Sc} fibrils, TMV rods and around their respective backgrounds, where the areas were selected for intensity measurement. All rectangle boxes were 60 nm in length. Rectangle widths were adjusted to include the fibrils or TMV width in each image. All intensities used to calculate a given MPL value were taken from the same image, as intensities from different images were not necessarily directly comparable due to variations in incident beam intensity.

In summary the procedure was as follows: 1) image intensities were measured inside the selected rectangular areas centered on fibril segments (I_F) and over equal areas of background on either side of each fibril segment (I_{B1} and I_{B2}); 2) similarly, image intensities were measured inside the selected rectangular areas centered on TMV segments (I_{TMV}) and over equal areas of background on either side of each TMV segment (I_{B3} and I_{B4}); 3) For each image, the quantity I_{TMV} was calculated as the average of the quantities $I_{TMV}-(I_{B3}+I_{B4})/2$ within the image; 4) MPL values were calculated as MPL=131x[$I_F-(I_{B1} + I_{B2})/2$]/ (I_{TMV}), as it is well known that TMV has a MPL of 131 kDa/nm Figures 34 A and B shows the histogram extracted from 32 TB-TEM images of PrP^{Sc} –sCJD fibrils derived from cortex and cerebellum, respectively. MPL peak positions were determined by fitting the histograms to one or more Gaussian functions. The histograms in Figures 34 A and B show a predominant peak centered between 60-70 kDa/nm for both samples (cortex and cerebellum), in agreement with a predicted value for a β-solenoid-like molecular structural model. Previous studies based on based on electron micrographs of 2D crystals of PrP 27-30 and the fibrillogenic miniprion PrP^{Sc} 106, suggested a parallel left-handed β-helical model for the core

of the infectious conformer. This model is supported by subsequent X-ray diffraction studies on PrP 27-30 [55], which showed meridional reflections at 4.8, 6.4 and 9.6 Å, suggesting a four-rung β-solenoid structure, where each PrP 27-30 molecule constitute four-rungs of β-structure and spans 19.2 Å along the axis of the fibril. Therefore, for this model, a MPL= ~30 kDa / 1.92 nm (1 subunit per 1.92 nm) is expected. This value corresponds to fibrils containing one protofilament only. Although the present X-ray diffraction data strongly support the β-solenoid model for PrP^{Sc} fibrils, there is still not enough evidence whether it can be applying to the infectious conformer.

4.5.5. Assessment of PrP species infectivity in Tg(HuPrP) mice. Previous studies have shown that infectivity of brain samples derived from patients affected by prion diseases is determined by the animal model that is used. Inoculation of WT mice, which express mouse PrP, with prion species related to humans, which are composed of human PrP^{Sc}, leads to inefficient disease transmission due to so-called species or transmission barrier effects. However, by using Tg mice that express human PrP can mitigate these effects, as they are susceptible to develop human prion disease. Another factor that influences the outcomes from transmission studies is the presence of methionine or valine at residue 129, in both the inoculum and the mice.

To evaluate the level of prion infectivity present in the final PrP^{Sc} purified product obtained from the brain tissue of patient diagnosed with sCJD, a small inoculum was used to inoculate transgenic mice homozygous for human PrP (*Prnp* +/+) (Tg(HuPrP) mice.) Tg(HuPrP) mice succumbed to the disease, showing lethargy, scruffy coat, and progressive ataxia and cachexia at 453 $\pm$50 dpi and 414 $\pm$ 22 dpi, for mice inoculated with 30-μl, 20% (w/v) (dilution 1/10) of BH or purified PrP^{Sc}, respectively (from case 3) (Table 6). A cohort group of Tg(HuPrP) mice was kept non-inoculated as negative controls. These results demonstrated that PrP^{Sc}-derived from sCJD samples remained infectious. Immunoblot analysis of these PrP^{Sc} PK-resistant species present in Tg(HuPrP) mice brain, revealed the presence of the characteristic ladder-like pattern of the three di-, mono-, and nonglycosylated isoforms (Figure 35). A further examination of these PrP species by negative stain and bright-field TEM imaging showed well-defined fibrillar structures, similar to previously reported amyloid fibrils (Figure 36).

4.6. Discussion

Sporadic CJD (sCJD) is the most common prion disease in humans, accounting for more than 80% of all cases and reporting a worldwide incidence of about 1.5 cases per 1 million population per year. It has been well documented that mammalian prions occur in a variety of strains. Strain properties are not dictated by the primary structure of the PrP protein; although it has been demonstrated that PrP^{Sc} exists in different molecular subtypes, encompassing differences in size and glycosylation patterns, degree of protease resistance, aggregation state, and conformational stability. Indeed, typing PrP^{Sc} associated with sCJD can be developed based on limited PK-digestion profile, polymorphism at codon 129 of *PRNP*, and the relative intensities of PrP bands (corresponding to the PrP glycoform ratio). Supporting evidence came from previous studies based on sCJD showing that human prion diseases with a distinct neuropathological profile may result from different conformers of PrP^{Sc} [316]. Two types of PrP^{Sc} (type 1 and 2) differing in their relative molecular mass and glycoforms ratio, as well as the polymorphism at codon 129, have been shown to determine the clinical and pathological variability of sCJD [316].

In a recent study, Pirisinu and coworkers [324] demonstrated the presence of a so-called PK-sensitive PrP^{Sc} (sPrP^{Sc}), an abnormal isoform of PrP^{Sc} derived from the misfolding of PrP^{C}. sPrP^{Sc} is also accumulated with nonglycosylated PK-resistant fragments in the 7-14 kDa range. According to previous studies, sPrP^{Sc} may contribute up to 90% of the whole PrP^{Sc} even in classical TSEs such as sCJD. In our case, the sample derived from cerebellum from a patient that suffered sCJD, case 2 (Figure 28) showed total digestion by PK, while the three characteristic bands, corresponding to di-, mono-, and nonglycosylated isoforms can be visualized in the fractions that were kept under non-PK digestion conditions. These findings suggest that for this sample, sPrP^{Sc} was the causative agent of the disease. Furthermore, a 21 kDa band can be seen as a high-intensity band for the diglycosylated isoform, suggesting that this sample can be classified as type 2B.

PrP^{Sc} glycosylation is another factor that seems to contribute to the molecular basis of strain variation. Previous studies have shown that distinct glycoform ratios are associated with a distinct subtype of prion diseases. Hence, since glycosylation is a co-translational process, the different glycoform ratios may reflect distinct neuronal populations, as a consequence of a strain-specific cellular tropism. In this study, a high-intense band was seen in cerebellum in both cases 3 and 4 (Figure 29 and 30, respectively), compared with cortex PrP^{Sc} signal demonstrated in both case samples. These findings suggest that PrP^{Sc} showed brain tropism towards this region in the brain of these patients. It is still debatable whether the distinct properties of PrP^{Sc} in these samples directly reflect PrP^{Sc} conformation or are instead determined by interactions between PrP^{Sc} and other molecules specific for that region in the brain.

Western blot of PrP from case 3 showed a 19 kDa band and two high-intensity bands corresponding to di- and nonglycosylated isoforms suggesting that this sample can be classified as type 2A, while PrP from case 4 showed a 19 kDa band, but with the di- and mono-glycosylated isoforms showing high-intensity bands, which suggest that this sample belongs to type 2 A/B. Western blot of PrP showed a type 1A/B pattern for sample derived from case 1, with a 19 kDa band and high-intensity bands for di- and monoglycosylated isoforms, suggesting that this sample can be classified as type 1 A/B. It remains unknown whether the glycoprofile of abnormal PrP influences on phenotype. In this research, only case 4 was confirmed to be MV129.

4.6.1. Effect of polymorphism at *PRNP* residue 129 on sCJD onset. The origin of sCJD is unknown, although the initiating event is thought to be the stochastic misfolding of endogenous PrP^{C}. This event, explained by the "protein-only" hypothesis, states that conversion of PrP^{C} into the abnormal PrP^{Sc} involves some direct interaction between the two isoforms, a process favored by sequence complementary [317,318].

This theory has been supported by previous findings, where the majority of cases of sCJD were homozygous at residue 129 for methionine (M) or valine (V) [319], and with heterozygotes appear significantly protected against developing sCJD [320]. Another key piece of evidence

supporting this argument came from findings that elderly survivors of the kuru epidemic that had multiple exposures at mortuary feasts, are predominantly *PRNP* codon 129 heterozygotes, have also shown to have longer incubation times [321]. This group also show marked Hardy-Weinberg disequilibrium, a principle that states that allele and genotype frequencies in a population will remain constant between generations in the absence of other evolutionary influences (like, genetic drift, mate choice, assertive mating, natural selection, sexual selection, mutation, gene flow, meiotic drive, genetic hitchhiking, population bottleneck, founder effect, and inbreeding)[322]. However, the role that this polymorphism has on the structure, stability, folding, and dynamics of the PrP is still unknown. A recent study based on NOE-derived constraints and chemical shift found remarkably little difference between the two sequences on the global stability of PrP^C under denaturant-unfolding transition and hydrogen exchange behavior [319]. This study suggests that M129V polymorphism does not affect prion propagation through its effect on PrP^C, instead, its influence is likely to be downstream in the disease mechanism, through the conformation or stability of PrP^{Sc}, its intermediates, or on the kinetics of their formation.

Although no significant differences were found regarding the molecular weight of PrP^{Sc} PK-resistant fragments, there were some cases where PrP^{Sc} was predominantly abundant in cerebellum samples-derived patients (case studies 2 and 3), suggesting a strain-specific PrP^{Sc} accumulation pattern. Recent research has shown how partial cellular tropism can lead to strain-specific PrP^{Sc} accumulation patterns, which eventually will generate different pathological phenotypes. In this case, the high density of neuronal connections in cerebellum (which holds about 30% of the neurons in 10% of the total volume of the brain), profoundly influences the neuropathological features of the disease [321].

In this study, only the patient presented in case 4 was confirmed to be heterozygous at codon 129 (M129V), with PrP^{Sc} showing no significant differences in accumulation in samples derived from brain cortex and cerebellum. Analysis of these samples by Western blot showed an nonglycosylated band at ~19 kDa, and two predominant bands (di- and mono- glycosylated), which according to previous studies might lead to classify these samples as type 2 A/B. Previous research has found that approximately 95% of the sCJD patients who are MM homozygous have PrP^{Sc} type

1 whereas 86% of the patients who are either VV homozygous or MV heterozygous have PrP^{Sc} type 2. Therefore, MM homozygosity favors the formation of PrP^{Sc} type 1 and the presence of one or two V at codon 129 favors the formation of PrP^{Sc} type 2 [297]. From these observations, it seems likely that the influence of residue 129 on prion disease results from its effect on the conformational properties of PrP^{Sc}, such that the type 1 and type 4 conformations are formed only by the methionine variant, whereas type 3 is favored by valine and the type 2 conformation is influenced equally well by either.

4.6.2. MPL analysis of sCJD PrP^{Sc} fibrils by TB-TEM. MPL histograms for PrP^{Sc} fibrils derived from cortex (case 1) and cerebellum (case 4) show a broad peak centered between 60-70kDa/nm for both samples, with an FWHM= ~25kDa/nm and ~30 kDa/nm, respectively (Figure 34, A and B, respectively). These MPL values were determined from TB-TEM images over an MPL range from 10 kDa/nm to 60 kDa/nm. As aforementioned in chapter 3, the differences in the FWHM values might be due to background intensity fluctuations, which in turn will generate MPL variations. Several factors are involved in these fluctuations, such as sample quality, presence of extraneous material on the sample grids, nonuniformity structures of the fibrils, which encompass unresolved breaks in the fibrils, and non-fibrillar content in the fibrils. Previous studies have reported the effect of these factors also in STEM measurements [241]. In this study, the TB-TEM images were recorded with an electron dose of 0.70 e/Å^2 s at 80 kV acceleration voltage, and a beam exposure time of 32 s (integration time). Comparison of TB-TEM electron beam exposure at 2.5 s was developed, that showed no evidence for rapid mass loss as it was previously reported [241].
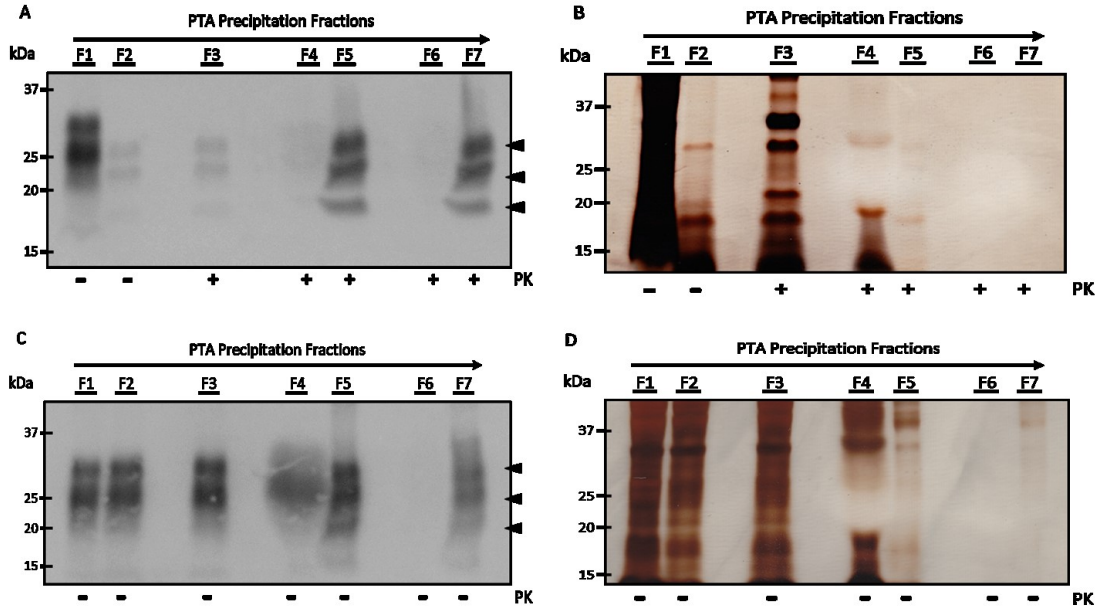
Figure 25. Western blot and silver stain analyses of PrP^{Sc} PK-resistant fragment derived from cerebral cortex-obtained from a patient affected by sCJD: Case 1. The samples were subjected to limited proteolysis, followed by PTA precipitation and analyzed at each step during the purification. (A, C) Western blot analysis showing the three characteristic PrP^{Sc} glycoforms patterns (di-, mono-, and un- glycosylated forms) detected on the final purified product (pointed by the black arrows), with molecular weights ranging between ~21-30 kDa. A small band at ~16 kDa can be seen in the non-PK digested fractions (A: F1; C: F5-F7). (B, D) SDS-PAGE stained by silver nitrate showing the brain homogenate (BH) and PTA purified fractions. The equivalent 5-μl 10% (w/v) BH and 5-μl samples were loaded per lane. F1: 20% BH, F2: 10% BH after first step of clarification; F3: after PK-digestion treatment; F4: first supernatant collected; F5: first pellet; F6: second supernatant collected; F7: final PrP^{Sc} pellet purified. An alternative non-enzymatic digest control was carried out in parallel, where the samples were PTA-precipitated in a buffer containing proteases inhibitors and kept under non-PK enzymatic digestion conditions (C, D). +/- Symbols indicate when PK-digestion was applied during the purification. As the amount of protein was high in the final PrP^{Sc} product, no sucrose gradient was developed for these samples.
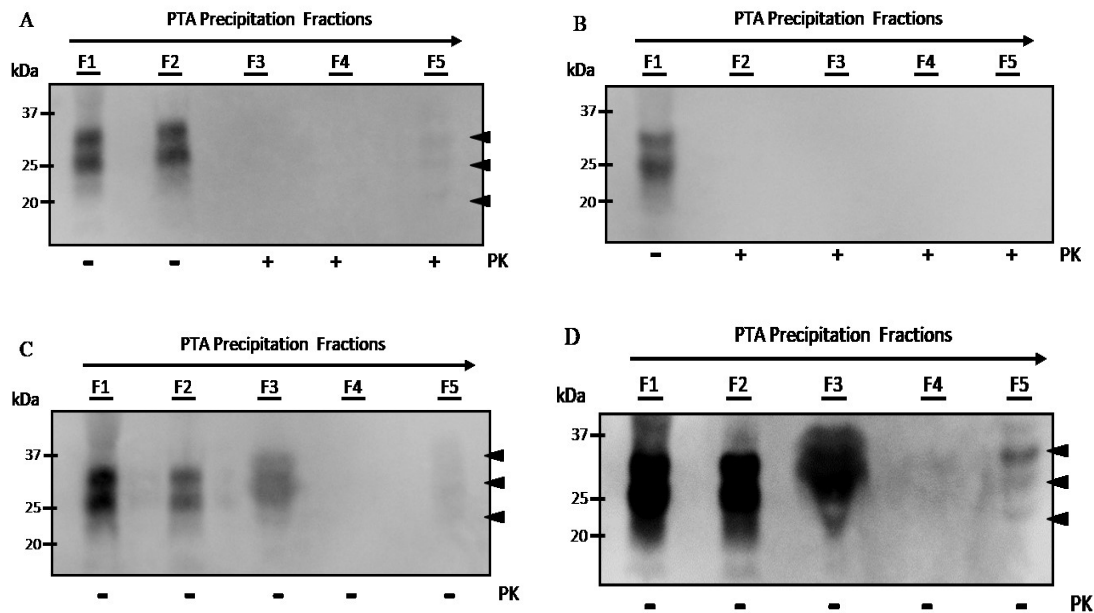
Figure 26. Western blot analysis of PrP^{Sc} PK-resistant fragment derived from cerebral cortex (A, C) and cerebellum (B, D) obtained from a patient affected by sCJD: Case 2. The samples were subjected to limited proteolysis, followed by PTA precipitation and analyzed at each step during the purification. Western blot analysis of PrP^{Sc} from cerebral cortex (left panels: A, C)-and cerebellum (right panels: B, D) shows the three characteristic PrP^{Sc} glycoforms patterns (di-, mono-, and un- glycosylated forms), detected on the final purified product and pointed by the black arrows, with molecular weights ranging between ~21-30 kDa. The equivalent 5-µl of 10% (w/v) BH and 5-µl samples were loaded per lane. F1: 20% BH, F2: 10% BH after first step of clarification; F3: after PK-digestion treatment; F4: first supernatant collected; F5: first and final pellet containing PrP^{Sc} purified. An alternative non-enzymatic digest control was carried out in parallel, where the samples were PTA-precipitated in a buffer containing proteases inhibitors and kept under non-PK enzymatic digestion conditions (C, D). +/- Symbols indicate when PK-digestion was applied during the purification.
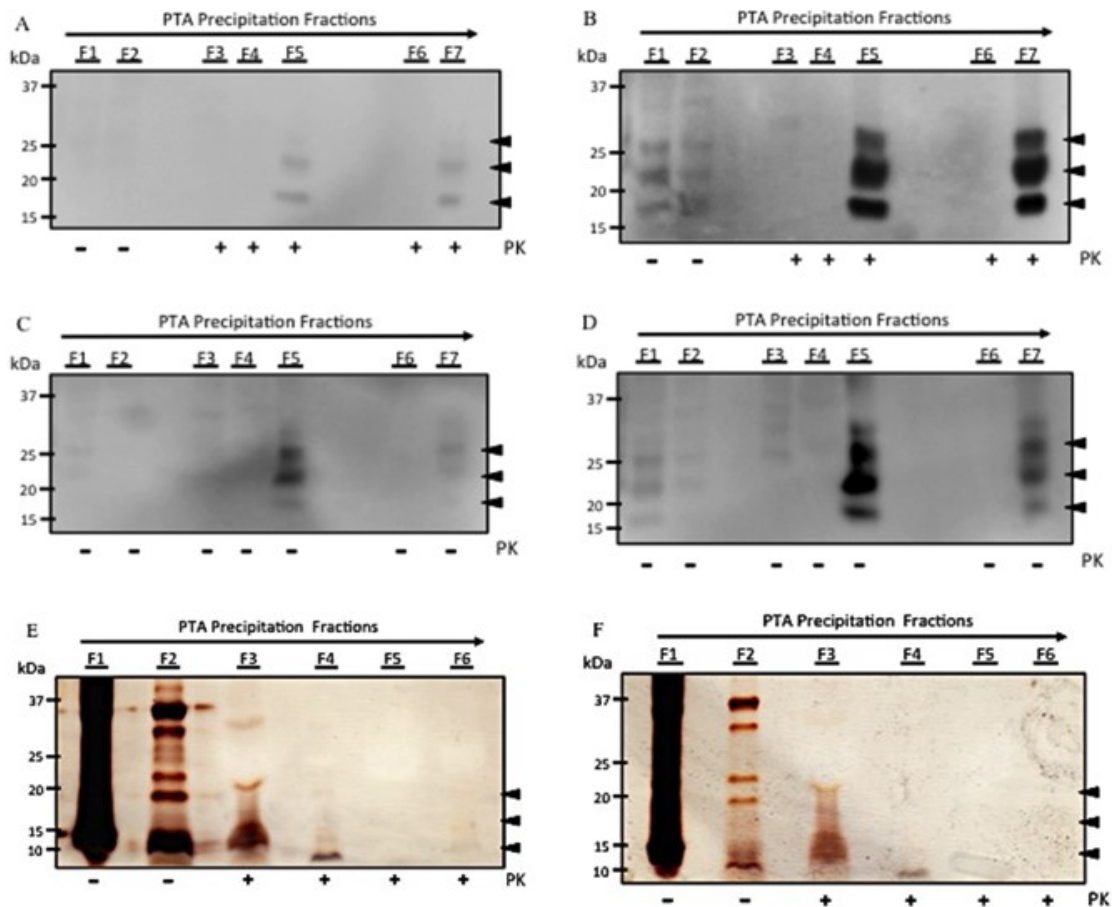
Figure 27. Western blot and silver stain analyses of PrP^{Sc} PK-resistant fragment derived from cerebral cortex (A, C, E) and cerebellum (B, D, E) obtained from a patient affected by sCJD: Case 3. The samples were subjected to limited proteolysis, followed by PTA precipitation and analyzed at each step during the purification. Western blot analysis of PrP^{Sc} from cerebral cortex (left panels: A, C)-and cerebellum (right panels: B, D) shows the three characteristic PrP^{Sc} glycoforms patterns (di-, mono-, and un- glycosylated forms), detected on the final purified product and pointed by the black arrows, with molecular weights ranging between ~16-30 kDa. (E, F) SDS-PAGE stained by silver nitrate showing the brain homogenate (BH) and PrP^{Sc} -PTA purified fractions. The equivalent 5-μl of 10% (w/v) BH and 5-μl samples were loaded per lane. F1: 20% BH, F2: 10% BH after first step of clarification; F3: after PK-digestion treatment; F4: first supernatant collected; F5: second supernatant collected; and F6: final pellet collected containing PrP^{Sc} purified. An alternative non-enzymatic digest control was carried out in parallel, where the samples were PTA-precipitated in a buffer containing proteases inhibitors and kept under non-PK enzymatic digestion conditions (C, D). +/- Symbols indicate when PK-digestion was applied during the purification.

Figure 28. Western blot and silver stain analyses of PrP^Sc PK-resistant fragment derived from cerebral cortex (A, C) and cerebellum (B, D) obtained from a patient affected by sCJD: Case 4. The samples were subjected to limited proteolysis, followed by PTA precipitation and analyzed at each step during the purification. Western blot analysis of PrP^Sc from cerebral cortex (left panels: A, C)-and cerebellum (right panels: B, D) shows the three characteristic PrP^Sc glycoforms patterns (di-, mono-, and un- glycosylated forms), detected on the final purified product and pointed by the black arrows, with molecular weights ranging between ~16-30 kDa. (C, D) SDS-PAGE stained by silver nitrate showing the brain homogenate (BH) and PrP^Sc -PTA purified fractions. The equivalent 5-μl of 10% (w/v) BH and 5-μl samples were loaded per lane. F1: 20% BH, F2: 10% BH after first step of clarification; F3: after PK-digestion treatment; F4: first supernatant collected; F5: second supernatant collected; and F6: final pellet collected containing PrP^Sc purified. +/- Symbols indicate when PK-digestion was applied during the purification.
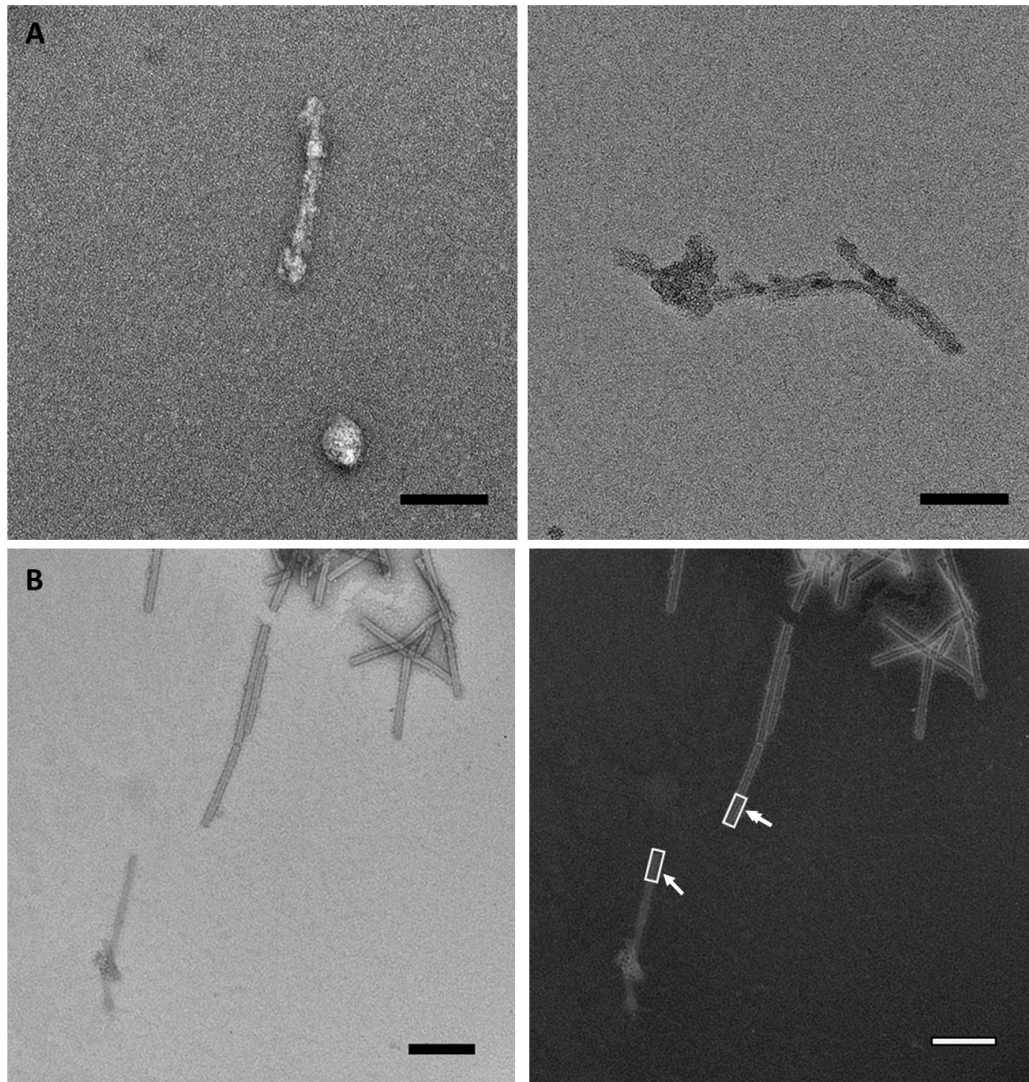
Figure 29. TEM images of PrP^{Sc} PK-resistant fibrils derived from brain cortex of a patient who suffered sCJD (case 1). (A) Bright-field images of negatively stained samples are shown in the upper panels. Negative stain method was used to evaluated the morphology and structural integrity of PrP^{Sc} fibrils, after purification. Amorphous oligomeric aggregates, as well as collagen fibrils can be seen clumping together to PrP^{Sc} fibrils. (B) Dark-field TB-TEM images of unstained PrP^{Sc} PK-resistant fibrils and TMV rods are shown in the lower panels. Single-headed arrows indicate example of selected segments in the PrP^{Sc} fibril analyzed for MPL determinations. Double-headed arrow indicates the segments on TMV rods. MPL values for PrP^{Sc} fibrils were calibrated with TMV (used as internal standard for mass calibration), assuming the average TMV MPL value to be 131 kDa/nm. (Scale bars, 100 nm and 500 nm for bright-field and dark-field images, respectively).

Figure 30. TEM images of PrP^{Sc} PK-resistant fibrils derived from brain cerebellum of a patient who suffered sCJD (case 3). Bright-field images of negatively stained samples showed highly dense package of amorphous and fibrillar aggregates (A), as well as fibrillar-like structures aggregated (B) (Scale bars, 500 nm (A) and 50 nm (B).
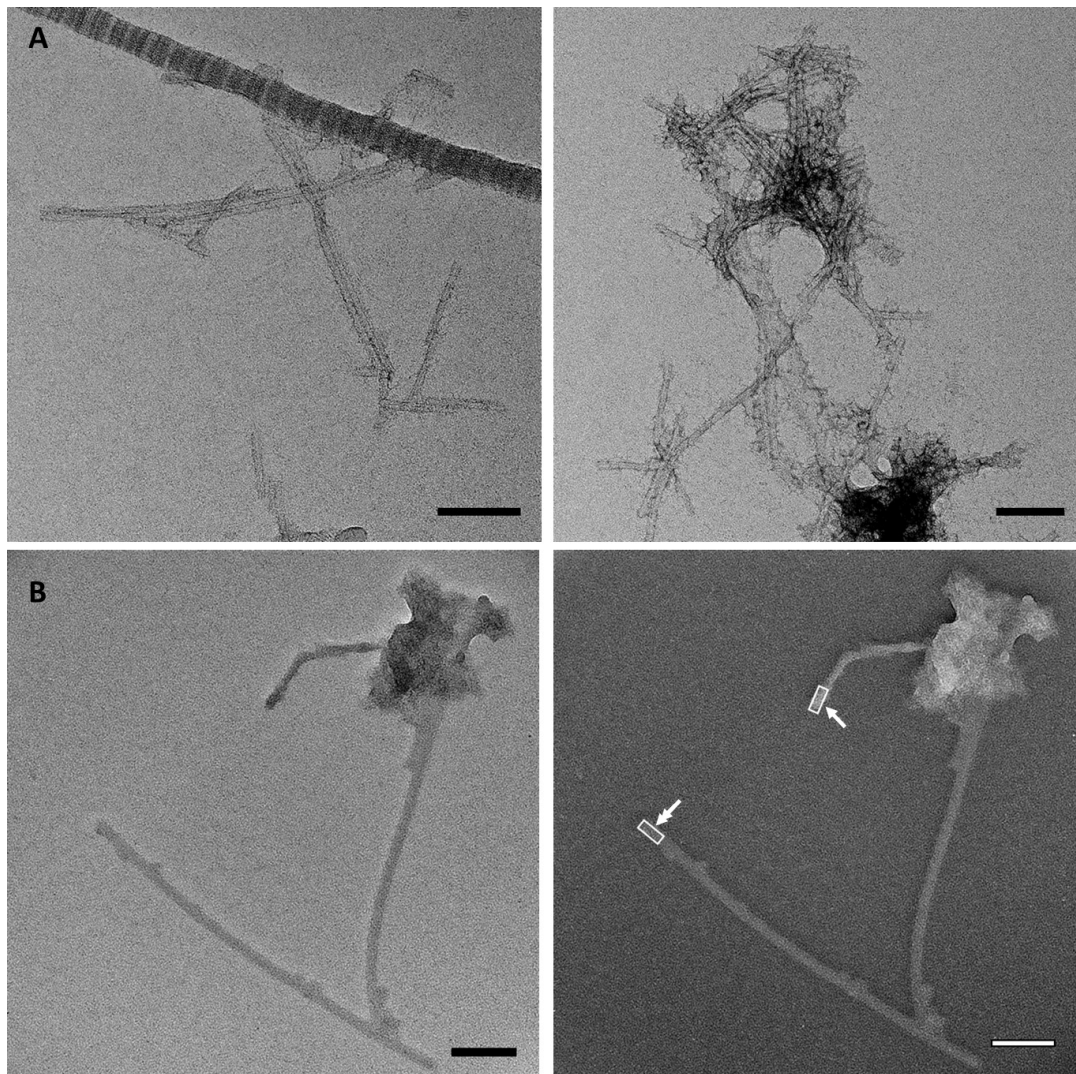
Figure 31. TEM images of PrP^Sc PK-resistant fibrils derived from brain cerebellum of a patient who suffered sCJD (case 4). (A) Bright-field images of negatively stained samples are shown in the upper panels. Negative stain method was used to evaluated the morphology and structural integrity of PrP^Sc fibrils, after purification. Amorphous oligomeric aggregates, as well as collagen fibrils can be seen clumping together to PrP^Sc fibrils. (B) Dark-field TB-TEM images of unstained PrP^Sc PK-resistant fibrils and TMV rods are shown in the lower panels. Single-headed arrows indicate example of selected segments in the PrP^Sc fibril analyzed for MPL determinations. Double-headed arrow indicates the segments on TMV rods. MPL values for PrP^Sc fibrils were calibrated with TMV (used as internal standard for mass calibration), assuming the average TMV MPL value to be 131 kDa/nm. (Scale bars, 100 nm and 500 nm for bright-field and dark-field images, respectively).

Figure 32. MPL histogram extracted from TB-TEM images of PrP^{Sc} unstained fibrils derived from cortex-case 1 (A) and cerebellum-case 4 (B) from patients that suffered sCJD. The solid curve is fit to one Gaussian function. The vertical dashed line indicates the ideal MPL value predicted by experimentally based structural models. The preliminary MPL measurements from these samples give a ~60 kDa/nm value, with FWHM of ~25 kDa/nm and ~30 kDa/nm, for PrP^{Sc} fibrils derived from cortex and cerebellum, respectively, suggesting a four-rung β-solenoid conformation for these fibrils.
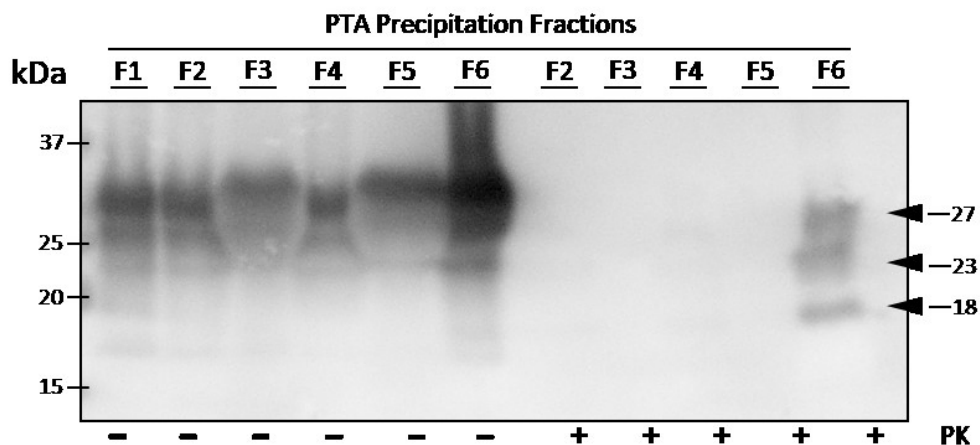
Figure 33. Immunoblot analysis of PrP species extracted from Tg(HuPrP) mice brain that were inoculated with PrP^Sc PK-resistant fragments and purified by PTA-precipitation from brain tissue derived from a patient affected by sCJD. Tg(HuPrP) mice were inoculated with a 30-μl inoculum (dilution 1/10) derived from sCJD derived from cerebral cortex (case 1). Tg(HuPrP) mice brains were subjected to limited proteolysis, followed by PTA-precipitation and analyzed at each step during the purification. The three characteristic PrP^Sc glycoform patterns (di-, mono-, and un-glycosylated) are revealed in the final purified product (F6) (pointed by the black arrows), with molecular weights between ~17-27 kDa. The equivalent 5-μl 10% (w/v) BH and 5-μl samples were loaded per lane. F1: 20% BH, F2: 10% BH after first step of clarification; F3: after PK-digestion treatment; F4: first supernatant collected; F5: second supernatant collected; and F6: final purified pellet. An alternative non-enzymatic digest control was carried out in parallel, where the samples were PTA-precipitated in a buffer containing proteases inhibitors and kept under non-PK enzymatic digestion conditions (Second PTA-fractions F2-F6). +/- Symbols indicate when PK-digestion was applied during the purification.

Figure 34. Bright-field TEM images of PrP^{Sc} PK-resistant species obtained from Tg(HuPrP) mice brain inoculated with PrP^{Sc} sCJD species derived from human cerebral cortex (A) and cerebellum B) (case 1).

CHAPTER 5

CHARACTERIZATION OF GERSTMANN-STRÄUSSLER-SCHEINKER (GSS) SYNDROME WITH A MUTATION AT CODON A117V AND POLYMORPHISM M129V OF PRION PROTEIN GENE

Claudia Y. Acevedo-Morantes[1,2], Xiongyao Wang[1], Brian Tancowny[1], Susana Teijeira[3], Beatriz San Millán[3], and Holger Wille [1,2]

[1]Centre for Prions and Protein Folding Diseases and [2]Department of Biochemistry, University of Alberta, Edmonton, AB, Canada, [3]Galicia Sur Health Research Institute, IIS Galicia Sur, SERGAS-UVIGO, Vigo, Spain, [4]Pathology Department, Complexo Hospitalario Universitario de Vigo (CHUVI), IIS Galicia Sur, SERGAS, Vigo, Spain

Summary

The wide range of phenotypic variation in human prion diseases is caused by aberrantly folded versions of the prion protein, termed PrP^{Sc}. Human prion diseases present as sporadic, familial, infectious, or iatrogenic diseases. Gerstmann-Sträussler-Scheinker syndrome (GSS), is an inherited autosomal dominant prion disease, clinically characterized by ataxia and cognitive impairment. A typical hallmark of the disease is the accumulation of PK-resistant fragments of ~7kDa to 15 kDa in the brain. The presence of mutations and/or polymorphisms determines the neuropathological features of the disease. In this study, PrP species purified from brain tissue of a patient with the A117V mutation who was heterozygous at codon 129 (M129V) were examined. These results showed no significant differences between PrP species derived from brain cortex and cerebellum. Furthermore, these PrP species comprises the plausible precursor 8 kDa PK-resistant fragment suggesting an early start of accumulation, alongside with the 16 kDa thermolysin-resistant signature. Our data suggest a similar signature when compared to previously reported findings, suggesting a common molecular pathway.

5.1. Introduction

Gerstmann-Sträussler-Scheinker Syndrome (GSS) is a rare inherited fatal neurodegenerative disease, typically present with slowly progressive cerebellar ataxia (degeneration of cerebellum, the part of the brain that controls coordination, balance, equilibrium and muscle tone), as well as late cognitive decline [5]. GSS was first reported by the Austrian physicians Josef Gerstmann, Ernst Sträussler, and Ilya Scheinker in 1936 [26].

GSS is associated with autosomal-dominant inheritance, caused by heterozygous mutation in the *PRNP* gene on chromosome 20p13. fCJD and fatal familial insomnia (FFI) are other allelic genetic prion diseases caused by a mutation in this gene [5]. However, GSS can be distinguished from other genetic prion diseases at an earlier age at onset; longer disease duration, and prominent cerebellar ataxia [49]. GSS onset is between 40 and 60 years, with an average disease duration of a few to seven years. Cognitive dysfunction is generally not shown early on. However, with progression, bradyphrenia (slowness of thought processing) may become evident. Common symptoms are pyramidally associated with spasticity and/or extrapyramidal involvement with bradykinesia (slow movement), increased muscle tone with or without cogwheeling (muscular rigidity), and masked facies (loss of facial expressions).

Psychiatric or behavioral symptoms are atypical. The disease progresses at a relatively slow but relentless pace throughout the illness. Cerebellar dysfunction results in severe dysarthria (difficult articulation of speech), gait and appendicular ataxia (loss of full control of bodily movements), ocular dysmetria (constant under- or overshooting of the eyes when attempting to focus the gaze on something) and lack of coordination in swallowing. In the terminal stage, the individual is immobilized due to the disabling ataxia, unable to eat because of severe lack of coordination in swallowing, and unable to communicate due to acute dysarthria. This pattern of progression is associated with the cerebellar amyloid deposition nature of this disease, as it propagates into the brain stem and eventually the cerebrum [5].

5.2. Classification of GSS

GSS is classified as a TSE due to the causative role-played by the *PRNP* gene. GSS is inherited as an autosomal dominant trait and segregates with variant genotypes resulting from the combination of a pathogenic mutation (P102L, P105L, A117V, G131V, F198S, D202N, Q212P, and Q217R) and the methionine (M) / valine (V) polymorphism at codon 129 in the *PRNP* gene that can influence the clinical phenotype produced by the mutation [323].

GSS molecular fingerprint. PK-treatment of PrP^{Sc} derived from most TSEs results in PK-resistant fragments (PrPres) with variable glycosylated C-terminal regions, which run in a typical ladder-like electrophoretic migration pattern of 19 to 21 kDa (nonglycosylated isoform) and 27 to 30 kDa (for the remaining isoforms). In contrast, GSS subtypes are characterized by nonglycosylated PrPres consisting of PrP internal fragments, truncated at the N- and C- terminal, with a molecular weight between ~ 7 to15 kDa, influenced by the specific *PRNP* mutation [324]. GSS P102L shows a particular pattern, with an accumulation of both 21 and 8 kDa. Transmission studies in transgenic mice expressing mutated murine PrP equivalent to human P102L (Tg101LL) have shown that the 21-kDa PrPres fragment is responsible for the biological properties of GSS, as it remains transmissible. Nevertheless, the 8 kDa PrPres fragment induced PrP-amyloid deposition, it did not replicate the infectivity in the Tg101LL mice. GSS cases associated with A117V show atypical PrPres fragments of 6 to 7 kDa, showing a wide range of clinical and pathological presentations even within the same family. Transmission studies of GSS A117V using transgenic mice over-expressing the human 117V PrP, are characterized by low clinical attack rates, long incubation periods (>600 days), and accumulation of inherently unstable PrP^{Sc} aggregates. Inefficient transmission of GSS cases with 6 to 8 kDa PrPres has shed some doubts to the hypothesis that GSS is a non-transmissible proteinopathy rather that authentic prion disease. Nonno and coworkers demonstrated that GSS cases are composed of PrP^{Sc} infectious particles, capable of inducing propagation and spongiform degeneration in the brain of voles [324].

5.3. Diagnosis of GSS

Genetic prion diseases constitute a continuum of clinical and pathologic manifestations broadly segregated into three dominant phenotypes designated as fCJD, GSS, and FFI. Although there is considerable overlap in the clinical features, a formal diagnostic criterion for each genetic form is still lacking. Recognizing a disease profile will be useful for diagnosis and care.

Clinical diagnosis of GSS relies upon a combination of the following: 1) clinical features: comprised of a combinations of adult-onset neurologic signs and symptoms, such as: dementia, dyscoordination of movements (ataxia, dysarthria), myoclonus (muscle jerks), weakness and/or spasticity, seizures and stroke-like episodes; 2) neuropathologic findings such as multiple amyloid plaques, recognized by anti-prion protein antibodies; 3) family history consistent with autosomal dominant inheritance; and 4) *PRNP* pathogenic variant (determined by molecular genetic testing).

Differential diagnosis is also performed to support the diagnosis and evaluation of other diseases of the central nervous system, and they include: 1) EEG with periodic sharp wave complexes (PSWCs), consisting of triphasic or sharp wave burst every 0.5 to 2.0 seconds. PSWCs are more likely to appear in pathogenic variants that produce a CJD-like clinical phenotype, hence a relatively small percentage of individuals with generic prion disease have a positive EEG; 2) Brain imaging like magnetic resonance imaging (MRI), diffusion-weighted MRI (DWI), and positron emission tomography (PET), which show atrophy or metabolic activities in the brain, depending on what technique is used; and 3) cerebrospinal fluid (CSF), where an elevation of CSF protein concentration by 10% may be attributed to the release of the normal neuronal 14-3-3 protein into the CSF following neuronal death, although this finding is not specific for prion disease [5].

5.4. Case: Presentation

Here a case of a patient with neuropathologically confirmed GSS from BioBanco Complexo Hospitalario Universitario de Vigo (Vigo, Spain) was analyzed by limited proteolysis, sucrose gradient density and MPL measurements by TB-TEM. The patient presented with slow progressive

cognitive dysfunction. Classical EEG changes and brain CT imaging atrophy were observed. The patient underwent brain post-mortem biopsy.

5.5. Case

A 49-year-old man, former smoker and drinker. He suffered meningitis at the age of 7. He went under appendectomy. The patient was hospitalized on July 11, 2008, due to episodes of tonic-clonic seizure in his extremities, with generalized rigidity, stertorous breathing, and developing somnolence. The patient was conscious, although with limited language, direct gaze, and no nystagmus. Generalized muscular atrophy. Symmetric osteo-tendon reflex (OTR). Difficulty walking. EEG revealed frontotemporal waves with acute theta rhythms in the left regions. A computed tomography (CT) imaging showed brain atrophy. Histopathological assessment and genetic evaluation, confirmed characteristic features of GSS. He died on May 2012.

Comments: The mutation A117V and polymorphism MV129 reported in the sample. Sample donated from cortical and cerebellar brain tissue.

5.6. Results

5.6.1. Molecular analysis of PrP species derived from a GSS-patient carrying the *PRNP* A117V polymorphism by aggregation profiles. The aggregate distribution profile approach was used to examine the PrP species present in the GSS samples (of both cortex and cerebellum regions). Hence, non-digested brain homogenates were submitted to PTA-precipitation following separation on a cushion of 40-80% sucrose density gradient. Before proceeding with the centrifugation, the position of each gradient was labeled on the tube, resulting in six zonal density-gradient fractions (top fraction of 40%, 40%, 40%-60%., 60%, 60%-80%, and 80%). Resulting preparations were ultracentrifuged for 24 h and fractionated in six fractions. Each fraction was analyzed by Western blot probed with the monoclonal antibody D15.15 (PrP epitope 175-186). Although PrP species derived from cerebellum showed higher intensity bands, suggesting that GSS-PrP species accumulated at higher concentration in this region of the brain, there was no

significant difference in the pattern of distribution between PrP species derived from cortex and cerebellum, i.e., PrP species from both samples showed considerable heterogeneity and similar distribution profile along the density gradient. In the upper fraction (~40%) of the density gradient, PrP species of ~16 kDa and 20-25 kDa are revealed (Figures 37: A- B, F1, and F2). Fractions obtained from the ~40% to 60% zonal gradient showed bands of ~16 kDa and 21-35 kDa (Figures 37: A-B, F3, and F4). Fractions derived from the bottom of the zonal gradient, >60% sucrose, showed higher molecular weight bands of ~21 kDa, and 25-37 kDa (Figures 37: A, B, F5, and F6).

5.6.1.1. Case results. Patient's EEG showed frontotemporal periodic waves complexes. Brain CT revealed atrophy regions. Ataxia, dysarthria, and bradyphrenia were visualized, in agreement with previously reported studies for GSS [5]. Exposure of non-enzymatically digested brain homogenates derived from cortex and cerebellum to PTA-precipitation and pass through a 40-80% sucrose gradient cushion revealed the high heterogeneity of these samples, with PrP species varying in molecular weight from ~16 - 37 kDa (Figure 37). PK digestion, following PTA-or methanol precipitation, also revealed the presence of the ~8 to 15 kDa PrP species, characteristic of GSS profile (Figure 40). Since the concentration of PrP^{Sc} final product showed to be high, determined by a strong signal intensity in the Western blot, the sample was selected for further examination by TEM.

5.6.2. Analysis of PrP content in GSS samples derived from sucrose density gradients by bright-field TEM imaging. Bright-field TEM images of negatively stained PrP species obtained from non-PK-digested samples of GSS-cortex and cerebellum tissues were used to evaluate PrP morphology and structural integrity after PTA-precipitation and sucrose gradient fractionation. PrP species in the same sample have different profiles of aggregation in sucrose gradients, as was revealed by Western blotting (Figure 37). Negative stain of PrP^{Sc} species derived from cortex revealed the presence of highly aggregated oligomeric amorphous deposits binding to lipids. These findings were expected, as lipids have a similar density as the upper fraction of the sucrose gradient (40%, ρ=1.006 g/ml), and PrP species have a high affinity to bind them [301] (Figure 38, A-D). These aggregates were found along with the sucrose gradient fractions. The highest proportion of fibrillar-like structures were found in the zonal interface of around 60%-80% sucrose gradient, as it was expected since PrP species have a similar buoyant density as this sucrose fraction (~1.21. g/ml)

(Figure 38, E-J). A similar pattern of distribution was found for PrP species derived from cerebellum. Negative stain of samples obtained from GSS-cerebellum revealed the upper zone of the sucrose gradient enriched with an abundant amount of lipids, higher than in GSS-cortex samples, and with amorphous oligomeric aggregates bound to them (Figure 39, A-G). Similarly, to cortex-derived samples, fibrillar-like structures were found in the zonal interface of around 60%-80% sucrose gradient, as it was expected since PrP species have a similar buoyant density as this sucrose fraction (~1.21 g/cm^3) (Figure 39, H-I).

5.6.3. Analysis of PrP content in GSS samples derived from cortex and cerebellum, by enzymatic digestions and bright-field TEM imaging. GSS PrP species derived from cortex and cerebellum were examined by enzymatic digestions using the following enzymes: 1) PK (25 µg/ml), 2) PE (5 µg/ml), and 3) TL (5 µg/ml); as well as sequential digestions using a combination of these enzymes: 1) PK/PE, 2) PE/TL, and 3) TL/PK. The enzymatic digestions were followed by precipitation with methanol or PTA. Immunoblot analysis of GSS-cortex samples enzymatically digested and methanol precipitated is shown in Figure 40, (A). Total digestion by PK is revealed, suggesting that PrP^{Sc} PK-sensitive species are present in this sample. Digestion by PE revealed a faint band at ~8 kDa and 16 kDa, as well as a prominent band between 21-27 kDa. Digestion by TL showed a series of prominent bands from ~21 kDa-30 kDa, as well as a prominent ~16 kDa band. A similar pattern was observed with the double digestion PE/TL. Surprisingly, the double digestion PK/PE revealed an 8 kDa PrP fragment pathognomonic for end-stage GSS [325]. A further examination of these fragments by bright-field TEM imaging showed: PE-digestion present high density packed of amorphous oligomeric aggregates (Figure 41, A, B). PrP species derived from TL-digestion showed more fibrillar-like structures when compared to PE-digestion (Figure 41, C, D). PrP species derived from sequential enzymatic digestion with TL, followed by PK-digestion, revealed more fibrillar-like structures, highly aggregated, and varying in size (Figure 41, E, F).

Immunoblot analysis of GSS-cerebellum samples enzymatically digested and methanol precipitated is shown in Figure 40 (B). Although the intensity in the GSS-bands is higher in comparison with the pattern observed for GSS-cortex, the electrophoretic mobility in both samples is similar, suggesting that there is not a significant difference in the PrP species content in both samples, cortex, and cerebellum. A closer view by bright-field TEM imaging of these samples

revealed similar amorphous aggregated oligomeric PrP species, similar to that observed in GSS-cortex samples. PrP species derived from the digestion with PE revealed high-density package of fibrillar-like structures (Figure 40, A-C). PrP species derived from the PK-digestion showed less amount of fibrillar-like structures when compared to PE-digestion (Figure 41, D-F). PrP species derived from TL-digestion showed a condensed pack of small fibrillar-like structures, in comparison to PE and PK digestions (Figure 41, G-H).

Immunoblot analysis of GSS-cortex and cerebellum samples enzymatically digested and PTA precipitated is shown in Figure 40 (D, E). For GSS-cortex, total PK-digestion is revealed, supporting the argument that PrP^{Sc} PK-sensitive species might be present in this sample. Only TL-digestion revealed three prominent bands, with a molecular weight at ~10–15 kDa, 21 kDa, and 27 kDa (Figure 40, D). For GSS-cerebellum, a faint band at ~8 kDa is revealed in all digestions, with TL-digestion generating highly prominent bands with a molecular weight similar to GSS-cortex samples, ~10–15 kDa, 21 kDa, and 27 kDa. (Figure 40, E). A further examination by the negative stain of PrP species and bright-field TEM imaging revealed GSS-cortex-PrP species derived from the digestion with TL revealed a prominent amount of fibrillar-like structures, densely packed (Figure 43, A-C). GSS-cerebellum-PrP species derived from the TL-digestion showed more ragged fibrillar-like structures when compared to PrP species derived from cortex samples (Figure 43, D-E). A GSS sample from cortex and cerebellum was left non-PK-digested (Figure 43, F).

5.6.4. Quantification of PrP^{Sc} concentration in the final purified product. To assess the concentration of PrP^{Sc} in the final PTA-precipitated pellet, a colorimetric ELISA was developed using the anti-prion monoclonal antibody D15.15 (epitope 175-186). Eight-standards with concentrations ranging from 0 to 2.5 μg/ml, were used to normalize the concentration of the samples. Each sample was run in triplicate. For PrP^{Sc} species derived from GSS samples, the concentration was 1.19 μg/ml and 1.23 μg/ml for cortex and cerebellum, respectively (Figure 19).

5.6.5. Assessment of prion infectivity in Tg(HuPrP) mice. Previous studies have shown that infectivity of brain samples derived from patients affected by prion diseases is determined by the animal model that is used. Inoculation of WT mice, which express mouse PrP, with prion species related to humans, which are composed of human PrP^{Sc}, leads to inefficient disease transmission

due to so-called species or transmission barrier effects. However, by using Tg mice that express human PrP can mitigate these effects, as they are susceptible to develop human prion disease. Another factor that influences the outcomes from transmissions studies is the presence of methionine or valine at residue 129, in both the inoculum and the mice.

In order to evaluate the level of prion infectivity present in the final PrP^{Sc} purified product derived from a patients diagnosed with GSS, who expressed the polymorphism A117V, a small inoculum derived from GSS-brain of affected patient was used to inoculate transgenic mice homozygous for human PrP (*Prnp* +/+) ((Tg(HuPrP) mice). Surprisingly, GSS-A117V inoculum showed an infectious profile, as the inoculated mice succumbed to the disease, displaying the characteristics symptoms, i.e., hunched, ataxic, scruffy coat and weight loss at 313 + 91 dpi for mice inoculated with 30-µl, 20% (w/v) (dilution 1/10) BH, and 282 + 87 dpi for those mice that were inoculated with 30-µl, 20% (w/v) (dilution 1/10) purified PrP^{Sc} (Table 6).

A cohort group of Tg(HuPrP) mice was maintained non-inoculated as negative controls. These results demonstrated that PrP^{Sc}-derived from GSS samples remained infectious. Immunoblot analysis of these PrP^{Sc} PK-resistant species present in Tg(HuPrP) mouse brain, revealed the presence of the characteristic ladder-like pattern of the three di-, mono-, and nonglycosylated isoforms (Figure 44). A further examination of these PrP species by negative stain and bright-field TEM imaging showed well-defined fibrillar structures, similar to previously reported amyloid fibrils (Figure 45).

5.7. Discussion

GSS is an uncommon adult-onset neurodegenerative disorder, that is inherited as an autosomal dominant trait and segregates with variant phenotypes resulting from the combination of a pathogenic mutation, like A117V, and a common polymorphism at codon 129 (M/V) in the *PRNP* gene. Previous studies have shown that a hallmark of GSS patients, regardless of the *PRNP* mutation, is the presence of low molecular weight N- and C- terminally truncated PrP fragments. Although these fragments can be detected in unprocessed brain homogenates, they are more evident

after PK-digestion. Hence, GSS is characterized by the accumulation of these PrP^{Sc} PK-resistant fragments of ~7 to 15 kDa in the brain, spanning residues ~81 to 150 [323,326].

In this study, the ~7 kDa PrP PK-resistant fragment was extracted from brain tissue of a patient diagnosed with GSS. These PrP species shared similar physicochemical properties of PrPres, i.e., insolubility in nondenaturing detergents, infectivity, and resistance to PK-digestion. Noteworthy, PrP^{Sc} was more prominent in preparations where methanol was used as precipitant, in comparison with PTA. Other PrP species with different molecular weights, ranging from ~7kDa to 17 kDa, were also detected. These findings are supported from previous observations that detergent-soluble fractions extracted from total brain homogenates contained ~60% of full-length PrP, and that were protease-sensitive, whereas the remainder of full-length molecules, and the N- and C- terminally truncated fragment of 16-17 kDa partitioned in the insoluble fractions. As expected, no PrP signal was observed when a brain homogenate from a healthy donor was submitted to this procedure [323].

Further examination by negative stain and bright-field TEM imaging revealed the presence of amorphous oligomeric aggregates and fibrillar-like structures. Regarding the structural integrity of the PrP species, no significant difference was visualized between methanol and PTA precipitation. Although methanol did precipitate more abundant PrP species and other non-PrP particles, that were binding to PrP species. Nevertheless, it cannot be inferred that these amorphous oligomeric aggregates are intermediates off-pathway during the fibrillization process.

Surprisingly, GSS PrP species showed an infectious profile, as Tg(HuPrP) mice that were inoculated with these particles, displayed the characteristic symptoms of prion disease and succumbed to the illness at similar times post-inoculation as previously reported [93]. Further analysis of these samples revealed the typical electrophoretic mobility profile and the fibrillar structure hallmark of prion fibrils. These findings allow the conclusion that infectivity of GSS-A117V PrP particles, follow a pattern of classical prion diseases.

5.8.   Figures
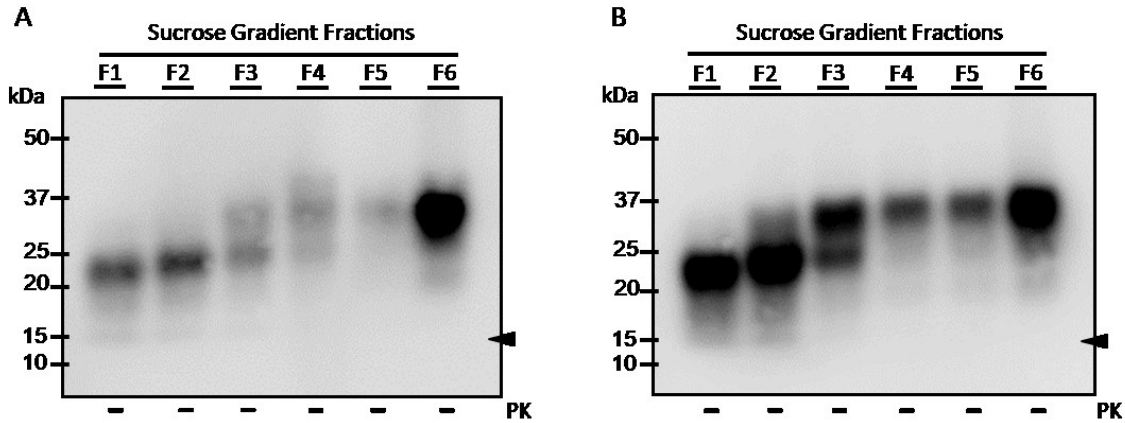
Figure 35. Immunoblots of GSS samples from cerebral cortex (A)-and cerebellum (B) derived from a patient affected by GSS and examined by sucrose fractionations coupled to ultracentrifugation. Final pellets obtained from non-PK digested and PTA-precipitated samples were passed through a cushion of sucrose gradient (40%, 60%, and 80%). The equivalent 5 μl of samples was loaded per lane. Species varying in molecular weight were detected in all fractions. The 16 and ~21 kDa bands were detected in the upper fraction of the sucrose gradient (~40%), in both, cortex and cerebellum (F1 and F2). Fractions corresponding to ~40-60% sucrose gradient (F3 and F4, for both samples) showed similar species, with molecular weights between 25-35 kDa. PrP species with higher molecular weight, between ~27-37 kDa, were found in the highest concentration of the sucrose gradient >60%, as well as a faint band corresponding to ~21 kDa species. Black arrows indicate the position of the 16-kDa PrP species.
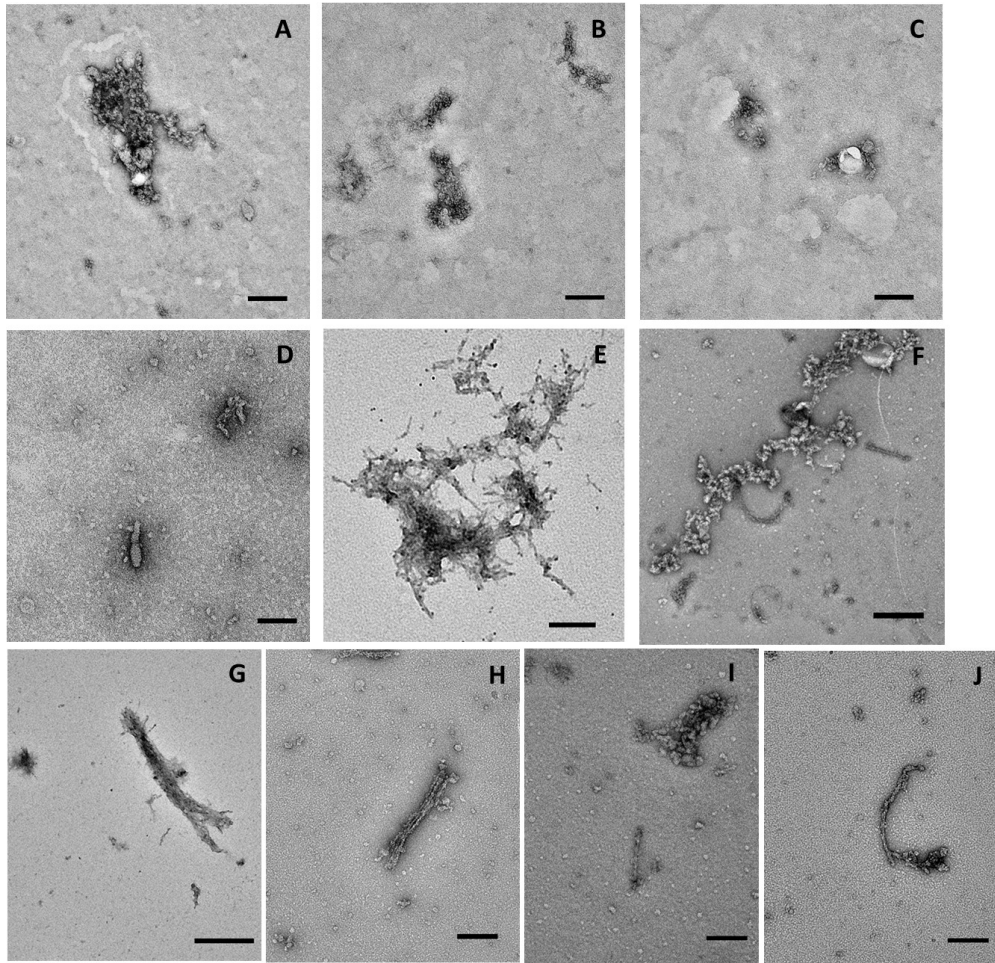
Figure 36. Bright-field TEM images of negatively stained PrP species derived from cortex tissue of a GSS-affected patient and purified by sucrose gradient fractionation. Negative stain was used to evaluate PrP species morphology and structural integrity after its purification. Amorphous oligomeric aggregates binding to lipids were found in the zonal fraction density at around 40% sucrose, as expected based on their similar buoyant density gradient ($\sim$1.0 g/cm^3) (A-D). Fibrillar-like structures were found in the zonal interface of around 60%-80% sucrose gradient, as it was expected since PrP species have a similar buoyant density as this sucrose fraction ($\sim$1.21. g/ml) (E-J). Scale bars, A-C, H-J: 200 nm; D-F: 100 nm; G: 500 nm.
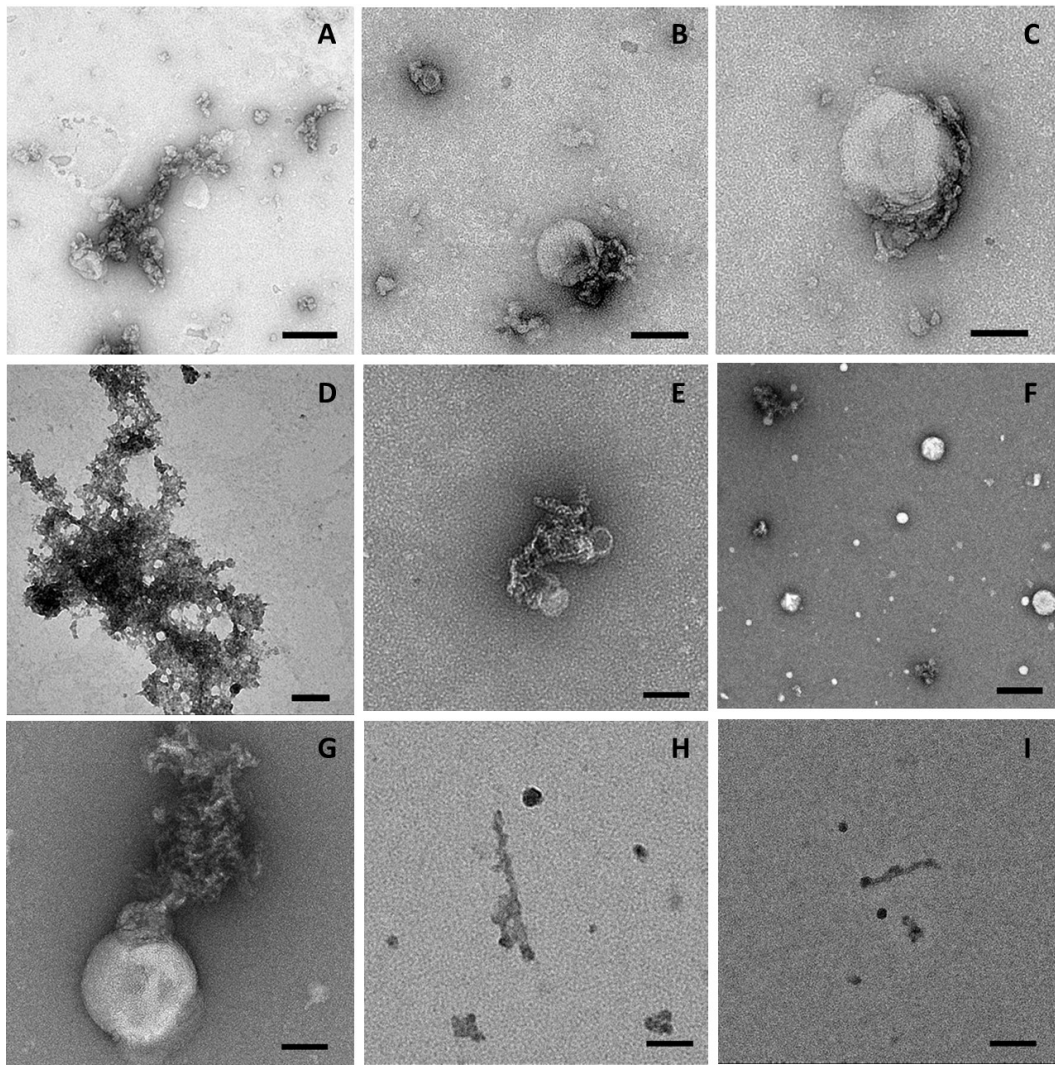
Figure 37. Bright-field TEM images of negatively stained PrP species derived from cerebellum tissue of a GSS-affected patient and purified by sucrose gradient fractionation. Negative stain was used to evaluate PrP species morphology and structural integrity after PTA-purification. Abundant lipids were found in the upper zone of the sucrose gradient, where amorphous oligomeric aggregates were binding to them. This zonal fraction density, at around 40% sucrose, has a similar buoyant density gradient to PrP^{Sc} (~1.006 g/ml) (A-G). Fibrillar-like structures were found in the zonal interface of around 60%-80% sucrose gradient, as was expected since PrP species have a similar buoyant density as this sucrose fraction (~1.21. g/ml) (H-I). Scale bars, A, D: 200 nm; B, C, E, G-I: 100 nm; F: 500 nm.
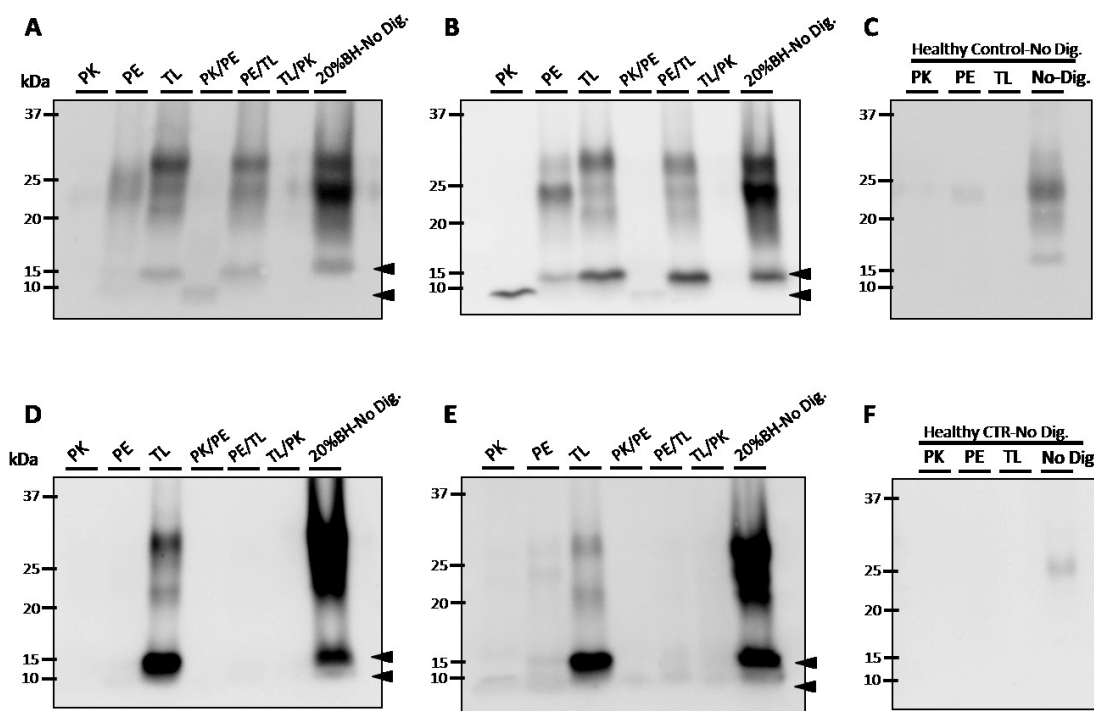
Figure 38. Immunoblot analysis of PrP content following digestion of GSS samples (cortex and cerebellum) with proteinase K (PK), thermolysin (TL) or pronase E (PE). 50-μg of GSS protein from cerebral cortex (A, D) and cerebellum (B, E) obtained from a patient affected by GSS and 50 μg of sample from cortex obtained from a healthy donor (C, F), were subjected to individual digestions using PK (25 μg/ml), PE (5 μg/ml), or TL (5 μg/ml). Sequential digestions were developed using a combination of two enzymes: PK/PE, PE/TL or TL/PK. Following the digestions, samples were precipitated by methanol or by PTA. (A-B) Methanol precipitates of lysates derived from cortex (A) showed a total digestion by PK, but identify a prominent 16 kDa species after TL and PE/TL digestions, and an 8 kDa species after PK/PE digestion. Similarly, lysates derived from cerebellum (B) showed an 8 kDa prominent species after PK and PK/PE digestions, and a 16 kDa species after PE, TL and PE/TL digestions. (D-E). PTA precipitates of lysates derived from cortex (D) identify a prominent 16 kDa species after TL digestion. Lysates derived from cerebellum (E) showed a faint 8 kDa species after PK, PE, PK/PE, PE/TL, TL/PK digestions, and a prominent 16 kDa species after TL digestion. Arrows indicate the position of the 8 kDa and 16 kDa PrP species. Samples that were maintained under non-PK-digested conditions are labeled as "No Dig.". Analyses were performed with Sha31 antibody.
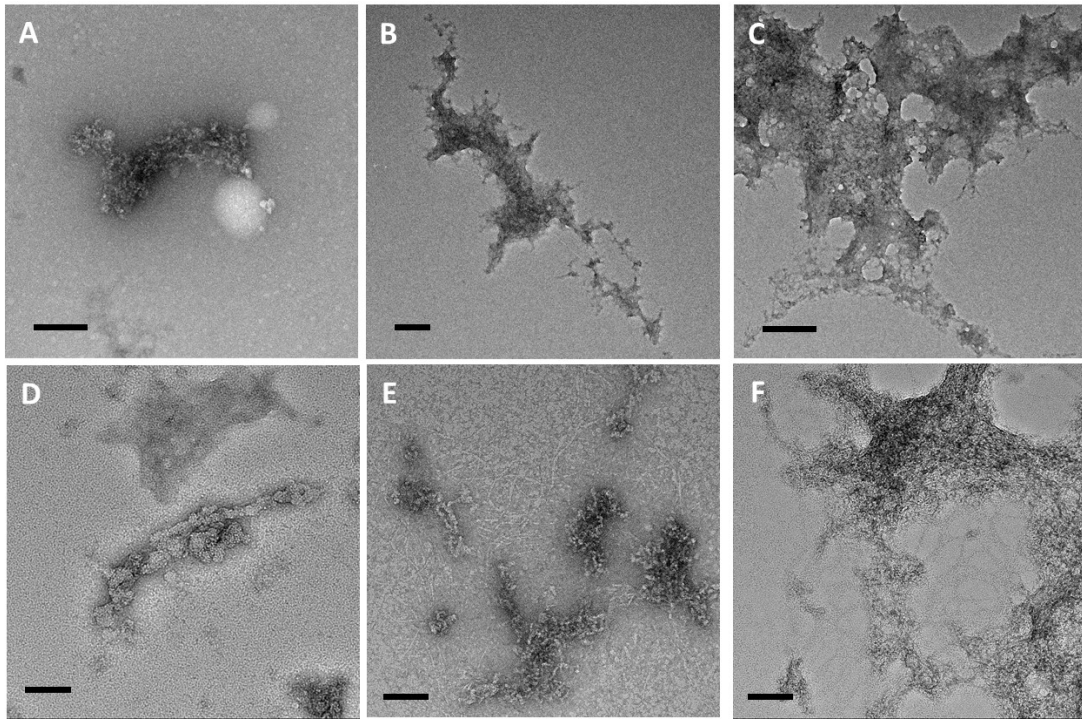
Figure 39. Bright-field TEM images of PrP content following digestion of GSS samples (cortex) with proteinase K (PK), thermolysin (TL) or pronase E (PE) and precipitated by methanol. Negative stain was used to evaluate PrP species morphology and structural integrity after enzymatic digestion and precipitated by methanol. (A, B) PrP species derived from the digestion with PE (5 µg/ml) revealed a high density pack of soluble oligomers and amorphous aggregates; (C, D) PrP species derived from the TL-digestion showed a more fibrillar-like structures, when compared to PE-digestion; (E, F) PrP species derived from a sequential enzymatic digestion with TL and PK (in that order) revealed a more fibrillar-like structures, highly aggregated and varying in size. Scale bars, A, B: 200 nm; C: 500 nm; D: 100 nm; E-F: 100 nm
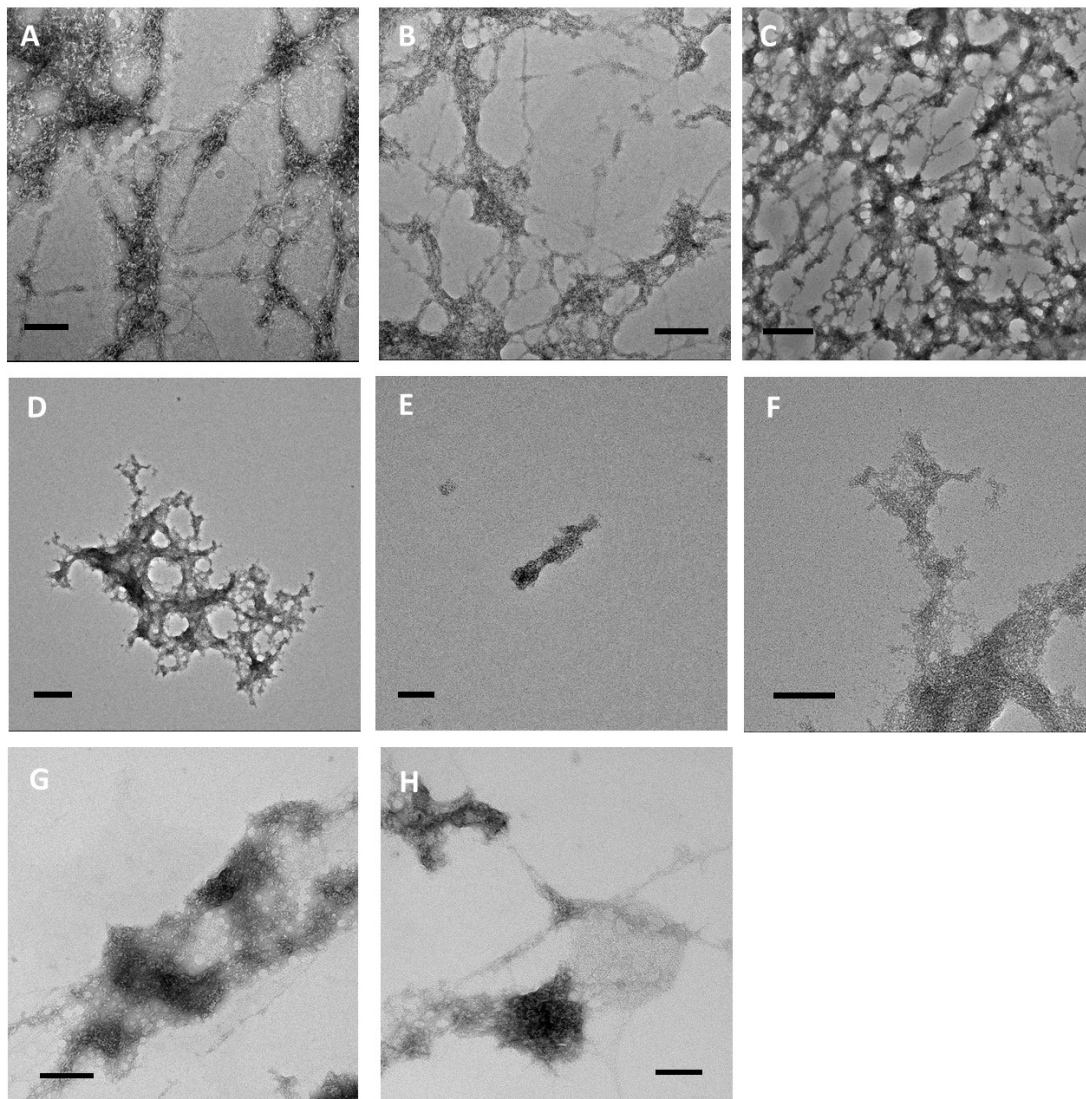
Figure 40. Bright-field TEM images of PrP content following digestion of GSS samples (cerebellum) with proteinase K (PK), thermolysin (TL) or pronase E (PE) and precipitated by methanol. Negative stain was used to evaluate PrP species morphology and structural integrity after enzymatically digested and precipitated by methanol. (A-C) PrP species derived from the digestion with PE (5 μg/ml) revealed a highly density package of fibrillar-like structures; (D-F) PrP species derived from the PK-digestion showed lower amount of fibrillar-like structures, when compared to PE-digestion; (G-H) PrP species derived from the TL-digestion showed a condensed pack of small fibrillar-like structures, in comparison to PE and PK digestions. Scale bars: A, B, G: 200 nm; C: 500 nm; D: 200 nm; E: 50 nm; F, H: 100 nm.
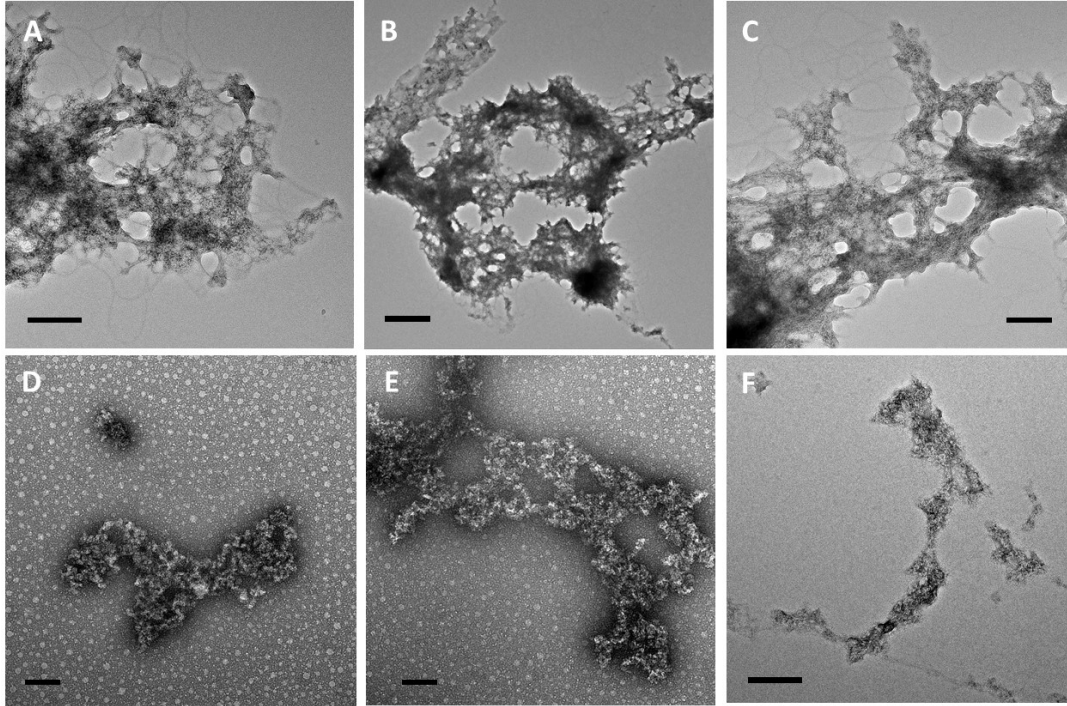
Figure 41. Bright-field TEM images of PrP content following digestion of GSS samples (cortex (A-C) and (D, E) cerebellum) with proteinase K (PK), thermolysin (TL) or pronase E (PE) and precipitated by PTA. Negative stain was used to evaluate PrP species morphology and structural integrity after enzymatic digestion and precipitation by PTA. (A-C) GSS-cortex-PrP species derived from the digestion with TL revealed a prominent amount of fibrillar-like structures, density packed; (D-E) GSS-cerebellum-PrP species derived from the TL-digestion showed a more ragged fibrillar-like structures, when compared to PrP species derived from cortex samples. (F) A GSS sample from cortex and cerebellum was maintained under non-PK-digested conditions. Scale bars, 200 nm.
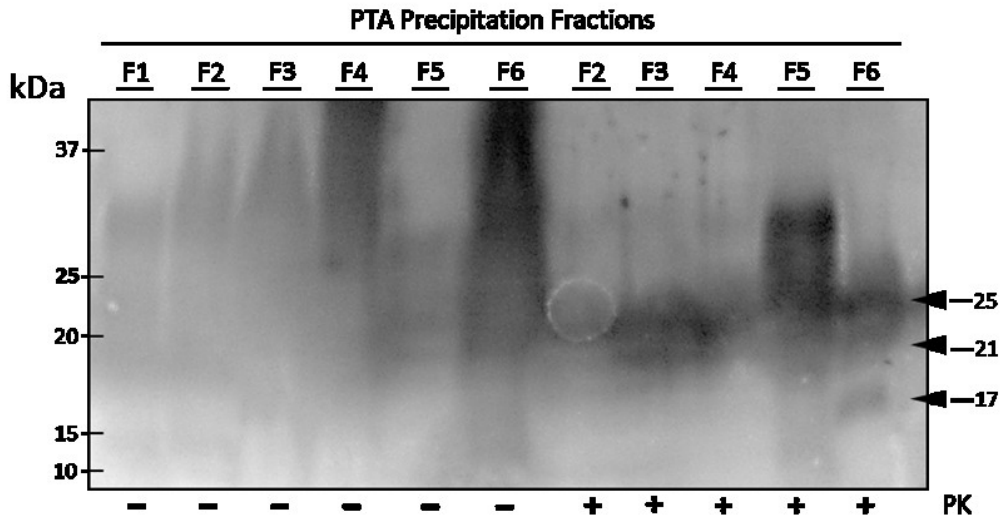
Figure 42. Immunoblot analysis of PrP species extracted from Tg(HuPrP) mouse brain were inoculated with PrP^{Sc} PK-resistant fragments and purified by PTA-precipitation from brain tissue derived from a patient affected by GSS. Tg(HuPrP) mice were inoculated with a 30-µl inoculum (dilution 1/10) derived from GSS derived from cortex. Tg(HuPrP) mice brains were subjected to limited proteolysis, followed by PTA-precipitation and analyzed at each step during the purification. The three characteristic PrP^{Sc} glycoform patterns (di-, mono-, and un-glycosylated) are revealed in the final purified product (F6) (black arrows), with molecular weights between ~17-27 kDa. The equivalent 5-µl 10% (w/v) BH and 5-µl samples were loaded per lane. F1: 20% BH, F2: 10% BH after first step of clarification; F3: after PK-digestion treatment; F4: first supernatant collected (not a first pellet was collected here); F5: second supernatant collected; and F6: final purified pellet. An alternative non-enzymatic digest control was carried out in parallel, where the samples were PTA-precipitated in a buffer containing proteases inhibitors and kept under non-PK enzymatic digestion conditions (second PTA-fractions F2-F6). +/- Symbols indicate when PK-digestion was applied during the purification.
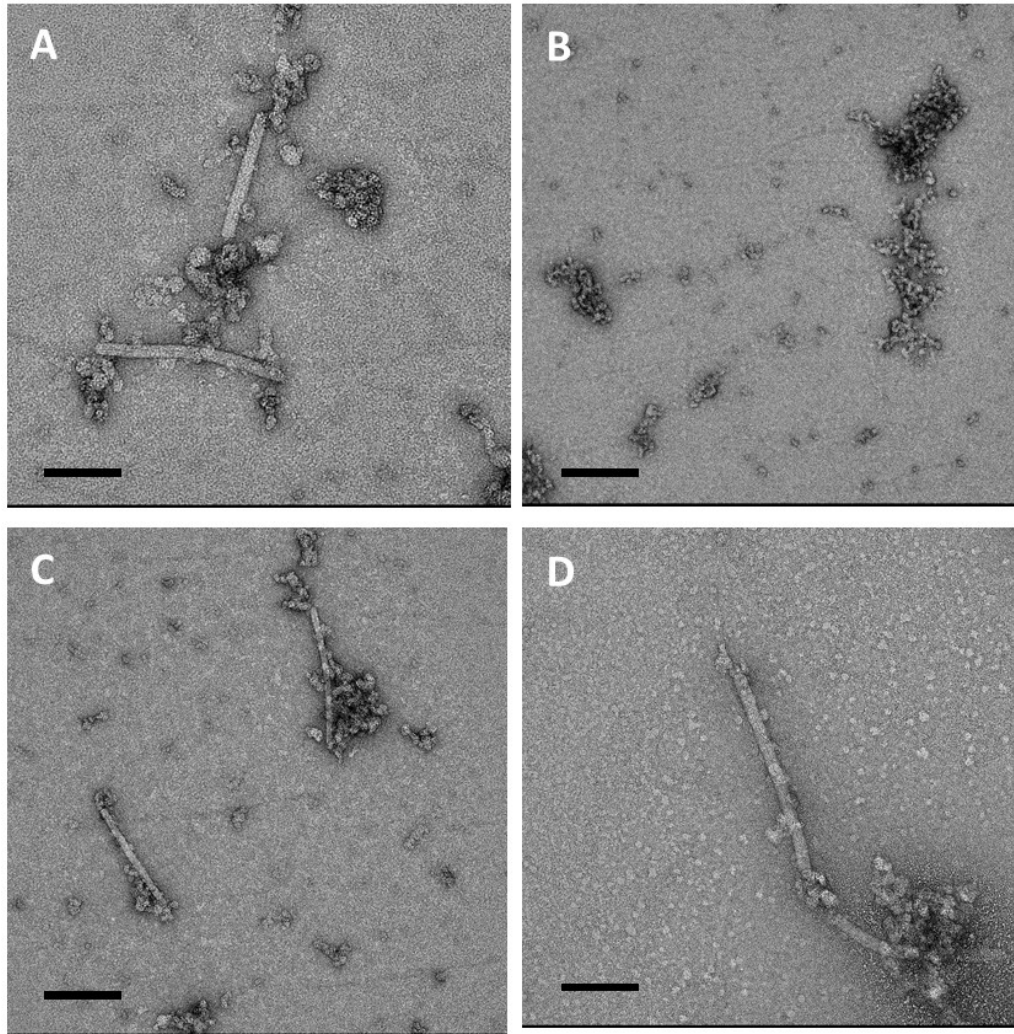
Figure 43. Bright-field TEM images of PrP^{Sc} PK-resistant species obtained from Tg(HuPrP) mice brain inoculated with PrP^{Sc} GSS species derived from cerebral cortex (A and B) or cerebellum (C and D). Scale bars: 200 nm

CHAPTER 6 CONCLUSIONS

> "I don't know anything, but I do know that everything is
> interesting if you go into it deeply enough."
>
> Richard Feynman

6.1. Summary

My interest in the study of prions was imprinted seven years ago when I was conducting a literature review on cancer. I was intrigued by how aberrant folding of proteins is linked to a vast list of pathologies, although their relationship in the development of diseases remains unknown. How do aggregates form and what are their structural properties? Are protein misfolding diseases a cause or a consequence of "a loss-of-function" or "toxic gain-of-function"? These questions intrigued me. I have a particular interest in the mechanisms of infectivity of prions; how misfolded proteins can self-assemble, and in a chain-reaction mechanism, spread themselves, becoming highly infectious. In this thesis, I focused on expanding our knowledge on the biology and particular characteristics of PrP species derived from the most common human prions diseases, fCJD, sCJD, and GSS, as well as to contribute in providing new constraints based on MPL measurements to evaluate the currently proposed models for the structure of PrP^{Sc}. This knowledge will provide insights into the conformational structure of PrP^{Sc} particles and their influence on the development of a variety of prion-like diseases. In the first chapter, I wrote a comprehensive review regarding the biology of prions, the effect of prions in the development of diseases in humans and animals, their conformational structural and the contributions and limitations of the state-of-the-art technology in elucidating the structure of the misfolded and infectious PrP^{Sc} particles. In chapter 2, I described the experimental procedures that were applied and / or developed during this project. In Chapters 3 and 4, examination of brain tissue derived from patients who suffered from fCJD and sCJD, respectively, revealed the characteristic fibrillar structure of these particles; as well MPL measurements provide new data that support a β-helix conformation for these particles. In chapter 4, I analyzed a human brain sample derived from a patient affected by GSS. Here, to characterize PrP species, the samples were fractionated and analyzed by enzymatic digestions followed by TEM imaging. Since each chapter contained a detailed discussion, I will only briefly review the results and present final thoughts regarding the current proposed structural models of PrP species. I will finish by discussing future directions that may help unravel the elusive structural conformation of PrP^{Sc} species.

6.2. Characterization of fCJD PrP^{Sc} species

Inherited prion diseases like fCJD are characterized by distinct disease phenotypes, neuropathological hallmarks, and pattern of PrP deposition. Immunoblot analysis of fCJD showed the typical ladder-like pattern of PK-resistant fragments, PrP27-30, cleaved at residues ~82 and ~97, with the three characteristics PrP bands corresponding to different glycosylation pattern. In this study, PrP species derived from brain tissue of a patient diagnosed with fCJD revealed an electrophoretic mobility profile running between ~16-27 kDa. Further examination of this sample by TEM imaging showed the typical fibrillar structures of these particles and MPL measurements of ~60 kDa/nm, suggesting a β-helix structural conformation. Evaluation of the infectivity of these particles in Tg(HuPrP) mice, revealed that in fact, these particles kept their infectious nature, a hallmark of prion particles. However, a higher resolution analysis would bring detailed information regarding the elusive nature of these particles.

6.3. Characterization of sCJD PrP^{Sc} species

In sCJD, PrP^{Sc} species separate into two main glycotypes: Type 1 and Type 2, with electrophoretic mobility profile of the nonglycosylated isoform at 21 and 19 kDa, respectively; regardless that both types show similar glycosylation profiles. In this study, PrP species obtained from brain tissue of four patients diagnosed with sCJD, revealed similar electrophoretic mobility profiles, with heterogeneous molecular weight. These findings provide evidence of the highly variable nature of these particles. Further examination by TEM imaging revealed the characteristic fibrillar structures, as well as abundant amorphous oligomeric aggregate deposits. Samples that displayed high concentrations of PrP^{Sc} fibrils and presented a well-defined fibrillar structure were chosen for MPL measurements. MPL values of ~60 kDa/nm suggested that these fibrils are organized in a β-helix structural conformation. Evaluation of their infectivity and transmission were determined in Tg(HuPrP) mouse bioassays, which revealed that these particles remain

infectious, a hallmark of prion particles. However, as aforementioned, a higher resolution analysis would bring detailed information regarding the elusive nature of these particles.

6.4. Characterization of GSS PrP^{Sc} species

Genetic prion diseases are inherited as an autosomal dominant trait and are clinically characterized by ataxia, cognitive impairment, and myoclonus (abrupt jerking movements of muscle groups and/or entire limbs). Three main phenotypes represent the core of genetic prion diseases: fCJD, FFI, and GSS. A typical hallmark GSS is the accumulation of PK-resistant fragments of ~7kDa to 15 kDa in the brain. The presence of mutations and/or polymorphisms determines the neuropathological features of the disease. In this study, PrP species purified from brain tissue of a patient with the A117V mutation who was heterozygous at codon 129 (M129V) were examined. In the first trials, non-digested, PTA-precipitated samples were passed through a sucrose gradient cushion. Highly heterogeneous PrP species were fractionated, based on their electrophoretic mobility, with molecular weights ranging from ~16 kDa to 37 kDa. A higher concentration of lipids was found in cerebellum fractions, with PrP species binding to them.

A close look at these PrP species by TEM imaging revealed highly amorphous oligomeric aggregates deposits and well-defined fibrils. Further assessment of these samples by a series of enzymatic digestions suggests that the species derived from cortex region are more sensitive to PK-digestion than those derived from cerebellum, as total digestion was revealed for samples from cortex, after PTA-precipitation and immunoblot analysis. No significant differences in the amount of non-PK-digested brain homogenate derived from both cortex and cerebellum were shown in the immunoblot, suggesting that PrP species derived from both regions were similar. These findings suggest brain tropism might affect the structural conformation of PrP species, regardless that they present the same neuropathological features. Examination of the PrP species digested revealed that GSS-cerebellum-PrP species derived from the TL-digestion showed more ragged fibrillar-like structures when compared to PrP species derived from cortex samples. Evaluation of the infectivity of these particles in Tg(HuPrP) mice, also revealed that in fact, these particles maintained their

infectious trait, a hallmark of prion particles. However, as aforementioned, a higher resolution analysis would bring detailed information regarding the elusive nature of these particles.

6.5. Elucidating the structure of PrP^{Sc} species: A new hope against misfolding diseases?

Elucidating the structure of amyloid fibrils will provide knowledge for the structure-based mechanisms of their molecular replication pathways. These findings will enable the generation of new structure-based drug design approaches in the development of therapeutic measures against prions and prions-like diseases, such as Alzheimer's disease (amyloid-β and tau), Parkinson's disease (α-synuclein), and Huntington's disease (Huntingtin), to name a few. Development of structure-based drug molecules needs to meet at least one of the three following requirements:
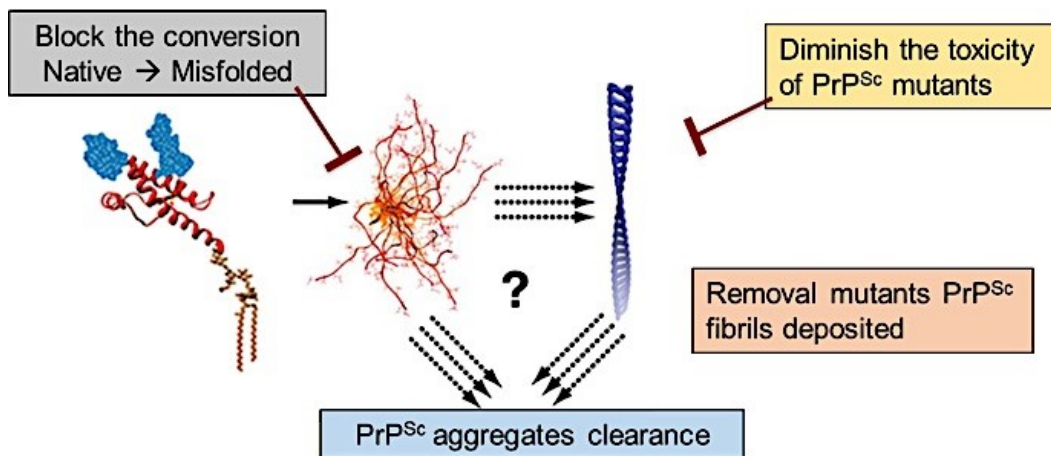
Figure 44. Proposed mechanisms for PrP^{Sc}-targeting compounds. Structure-based drug molecules. Small molecules selectively binding and stabilizing PrP^{C}, removal of mutant PrP^{Sc} fibrils deposited and / or diminishing their toxicity by binding to specific PrP-ligand antibodies, and removal of PrP^{Sc} aggregates by breakdown its products, followed by clearance, are among the proposed mechanisms for therapeutic measures for prion diseases (figure adapted from [327] and reprinted with permission from Bentham Publishers).

6.6 Future directions

Although prions have been recognized as infectious proteinaceous particles, little information is available regarding the conformational structural arrangement that they acquire. This gap in knowledge has limited our understanding regarding the molecular and biochemical properties of prion strains, the biological consequences they generate in the host, i.e., clinical symptoms, incubation periods, brain vacuolation profiles and PrP^{Sc} resistance to denaturation and proteolysis.

The results presented here do not account for the clinical stage of the disease. However, these findings may suggest that there are not any significant structural differences between PrP^{Sc} fibrils affecting cortex and cerebellum in patients affected by prion diseases. Hence, different neuropathological phenotype might be due to strain-specific accumulation pattern due to brain tropism that induces differential toxicity. Further analysis using a higher resolution technique might provide more detailed information regarding the conformational structure of PrP 27-30 fibrils involved in each disease and delineate a more accurate neuropathological profile that eventually leads to the development of the disease.
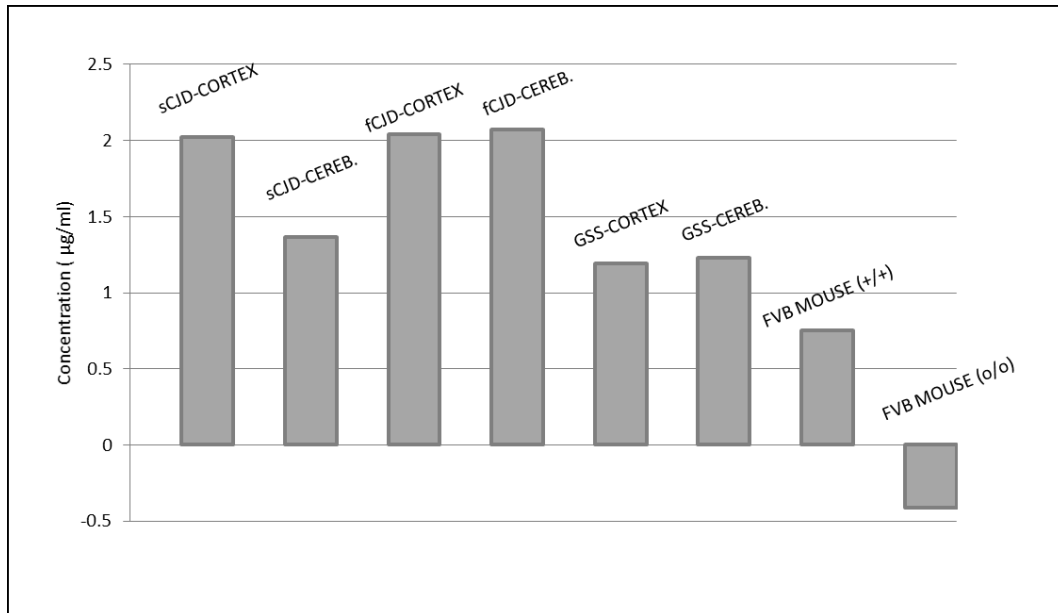
Figure S1. Quantification by ELISA of the relative concentration of PrP species in the final pellet purified by PTA-precipitation. Samples analyzed (from left to right): 1) sCJD cortex and cerebellum (case 3); 2) fCJD sample from cortex and cerebellum; 3) GSS sample from cortex and cerebellum; 4) wild-type FVB mouse expressing human PrPC (*Prnp* +/+) used as positive control; and 5) PrPC-null FVB mice (*Prnp* -/-) used as negative control.

References

1. Prusiner S. Shattuck Lecture- Neurodegenerative diseases and prions. *N Engl J Med*. 2001; 344(20): 1516-1526.

2. Weissmann C. The state of the prion. *Nat Rev Microbiol*. 2004; 2: 861-871.

3. Zomosa-Signoret V, Arnaud JD, Fontes P, Alvarez-Martinez MT, Liautard JP. Physiological role of the cellular prion protein. *Vet Res*. 2008; 39(09): 1-16.

4. Prusiner S. Novel proteinaceous infectious particles cause scrapie. *Science*. 1982; 216(4542): 136-144.

5. Mastrianni JA. The genetics of prion diseases. *Genet Med*. 2010; 12(4): 187-195.

6. Perrett D. From "protein" to the beginnings of clinical proteomics. *Proteomics Clin Appl*. 2007; 1(8): 720-738.

7. Tanford C, Reynolds J. Nature's Robots: A History of proteins. *Oxford Univ Press*. 2001; 30(5): 336-345.

8. Drews G. The roots of microbiology and the influence of Ferdinand Cohn on microbiology of the 19th century. *FEMS*. 2000; 24: 225-249.

9. Koch R. Die Ätiologie der Tuberkulose. *Berliner Klin Wochenschrift*. 1882; 19(15).

10. Piro A, Tagarelli A, Tagarelli G, Lagonia P, Quattrone A. Paul Ehrlich: The Nobel Prize in physiology or medicine 1908. *Int Rev Immunol*. 2008; 27(1-2): 1-17.

11. Lecoq H. Découverte du premier virus, le virus de la mosaïque du tabac : 1892 ou 1898? *Comptes Rendus l'Académie des Sci - Ser III - Sci la Vie*. 2001; 324(10): 929-933.

12. Hershey AD, Chase M. Independent functions of viral protein and nucleic acid in growth of bacteriophage. *J Gen Physiol*. 1952; 36(1): 39-56.

13. Watson JD, Crick FHC. Molecular structure of nucleic acids: A structure for deoxyribose nucleic acid. *Nature*. 1953; 171(4356): 737-738.

14. Koonin E. Does the central dogma still stand? *Koonin Biol Direct*. 2012; 7(27): 1-7.

15. Liberski PP. Kuru: A journey back in time from Papua New Guinea to the Neanderthals' extinction. 2013; 2: 472-505.

16. Fraenkel-Conrat H, Williams RC. Reconstitution of active tobacco mosaic virus from its inactive protein and nucleic acid components. *Biochemistry*. 1955; 41: 690-698.

17. Eklund C, Kennedy R, Hadlow W. Pathogenesis of scrapie virus infection in the mouse. *J Infect Dis*. 1967; 117(1): 15-22.

18. Gajdusek D. Slow-virus infections of the nervous system. *N Engl J Med*. 1967; 276(7): 392-400.

19. Zabel M, Reid C. A brief history of prions. *FEMS Pathog Dis*. 2015; 73(9): 1-8.

20. Charrel R, Attoui H, Butenko A, *et al*. Tick-borne virus diseases of human interest in Europe. *Clin Microbiol Infec*. 2004; 10(12): 1040-1055.

21. Gordon W. Advances in veterinary research. Looping ill, tick-born fever and scrapie. *Vet Rec*. 1946; 58: 516-525.

22. Creutzfeldt H. Über eine eigenartige herdförmige erkrankung des zentralnervensystems (Vorläufige mitteilung). *Zeitschrift für die gesamte Neurol und Psychiatr*. 1920; 57(1): 1-18.

23. Jakob A. Über eigenartige erkrankungen des zentralnervensystems mit bemerkenswertem anatomischen befunde. *Zeitschrift für die gesamte Neurol und Psychiatr*. 1921; 64(1): 147-228.

24. Budka H. Neuropathology of prion diseases. *Brit Med Bull*. 2003; 66(1): 121-130.

25. Manix M, Kalakoti P, Henry M, *et al.* Creutzfeldt-Jakob disease: Updated diagnostic criteria, treatment algorithm, and the utility of brain biopsy. *Neurosurg Focus*. 2015; 39(5): 1-11.

26. Gerstmann J, Sträussler E, Scheinker I. Über eine eigenartige hereditär- familiäre Erkrankung des Zentralnervensystems. *Zeitschrift für die gesamte Neurol und Psychiatr*. 1935; 154(1): 736-762.

27. Will R. Epidemiology of Creutzfeldt-Jakob disease. *Br Med Bull*. 1993; 49(4): 960-970.

28. Brown P, Cathala F, Castaigne P, Gajdusek D. Creutzfeldt-Jakob disease: Clinical analysis of a consecutive series of 230 neuropathologically verified cases. *Ann Neurol*. 1986; 20: 597-602.

29. Duffy P, Wolf J, Collins G, DeVoe A, Streeten B, Cowen D. Possible person-to-person transmission of Creutzfeldt-Jakob disease. *N Engl J Med*. 1974; 290: 692-693.

30. Will R. Acquired prion disease : iatrogenic CJD, variant CJD, kuru. *Brit Med Bull*. 2003; 66: 255-265.

31. Will R, Ironside J, Zeidler M, *et al*. A new variant of Creutzfeldt-Jakob disease in the UK. *Lancet*. 1996; 347: 921-925.

32. Lindenbaum S. An annotated history of kuru. *Med Antrop Theory*. 2009; (1): 95-127.

33. Whitfield J, Pako W, Collinge J, Alpers M. Mortuary rites of the South Fore and kuru. *Philos Trans R Soc B Biol Sci*. 2008; 363(1510): 3721-3724.

34. Plummer P. Scrapie-A disease of sheep. *Can J Comp Med Vet Sci*. 1946; 10(2): 49.

35. Greenlee J. Update on classical and atypical scrapie in sheep and goats. *Vet Pathol*. 2019; 56(1): 6-16.

36. Hadlow W. Scrapie and kuru. *Lancet*. 1959; 274(7097): 289-290.

37. Alpers MP. A history of kuru. *Papua New Guinea Med J*. 2007; 50(1-2): 10-19.

38. Dickinson AG, Mackay J. Genetical control of the incubation period in mice of the neurological disease, scrapie. *Heredity*. 1963; 19: 279-288.

39. Hunter G, Millson G. Studies on the heat stability and chromatographic behaviour of the scrapie agent. *J Gen Microbiol*. 1964; 37: 251-258.

40. Pattison IH. Resistance of the scrapie agent to formalin. *J Comp Pathol*. 1965; 75(2): 159-164.

41. Alper T, Haig DA, Clarke MC. The exceptionally small size of the scrapie agent. *Biochem Biophys Res Commun*. 1966; 22(3): 278-284.

42. Pattison IH, Jones KM. The possible nature of the transmissible agent of scrapie. *Vet Rec*. 1967; 80(1): 2-9.

43. Griffith J. Nature of the scrapie agent: Self-replication and scrapie. *Nature*. 1967; 215(5105): 1043-1044.

44. Hunter G, Gibbons R, Kimberlin R, Millson G. Further studies of the infectivity and stability of extracts and homogenates derived from scrapie affected mouse brains. *J Comp Pathol*. 1969; 79(1): 101-108.

45. Prusiner S, Hadlow W, Garfin D, *et al.* Partial purification and evidence for multiple molecular forms of the scrapie agent. *Biochemistry*. 1978; 17(23): 4993-4999.

46. Bolton D, McKinley M, Prusiner S. Identification of a protein that purifies with the scrapie prion. *Science*. 1982; 218(4579): 1309-1311.

47. Prusiner S, Bolton D, Groth D, Bowman K, *et al.* Further purification and characterization of scrapie prions. *Biochemistry*. 1982; 21(26): 6942-6950.

48. Masters C, Harris J, Gajdusek D, Gibbs C, Bernoulli C, Asher D. Creutzfeldt-Jakob disease: Patterns of worldwide occurrence and the significance of familial and sporadic clustering. *Ann Neurol*. 1979; 5(2): 177-188.

49. Schoene W, Masters C, Gibbs CJ Jr, *et al.* Transmissible spongiform encephalopathy (Creutzfeldt-Jakob disease): Atypical clinical and pathological findings. *Arch Neurol*. 1981; 38(8): 473-477.

50. Owen F, Poulter M, Shah T, *et al*. An in-frame insertion in the prion protein gene in familial Creutzfeldt-Jakob disease. *Mol Brain Res*. 1990; 7(3): 273-276.

51. Schenkein J, Montagna P. Self-management of fatal familial insomnia. Part 2: case report. *MedGenMed*. 2006; 8(3): 66.

52. Montagna P, Gambetti P, Cortelli P, Lugaresi E. Familial and sporadic fatal insomnia. *Lancet Neurol*. 2003; 2: 167-176.

53. Chesebro B, Race R, Wehrly K, *et al*. Identification of scrapie prion protein-specific mRNA in scrapie-infected and uninfected brain. *Nature*. 1985; 315(6017): 331-333.

54. Oesch B, Westaway D, Wälchli M, *et al*. A cellular gene encodes scrapie PrP 27-30 protein. *Cell*. 1985; 40(4): 735-746.

55. Wille H, Bian W, McDonald M, *et al.* Natural and synthetic prion structure from X-ray fiber diffraction. *PNAS*. 2009; 106(40): 16990-16995.

56. Büeler H, Fischer M, Lang Y, *et al*. Normal development and behaviour of mice lacking the neuronal cell-surface PrP protein. *Nature*. 1992; 356(6370): 577-582.

57. Wilesmith J, Wells G, Cranwell M, Ryan J. Bovine spongiform encephalopathy: epidemiological studies. *Vet Rec*. 1988; 123(25) :638-644.

58. Prusiner S, Groth D, Serban A, *et al.* Ablation of the prion protein (PrP) gene in mice prevents scrapie and facilitates production of anti-PrP antibodies. *PNAS*. 1993; 90: 10608-10612.

59. Aucouturier P, Carp R, Carnaud C, Wisniewski T. Prion diseases and the immune system. *Clin Immunol*. 2000: 96(2): 79-85.

60. Collinge J, Sidle K, Meads J, Ironside J, Hill A. Molecular analysis of prion strain variation and the aetiology of "new variant" CJD. *Nature*. 1996; 383(6602): 685-690.

61. Moore R, Hope J, McBride P, *et al*. Mice with gene targetted prion protein alterations show that Prnp, Sinc and Prni are congruent. *Nat Genet*. 1998; 18: 118-125.

62. Deleault N, Geoghegan J, Nishina K, Kascsak R, Williamson R, Supattapone S. Protease-resistant Prion Protein Amplification Reconstituted with Partially Purified Substrates and Synthetic Polyanions. *J Biol Chem*. 2005; 280(29): 26873-26879.

63. Barria M, Mukherjee A, Gonzalez-romero D, Morales R, Soto C. De novo generation of infectious prions *in vitro* produces a new disease phenotype. *PLoS Pathog*. 2009; 5(5): 1-10.

64. Ma J, Wang F. Prion disease and the 'protein-only hypothesis.' *Essays Biochem*. 2014; 56: 181-191.

65. Zhang Z, Zhang Y, Wang F, *et al.* De novo generation of infectious prions with bacterially expressed recombinant prion protein. *FASEB J*. 2013; 27: 4768-4775.

66. Collinge J. Prion Diseases of humans and animals: Their causes and molecular basis. *Annu Rev Neurosci*. 2001; 24(1): 519-550.

67. Peretz D, Supattapone S, Giles K, *et al.* Inactivation of prions by acidic sodium dodecyl sulfate. *J Virol*. 2006; 80(1): 322-331.

68. Morales R. Prion strains in mammals : Different conformations leading to disease. *PLoS Pathog*. 2017; 13(7): 1-5.

69. Seuring C, Greenwald J, Wasmer C, *et al*. The Mechanism of toxicity in HET-S/HET-s prion incompatibility. *PLoS Biol*. 2012; 10(12): 1-18.

70. Lacroute F. Non-Mendelian mutation allowing ureidosuccinic acid uptake in yeast. *J Bacteriol*. 1971; 106(2): 519-522.

71. Wickner R, Masison D, Edskes H. [PSI+] and [URE3] as Yeast prions. *Yeast*. 1995; 11: 1671-1685.

72. Derkatch I, Bradley M, Hong J, Liebman S. Prions affect the appearance of other prions : The Story of [PIN+]. *Cell*. 2001; 106: 171-182.

73. Cox B. Ψ, A cytoplasmic suppressor of super-suppressor in yeast. *Heredity*. 1965; 20(4): 505-521.

74. Roberts B, Wickner R. Heritable activity : a prion that propagates by covalent autoactivation. *Genes Dev*. 2003; 17: 2083-2087.

75. Brown J, Lindquist S. A heritable switch in carbon source utilization driven by an unusual yeast prion. *Genes Dev*. 2009; 23: 2320-2332.

76. Rogoza T, Goginashvili A, Ivanov M, *et al*. Non-Mendelian determinant [ISP+] in yeast is a nuclear-residing prion form of the global transcriptional regulator Sfp1. *PNAS*. 2010; 107(23): 10573-10577.

77. Wickner RB, Edskes HK, Roberts BT, *et al.* Prions: Proteins as genes and infectious entities. *Genes Dev*. 2004; 18(5): 470-485.

78. Holmes D, Lancaster A, Lindquist S, Halfmann R. Heritable remodeling of yeast multicellularity by an environmentally responsive prion. *Cell*. 2013; 153(1): 153-165.

79. Wickner RB, Edskes HK, Maddelein M, Taylor KL, Moriyama H. Prions of yeast and fungi. 1999; (1): 555-559.

80. Du Z, Zhang Y, Li L. The Yeast Prion [SWI+] abolishes multicellular growth by triggering conformational changes of multiple regulators required for flocculin gene expression. *Cell Rep*. 2015; 13: 2865-2878.

81. Cox B. Cytoplasmic Inheritance: Prion-like factors in yeast. *Curr Biol*. 1994; 4(8): 744-748.

82. Glover J, Kowal A, Schirmer E, Patino M, Liu J, Lindquist S. Self-seeded fibers formed by Sup35, the protein determinant of [PSI+], a heritable prion-like factor of *S*. *cerevisiae*. *Cell*. 1997; 89: 811-819.

83. Liebman S, Chernoff Y. Prions in Yeast. *Genetics*. 2012; 191: 1041-1072.

84. Wickner R, Shewmaker F, Bateman D, *et al*. Yeast prions : Structure , biology , and prion-handling systems. *Microbiol Mol Biol Rev*. 2015; 79(1): 1-17.

85. Wiliams E, Young S. Chronic Wasting Disease of captive mule deer: A spongiform encephalopathy. *J Wildl Dis*. 2013; 16(1): 89-98.

86. Collee JG, Bradley R, Liberski PP. Variant CJD (vCJD) and bovine spongiform encephalopathy (BSE): 10 and 20 years on: part 2. *Folia Neuropathol*. 2006; 44(2): 102-110.

87. Wyatt J, Pearson G, Smerdon T, Gruffydd-Jones T, Wells G, Wilesmith J. Naturally occurring scrapie-like spongiform encephalopathy in five domestic cats. *Vet Rec*. 1991; 129(11): 233-236.

88. Cunningham A, Kirkwood J, Dawson M, Spencer Y, Green R, Wells G. Bovine Spongiform

Encephalopathy infectivity in Greater Kudu (Tragelaphus strepsiceros). *Emerg Infect Dis*. 2004; 10(6): 1044-1049.

89.   Spiropoulos J, Lockey R, Sallis R, *et al.* Isolation of prion with BSE properties from farmed goat. *Emerg Infect Dis*. 2011; 17(12): 2253-2261.

90.   Wood J, Lund L, Done S. The natural occurrence of scrapie in moufflon. *Vet Rec*. 1992; 130(2): 25-27.

91.   Wilson D, Anderson R, Smith W. Studies in scrapie. *J Comp Pathol*. 1950; 60(4): 267-282.

92.   Kimberlin R, Marsh R. Comparison of scrapie and transmissible mink encephalopathy in hamsters. Biochemical studies of brain during development of disease. *J Infect Dis*. 1975; 131(2): 97-103.

93.   Liberski P. Gerstmann-Sträussler-Scheinker disease. In: Ahmad S, ed. *Neurodegenerative Diseases. Advances in Experimental Medicine and Biology*. New York, NY: Springer; 2012: 128-137.

94.   Parry H. Scrapie: A transmissible and hereditary disease of sheep. *Heredity*. 1962; 17(1): 75-105.

95.   Dickinson AG, Stamp JT, Renwick CC. Maternal and lateral transmission of scrapie in sheep. *J Comp Pathol*. 1974; 84(1): 19-25.

96.   Deleault N, Harris B, Rees J, Supattapone S. Formation of native prions from minimal components in vitro. *PNAS*. 2007; 104(23): 9741-9746.

97.   Wells G, Scott A, Johnson C, *et al*. A novel progressive spongiform encephalopathy in cattle. *Vet Rec*. 1987; 121(18): 419-420.

98.   Bruce M, Will R, Ironside J, *et al*. Transmissions to mice indicate that 'new variant' CJD is caused by the BSE agent. *Nature*. 1997; 389(6650): 498-501.

99.   Ryou C. Prions and prion diseases : Fundamentals and mechanistic details. *J Microbiol Biotechnol*. 2007; 17(7): 1059-1070.

100.   Prusiner S. Molecular biology of prion diseases. *Science*. 1991; 252(5012): 1515-1522.

101.   Jeffrey M, Halliday W, Bell J, *et al.* Synapse loss associated with abnormal PrP precedes neuronal degeneration in the scrapie-infected murine hippocampus. *Neuropathol Appl Neurobiol*. 2000; 26(1): 41-54.

102.   Jeffrey M, González L. Classical sheep transmissible spongiform encephalopathies: Pathogenesis, pathological phenotypes and clinical disease. *Neuropathol Appl Neurobiol*. 2007; 33(4): 373-394.

103.   Hourrigan J, Klingsporn A. Scrapie: Studies on Vertical and Horizontal Transmission. In: Gibbs CJ, ed. *Bovine Spongiform Encephalopathy: The BSE Dilemma*. New York, NY: Springer New York; 1996: 59-83.

104.   Burger D, Hartsough G. A scrapie-like disease of mink. In: Agriculture USD of, ed. *Report of a Scrapie Seminar. ARS 91-53*. 27th ed.; 1964: 641-645.

105. Williams E, Young S. Spongiform Encephalopathy of Rocky Mountain Elk. *J Wildl Dis*. 2013; 18(4): 465-471.

106. Imran M, Mahmood S. An overview of human prion diseases. *Virol J*. 2011; 8(559): 1-9.

107. Wilesmith J, Wells G. Bovine Spongiform Encephalopathy. In: Chesebro B.W., ed. *Transmissible Spongiform Encephalopathies: Current Topics in Microbiology and Immunology*. Vol 172. Berlin, Heidelberg: Springer; 1991; (172): 21-38.

108. Hill A, Desbruslais M, Joiner S, *et al.* The same prion strain causes vCJD and BSE. *Nature*. 1997; 389(6650): 448-450.

109. Soto C. Unfolding the role of protein misfolding in neurodegenerative diseases. *Nat Rev Neurosci*. 2003; 4(1): 49-60.

110. Pastore A, Zagari A. A structural overview of the vertebrate prion proteins. *Prion*. 2007; 1(3): 185-197.

111. Public Health Agency of Canada. CJD Statistics. *PHAC*. 2019; 1-4.

112. Kirschbaum W. Zwei eigenartige Erkrankung des Zentralnervensystems nach Art der spatischen Pseudosklerose (Jakob). *Z Neurol Psyciath*. 1924; 92: 175-220.

113. Gambetti P, Puoti G, Zou W. Variably protease-sensitive prionopathy: A novel disease of the prion protein. *J Mol Neurosci*. 2011; 45(3): 422-424.

114. Budka H. *Histopathology and Immunohistochemistry of Human Transmissible Spongiform Encephalopathies (TSEs)*. Vol 16. Prion Dise. (Groschup M, Kretzschmar H, eds.). Vienna: Springer; 2000.

115. Ironside J, McCardle L, Horsburgh A, Lim Z, Head M. Pathological diagnosis of variant Creutzfeldt-Jakob disease. *APMIS*. 2002; 110: 79-87.

116. Kovacs GG, Budka H. Molecular Pathology of Human Prion Diseases. 2009; (1): 976-999.

117. Schleeger M, Corianne C, Deckert-Gaudig T, *et al.* Amyloids : From molecular structure to mechanical properties. *Polymer*. 2013; 54(10): 2473-2488.

118. Greenwald J, Riek R. Biology of amyloid: Structure, function, and regulation. *Structure*. 2010; 18: 1244-1260.

119. Jackson M, Hewitt E. Why are functional amyloids non-toxic in humans? *Biomolecules*. 2017; 7(4): 1-13.

120. Chapman M, Robinson L, Pinkner J, *et al.* Role of *Escherichia coli* Curli Operons in Directing Amyloid Fiber Formation. *Science*. 2002; 295: 851-855.

121. Mankar S, Anoop A, Sen S, Maji SK. Nanomaterials: amyloids reflect their brighter side. *Nano Rev*. 2011; 2(6032): 1-12.

122. True H, Lindquist S. A yeast prion provides a mechanism for genetic variation and phenotypic diversity. *Nature*. 2000; 407(6803): 477-483.

123. Kenney JM, Knight D, Wise MJ, Vollrath F. Amyloidogenic nature of spider silk. *Eur J Biochem*. 2002; 269(16): 4159-4163.

124. Hee JS, Mitchell SM, Liu X, Leonhardt RM. Melanosomal formation of PMEL core amyloid is driven by aromatic residues. *Sci Rep*. 2017; 7: 1-15.

125. Seth R, Sun L, Ea C, Chen Z. Identification and characterization of MAVS, a mitochondrial antiviral signaling protein that activates NF-κB and IRF3. *Cell*. 2005; 122(5): 669-682.

126. Zeng L, Zou W, Wang G. Cellular prion protein (PrPC) and its role in stress responses. *Int J Clin Exp Med*. 2015; 8(5): 8042-8050.

127. Mouillet-Richard S, Ermonval M, Chebassier C, *et al*. Signal transduction through prion protein. *Science*. 2000; 289(5486): 1925-1928.

128. LaCasse RA, Striebel JF, Favara C, Kercher L, Chesebro B. Role of Erk1/2 activation in prion disease pathogenesis: Absence of CCR1 leads to increased Erk1/2 activation and accelerated disease progression. *J Neuroimmunol*. 2008; 196(1-2): 16-26.

129. Rachidi W, Vilette D, Guiraud P, *et al.* Expression of prion protein increases cellular copper binding and antioxidant enzyme activities but not copper delivery. *J Biol Chem*. 2003; 278(11): 9064-9072.

130. Didonna A, Sussman J, Benetti F, Legname G. The role of Bax and caspase-3 in doppel-induced apoptosis of cereellar granule cells. *Prion*. 2012; 6(3): 309-311.

131. Spudich A, Frigg R, Kilic E, *et al.* Aggravation of ischemic brain injury by prion protein deficiency: Role of ERK-1/-2 and STAT-1. *Neurobiol Dis*. 2005; 20(2): 442-449.

132. Grad LI, Cashman NR. Prion-like activity of Cu/Zn superoxide dismutase Implications for amyotrophic lateral sclerosis. *Prion*. 2014; 8(1): 33-41.

133. Bragason B, Palsdottir A. Interaction of PrP with NRAGE, a protein involved in neuronal apoptosis. *Mol Cell Neurosci*. 2005; 29(2): 232-244.

134. Puig S, Thiele D. Molecular mechanisms of copper uptake and distribution. *Curr Opin Chem Biol*. 2002; 6(2): 171-180.

135. Tsui-Pierchala B, Encinas M, Milbrandt J, Johnson Jr E. Lipid rafts in neuronal signaling and function. *Trends Neurosci*. 2002; 25(8): 412-417.

136. Schmitt-Ulms G, Legname G, Baldwin M, *et al*. Binding of neural cell adhesion molecules (N-CAMs) to the cellular prion protein. *J Mol Biol*. 2001; 314(5): 1209-1225.

137. Faris R, Moore RA, Ward A, *et al.* Cellular prion protein is present in mitochondria of healthy mice. *Sci Rep*. 2017; 7(41556): 1-16.

138. Manson J, West J, Thomson V, McBride P, Kaufman M, Hope J. The prion protein gene: a role in mouse embryogenesis? *Development*. 1992; 115(1): 117-122.

139. Moser M, Colello R, Pott U, Oesch B. Developmental expression of the prion protein gene in glial cells. *Neuron*. 1995; 14(3): 509-517.

140. Westergard L, Christensen H, Harris D. The cellular prion protein (PrPC): Its physiological

function and role in disease. *Biochim Biophys Acta*. 2007; 1772(6): 629-644.

141. Otvos L, Cudic MJ. Post-Translational Modifications in Prion Proteins. *Curr Protein Pept Sci*. 2002; 3(6): 643-652.

142. Watt N, Taylor D, Kerrigan T, *et al.* Prion protein facilitates uptake of zinc into neuronal cells. *Nat Commun*. 2012; 3(1134): 1-7.

143. Um J, Kaufman A, Kostylev M, *et al*. Metabotropic glutamate receptor 5 is a co-receptor for Alzheimer Aβ oligomer bound to cellular prion protein. *Neuron*. 2013; 79(5): 887-902.

144. Hu N, Nicoll A, Zhang D, *et al*. mGlu5 receptor and cellular prion protein mediate amyloid-β-facilitated synaptic long-term depression in vivo. *Nat Commun*. 2014; 4(5): 3374.

145. Kuwahara C, Takeuchi A, Nishimura T, *et al*. Prions prevent neuronal cell-line death. *Nature*. 1999; 400(6741): 225-226.

146. Chiarini L, Freitas A, Zanata S, Brentani R, Martins V, Linden R. Cellular prion protein transduces neuroprotective signals. *EMBO J*. 2002; 21(13): 3317-3326.

147. Vey M, Pilkuhn S, Wille H, *et al.* Subcellular colocalization of the cellular and scrapie prion proteins in caveolae-like membranous domains. *PNAS*. 1996; 93(25): 14945-14949.

148. Sunyach C, Jen A, Deng J, *et al*. The mechanism of internalization of glycosylphosphatidyl-inositol-anchored prion protein. *EMBO J*. 2003; 22(14): 3591-3601.

149. Prado M, Alves-Silva J, Magalhães A, *et al.* PrPC on the road: Trafficking of the cellular prion protein. *J Neurochem*. 2004; 88(4): 769-781.

150. Taylor D, Hooper N. The prion protein and lipid rafts (Review). *Mol Membr Biol*. 2006; 23(1): 89-99.

151. Parkyn CJ, Vermeulen EGM, Mootoosamy RC, *et al.* LRP1 controls biosynthetic and endocytic trafficking of neuronal prion protein. *J Cell Sci*. 2008; 121(6): 773-783.

152. Sarnataro D, Caputo A, Casanova P, *et al.* Lipid rafts and clathrin cooperate in the internalization of PrPC in epithelial FRT cells. *PLoS One*. 2009; 4(6): 1-15.

153. Wulf M, Senatore A, Aguzzi A. The biological function of the cellular prion protein: An update. *BMC Biol*. 2017; 15(1): 1-13.

154. Caughey B, Dong A, Bhat K, Ernst D, Hayes S, Caughey W. Secondary structure analysis of the scrapie-associated protein PrP 27-30 in water by infrared spectroscopy. *Biochemistry*. 1991; 30(31): 7672-7680.

155. Sarnataro D, Anna P, Altamura G, *et al.* The 37 / 67kDa laminin receptor affects 37 / 67kDa LR cell surface localization and interaction with the cellular prion protein. *Sci Rep*. 2016; 6(24457): 1-13.

156. Lawson V, Lumicisi B, Welton J, *et al.* Glycosaminoglycan sulphation affects the seeded misfolding of a mutant prion protein. *PLoS One*. 2010; 5(8): e12351.

157. Kovacs N, Petrov A, Lanier K, Williams L. Frozen in Time: The history of proteins. *Mol Biol Evol*. 2017; 34(5): 1252-1260.

158. Kiachopoulos S, Heske J, Tatzelt J, Winklhofer K. Misfolding of the prion protein at the plasma membrane induces endocytosis, intracellular retention and degradation. *Traffic*. 2004; 5: 426-436.

159. Kristiansen M, Messenger M, Klöhn P, *et al.* Disease-related prion protein forms aggresomes in neuronal cells leading to caspase activation and apoptosis. *J Biol Chem*. 2005; 280(46): 38851-38861.

160. Vella L, Sharples R, Lawson V, Masters C, Cappai R, Hill A. Packaging of prions into exosomes is associated with a novel pathway of PrP processing. *J Pathol*. 2007; 211: 582-590.

161. Caughey B, Baron G, Chesebro B, Jeffrey M. Getting a grip on prions: oligomers, amyloids, and pathological membrane interactions. *Annu Rev Biochem*. 2009; 78: 177-204.

162. Prusiner S, Scott M, DeArmond S, Cohen F. Prion protein biology review. *Cell*. 1998; 93(3): 337-348.

163. Come J, Frasert P, Lansbury P. A Kinetic model for amyloid formation in the prion diseases : Importance of seeding. *PNAS*. 1993; 90(13): 5959-5963.

164. Surewicz WK, Apostol MI. Prion protein and its conformational conversion: A structural perspective. Tatzelt J, ed. *Top Curr Chem*. 2011; 305: 135-168.

165. Caughey B, Raymond G, Callahan M, Wong C, Baron G, Xiong L. Interactions and conversions of prion protein isoforms. *Adv Protein Chem*. 2001; 57: 139-169.

166. Jarrett J, Lansbury Jr P. Seeding "one-dimensional crystallization" of amyloid: A pathogenic mechanism in Alzheimer's disease and scrapie? *Cell*. 1993; 73: 1055-1058.

167. Scott M, Groth D, Foster D, *et al.* Propagation of prions with artificial properties in transgenic mice expressing chimeric PrP genes. *Cell*. 1993; 73(5): 979-988.

168. Hope J. The nature of the scrapie agent: The evolution of the Virino. *Ann N Y Acad Sci*. 1994; 724(1): 282-289.

169. Caughey B, Kocisko D, Raymond G, Lansbury P. Aggregates of scrapie-associated prion protein induce the cell-free conversion of protease-sensitive prion protein to the protease-resistant state. *Chem Biol*. 1995; 2(12): 807-817.

170. Eigen M. Prionics or the kinetic basis of prion diseases. *Biophys Chem*. 1996; 63(1): A1-18.

171. Masel J, Jansen VAA, Nowak MA. Quantifying the kinetic parameters of prion replication. *Biophys Chem*. 1999; 77(2): 139-152.

172. Muntau A, Leandro J, Staudigl M, Mayer F, Gersting S. Innovative strategies to treat protein misfolding in inborn errors of metabolism : pharmacological chaperones and proteostasis regulators. *J Inherit Metab Dis*. 2014; 37: 505-523.

173. Bessen R, Marsh R. Biochemical and physical properties of the prion protein from two strains of the transmissible mink encephalopathy agent. *J Virol*. 1992; 66(4): 2096-2101.

174. Safar J, Wille H, Itri V, *et al.* Eight prion strains have PrPSc molecules with different

conformations. *Nat Med*. 1998; 4(10): 1157-1165.

175. Telling G, Parchi P, Dearmond S, *et al*. Evidence for the conformation of the pathologic isoform of the prion protein enciphering and propagating prion diversity. *Science*. 2002; 274(5295): 2079-2082.

176. Pattison J. The emergence of bovine spongiform encephalopathy and related diseases. *Emerg Infect Dis*. 1998; 4(3): 390-394.

177. Bruce M. Scrapie strain variation and mutation. *Br Med Bull*. 1993; 49(4): 822-838.

178. Bartz J, Bessen R, McKenzie D, Marsh R. Adaptation and selection of prion protein strain conformations following interspecies transmission of transmissible Mink encephalopathy. *J Virol*. 2000; 74(12): 5542-5547.

179. Collinge J, Clarke A. A general model of prion strains and their pathogenicity. *Science (80-)*. 2007; 318(5852): 930-936.

180. Bruce M, Chree A, McConnell I, Foster J, Pearson G, Fraser H. Transmission of bovine spongiform encephalopathy and scrapie to mice: strain variation and the species barrier. *Philos Trans R Soc London Ser B Biol Sci*. 1994; 343(1306): 405-411.

181. Barron R, Thomson V, Jamieson E, *et al*. Changing a single amino acid in the N-terminus of murine PrP alters TSE incubation time across three species barriers. *EMBO J*. 2001; 20(18): 5070-5078.

182. Scott M, Peretz D, Nguyen H, Dearmond S, Prusiner S. Transmission barriers for bovine, ovine , and human prions in transgenic mice. *J Virol*. 2005; 79(9): 5259-5271.

183. Nonno R, Di Bari M, Cardone F, *et al.* Efficient transmission and characterization of Creutzfeldt-Jakob disease strains in Bank Voles. *PLoS Pathog*. 2006; 2(2): 0112-0120.

184. Fraser PE. Prions and prion-like proteins. *J Biol Chem*. 2014; 289(29): 19839-19840.

185. Haldiman T, Kim C, Cohen Y, *et al*. Co-existence of distinct prion types enables conformational evolution of human PrPSc by competitive selection*. *J Biol Chem*. 2013; 288(41): 29846-29861.

186. Solforosi L, Milani M, Mancini N, *et al.* A closer look at prion strains: characterization and important implications. 2013; 7(2): 99-108.

187. Scheibel T, Lindquist SL. The role of conformational flexibility in prion propagation and maintenance for Sup35p. *Nat Struct Biol*. 2001; 8(11): 958-962.

188. Serio T, Cashikar A, Kowal A, *et al.* Nucleated conformational conversion and the replication of conformational information by a prion determinant. *Science*. 2000; 289(5483): 1317-1321.

189. Bessen R, Marsh R. Distinct PrP properties suggest the molecular basis of strain variation in transmissible mink encephalopathy. *J Virol*. 1994; 68(12): 7859-7868.

190. Sigurdson C, Manco G, Schwarz P, *et al*. Strain fidelity of chronic wasting disease upon murine adaptation. *J Virol*. 2006; 80(24): 12303-12311.

191. Sigurdson C, Nilsson K, Hornemann S, *et al.* Prion strain discrimination using luminescent conjugated polymers. *Nat Methods*. 2007; 4: 1023-1030.

192. Nilsson M. Techniques to study amyloid fibril formation in vitro. *Methods*. 2004; 34(1): 151-160.

193. Asante E, Linehan J, Desbruslais M, *et al*. BSE prions propagate as either variant CJD-like or sporadic CJD-like prion strains in transgenic mice expressing human prion protein. *EMBO J*. 2002; 21(23): 6358-6366.

194. Lloyd S, Onwuazor O, Beck J, *et al.* Identification of multiple quantitative trait loci linked to prion disease incubation period in mice. *PNAS*. 2001; 98(11): 6279-6283.

195. Bae S, Jung S, Kim H, Son H. Correlation analysis for the incubation period of prion disease. *Prion*. 2012; 6(3): 276-281.

196. Scott M, Foster D, Mirenda C, *et al.* Transgenic mice expressing hamster prion protein produce species-specific scrapie infectivity and amyloid plaques. *Cell*. 1989; 59(5): 847-857.

197. Scott M, Köhler R, Foster D, Prusiner S. Chimeric prion protein expression in cultured cells and transgenic mice. *Protein Sci*. 1992; 1(8): 986-997.

198. Saijo E, Kang HE, Bian J, *et al*. Epigenetic dominance of prion conformers. *PLoS Pathog*. 2013; 9(10): e1003692.

199. Schätzl H, Costa M, Taylor L, Cohen F, Prusiner S. Prion protein gene variation among primates. *J Mol Biol*. 1995; 245: 362-374.

200. Parchi P, Giese A, Capellari S, *et al.* Classification of sporadic Creutzfeldt-Jakob disease based on molecular and phenotypic analysis of 300 subjects. *Ann Neurol*. 1999; 46: 224-233.

201. Puckett C, Concannon P, Casey C, Hood L. Genomic structure of the human prion protein gene. *Am J Hum Genet*. 1991; 49: 320-329.

202. Mahal S, Asante E, Antoniou M, Collinge J. Isolation and functional characterization of the promoter region of the human prion protein gene. *Gene*. 2001; 268(1): 105-114.

203. Kübler E, Oesch B, Raeber A. Diagnosis of prion diseases. *Br Med Bull*. 2003; 66: 267-279.

204. Liao Y, Lebo R, Clawson G, Smuckler E. Human prion protein cDNA: Molecular cloning, chromosomal mapping, and biological implications. *Science*. 1986; 233(4761): 364-367.

205. Kretzschmar H, Stowring L, Westaway D, Stubblebine W, Prusiner S, Dearmond S. Molecular cloning of a human prion protein cDNA. *DNA*. 1986; 5(4): 315-324.

206. Boellaard JW, Brown P, Tateishi J. Gerstmann-Sträussler-Scheinker disease- the dilemma of molecular and clinical correlations. *Clin Neuropathol*. 1999; 18(6): 271-285.

207. Monari L, Chen S, Brown P, *et al.* Fatal familial insomnia and familial Creutzfeldt-Jakob disease: different prion proteins determined by a DNA polymorphism. *PNAS*. 2006; 91(7): 2839-2842.

208. Yanagihara C, Yasuda M, Maeda K, Miyoshi K, Nishimura Y. Rapidly progressive dementia syndrome associated with a novel four extra repeat mutation in the prion protein gene. *J Neurol Neurosurg Psychiatry*. 2002; 72(6): 788-791.

209. Miura T, Sasaki S, Toyama A, Takeuchi H. Copper reduction by the octapeptide repeat region of prion protein: pH dependence and implications in cellular copper uptake. *Biochemistry*. 2005; 44(24): 8712-8720.

210. Giachin G, Biljan I, Ilc G, Plavec J, Legname G. Probing early misfolding events in prion protein mutants by NMR spectroscopy. *Molecules*. 2013; 18: 9451-9476.

211. Adrover M, Pauwels K, Prigent S, *et al.* Prion fibrillization is mediated by a native structural element that comprises helices H2 and H3. *J Biol Chem*. 2010; 285(27): 21004-21012.

212. Rossetti G, Giachin G, Legname G, Carloni P. Structural facets of disease-linked human prion protein mutants: A molecular dynamic study. *Proteins*. 2010; 78(16): 3270-3280.

213. van der Kamp MW, Daggett V. Pathogenic Mutations in the hydrophobic core of the human prion protein can promote structural instability and misfolding. *J Mol Biol*. 2010; 404(4): 732-748.

214. Acevedo-Morantes C, Wille H. The structure of human prions: From biology to structural models-considerations and pitfalls. *Viruses*. 2014; 6: 3875-3892.

215. Schmitt-Ulms G, Ehsani S, Watts JC, Westaway D, Wille H. Evolutionary descent of prion genes from the ZIP family of metal ion transporters. *PLoS One*. 2009; 4(9): e7208.

216. Ehsani S, Tao R, Pocanschi CL, Ren H, Harrison PM, Schmitt-Ulms G. Evidence for retrogene origins of the prion gene family. *PLoS One*. 2011; 6(10): e26800.

217. Rieger R, Edenhofer F, Lasmézas CI, Weiss S. The human 37-kDa laminin receptor precursor interacts with the prion protein in eukaryotic cells. *Nat Med*. 1997; 3(12): 1383-1388.

218. Graham J, Kurian D, Agarwal S, *et al*. Na+/K+-ATPase is present in scrapie-associated fibrils, modulates PrP misfolding in vitro and links PrP function and dysfunction. *PLoS One*. 2011; 6(11): e26813.

219. Yoo B, Krapfenbauer K, Cairns N, Belay G, Bajo M, Lubec G. Overexpressed protein disulfide isomerase in brains of patients with sporadic Creutzfeldt-Jakob disease. *Neurosci Lett*. 2002; 334: 196-200.

220. Cortez L, Sim V. Implications of prion polymorphisms. *Prion*. 2013; 7(4): 276-279.

221. Palmer M, Dryden A, Hughes J, Collinge J. Homozygous prion protein genotype predisposes to sporadic Creutzfeldt–Jakob disease. *Nature*. 1991; 352(6333): 340-342.

222. Brown K, Mastrianni JA. The prion diseases. *J Geriatr Psychiatry Neurol*. 2010; 23(4): 277-298.

223. Doh-Ura K, Kitamoto T, Sakaki Y, Tateishi J. CJD discrepancy. *Nature*. 1991; 353(6347): 801-802.

224. Kitamoto T, Tateishi J. Human prion diseases with variant prion protein. *Philos Trans R Soc Lond B Biol Sci*. 1994; 343(1306): 391-398.

225. Tanaka Y, Minematsu K, Moriyasu H, *et al.* A Japanese family with a variant of Gerstmann-Straussler-Scheinker disease. *J Neurol Neurosurg Psychiatry*. 1997; 62: 454-457.

226. Hizume M, Kobayashi A, Teruya K, *et al.* Human prion protein (PrP) 219K is converted to PrPSc but shows heterozygous inhibition in variant Creutzfeldt-Jakob disease infection. *J Biol Chem*. 2009; 284(6): 3603-3609.

227. Kyle R. Amyloidosis: A convoluted story. *Br J Haematol*. 2001; 114: 529-538.

228. Sipe J, Cohen A. Review: History of the amyloid fibril. *J Struct Biol*. 2000; 130: 88-98.

229. Rambaran R, Serpell L. Amyloid fibrils: Abnormal protein assembly. *Prion*. 2008; 2(3): 112-117.

230. Wiltzius J, Sievers S, Sawaya M, *et al*. Atomic structure of the cross-beta spine of islet amyloid polypeptide (amylin). *Protein Sci*. 2008; 17: 1467-1474.

231. Jahn T, Makin O, Morris K, *et al*. The Common architecture of cross-β amyloid. *J Mol Biol*. 2010; 395: 717-727.

232. Volpatti L, Knowles T. Polymer physics inspired approaches for the study of the mechanical properties of amyloid fibrils. *J Polym Sci*. 2014; 52: 281-292.

233. Vázquez-Fernández E, Vos M, Afanasyev P, *et al.* The structural architecture of an infectious mammalian prion using electron cryomicroscopy. *PLoS Pathog*. 2016; 12(9): e1005835.

234. Nyrkova I, Semenov A, Aggeli A, Bell M, Boden N, McLeish T. Self-assembly and structure transformations in living polymers forming fibrils. *Eur Phys J B*. 2000; 17(3): 499-513.

235. Smith J, Knowles T, Dobson C, Macphee C, Welland M. Characterization of the nanoscale properties of individual amyloid fibrils. *PNAS*. 2006; 103(43): 15806-15811.

236. Knowles T, Fitzpatrick A, Meehan S, *et al.* Role of intermolecular forces in protein nanofibrils. *Science*. 2007; 318: 1900-1904.

237. Ritter C, Maddelein M, Siemer A, *et al.* Correlation of structural elements and infectivity of the HET-s prion. *Nature*. 2005; 435(7043): 844-848.

238. Wasmer C, Lange A, Melckebeke H, Siemer A, Riek R, Meier B. Amyloid fibrils of the HET-s(218–289) prion form a beta-solenoid with a triangular hydrophobic core. *Science*. 2008; 319: 1523-1527.

239. Tycko R, Wickner R. Molecular structures of amyloid and prion fibrils: Consensus vs. Controversy. *Acc Chem Res*. 2013; 46(7): 1487-1496.

240. Petkova A, Leapman R, Guo Z, *et al*. Self-propagating, molecular-level polymorphism in Alzheimer's β-Amyloid fibrils. *Science*. 2005; 307(5707): 262-265.

241. Chen B, Thurber K, Shewmaker F, Wickner R, Tycko R. Measurement of amyloid fibril mass-per-length by tilted-beam transmission electron microscopy. *PNAS*. 2009; 106(34): 14339-14344.

242. Ross E, Minton A, Wickner R. Prion domains: sequences, structures and interactions. *Nat Cell Biol*. 2005; 7(11): 1039-1044.

243. Sen A, Baxa U, Simon M, *et al*. Mass Analysis by scanning transmission electron microscopy and electron diffraction validate predictions of stacked beta-solenoid model of HET-s prion fibrils. *J Biol Chem*. 2007; 282(8): 5545-5550.

244. Wickner R, Shewmaker F, Kryndushkin D, Edskes H. Protein inheritance (prions) based on parallel in-register beta-sheet amyloid structures. *BioEssays*. 2008; 30: 955-964.

245. Sabate R, Rousseau F, Schymkowitz J, Ventura S. What makes a protein sequence a prion? *PloS Comput Biol Comput Biol*. 2015; 11(1): e1004013.

246. Bateman D, Wickner R. [PSI+] prion transmission barriers protect *Saccharomyces cerevisiae* from infection: Intraspecies "species barriers." *Genetics*. 2012; 190(2): 569-579.

247. DePace A, Santoso A, Hillner P, Weissman J. A critical role for amino-terminal glutamine/asparagine repeats in the formation and propagation of a yeast prion. *Cell*. 1998; 93(7): 1241-1252.

248. Doel S, McCready S, Nierras C, Cox B. The dominant PNM2(-) mutation which eliminates the ψ factor of *Saccharomyces cerevisiae* is the result of a missense mutation in the SUP35 gene. *Genetics*. 1994; 137: 659-670.

249. Murphy M, Iii H. Alzheimer's disease and the β-amyloid peptide. *J Alzheimer's Dis*. 2010; 19(1): 1-17.

250. Raskin J, Cummings J, Hardy J, Schuh K, Dean R. Neurobiology of Alzheimer's disease: Integrated molecular, physiological, anatomical, biomarker, and cognitive dimensions. *Curr Alzheimer Res*. 2015; 12(8): 712-722.

251. Tycko R, Ishii Y. Constraints on supramolecular structure in amyloid fibrils from two-dimensional solid-state NMR spectroscopy with uniform isotopic labeling. *J Am Chem Soc*. 2003; 125(22): 6606-6607.

252. Colvin M, Silvers R, Ni Q, *et al*. Atomic resolution structure of monomorphic Aβ42 amyloid fibrils. *J Am Chem Soc*. 2016; 138(30): 9663-9674.

253. Antzutkin O, Balbach J, Leapman R, Rizzo N, Reed J, Tycko R. Multiple quantum solid-state NMR indicates a parallel, not antiparallel, organization of beta -sheets in Alzheimer's beta-amyloid fibrils. *PNAS*. 2000; 97(24): 13045-13050.

254. Schmidt M, Sachse C, Richter W, Xu C, Fandrich M, Grigorieff N. Comparison of

Alzheimer Aβ(1-40) and Aβ(1–42) amyloid fibrils reveals similar protofilament structures. *PNAS*. 2009; 106(47): 19813-19818.

255. Luhrs T, Ritter C, Adrian M, *et al.* 3D structure of Alzheimer's amyloid-beta-(1–42) fibrils. *PNAS*. 2005; 102(48): 17342-17347.

256. Petkova A, Yau W, Tycko R. Experimental constraints on quaternary structure in Alzheimer's β-amyloid fibrils. *Biochemistry*. 2006; 45(2): 498-512.

257. Kajava A, Steven A. The turn of the screw: Variations of the abundant β-solenoid motif in passenger domains of Type V secretory proteins. *J Struct Biol*. 2006; 155: 306-315.

258. Pan K, Baldwin M, Nguyen J, *et al.* Conversion of α-Helices β-Sheets features in the formation of the scrapie prion proteins. *PNAS*. 1993; 90(23): 10962-10966.

259. Riesner D. Biochemistry and structure of PrPC and PrPSc. *Br Med Bull*. 2003; 66: 21-33.

260. Riek R, Hornemann S, Wider G, Billeter M, Glockshuber R, Wuthrich K. NMR structure of the mouse prion protein domain PrP(121-231). *Nature*. 1996; 382(6587): 180-182.

261. Riek R, Hornemann S, Wider G, Glockshuber R, Wüthrich K. NMR characterization of the full-length recombinant murine prion protein, mPrP(23-231). *FEBS Lett*. 1997; 413: 282-288.

262. Hornemann S, Schorn C, Wüthrich K. NMR structure of the bovine prion protein isolated from healthy calf brains. *EMBO Rep*. 2004; 5(12): 1159-1164.

263. Liu L, Jiang D, McDonald A, Hao Y, Millhauser G, Zhou F. Copper redox cycling in the prion protein depends critically on binding mode. *J Am Chem Soc*. 2011; 133(31): 12229-12237.

264. Hornshaw M, McDermott J, Candy J. Copper binding to the N-terminal tandem repeat regions of mammalian and avian prion protein. *Biochem Biophys Res Commun*. 1995; 207(2): 621-629.

265. Stöckel J, Safar J, Wallace A, Cohen F, Prusiner S. Prion protein selectively binds copper(II) ions. *Biochemistry*. 1998; 37(20): 7185-7193.

266. Harris D, Pauly P. Copper stimulates endocytosis of the prion protein. *J Biol Chem*. 1998; 273(50): 33107-33110.

267. Maiti N, Surewicz W. The Role of Disulfide Bridge in the folding and stability of the recombinant human prion protein. *J Biol Chem*. 2001; 276(4): 2427-2431.

268. Gasset M, Baldwin M, Fletrerickti R, Prusiner S. Perturbation of the secondary structure of the scrapie prion protein under conditions that alter infectivity. *PNAS*. 1993; 90: 1-5.

269. Nguyen J, Inouye H, Baldwin M, *et al.* X-ray diffraction of scrapie prion rods and PrP peptides. *J Mol Biol*. 1995; 252: 412-422.

270. Requena JR, Wille H. The structure of the infectious prion protein: Experimental data and molecular models. *Prion*. 2014; 8(1): 1-7.

271. Petrotchenko E, Borchers C. Modern Mass Spectrometry-based structural proteomics. *Adv*

Protein Chem Struct Biol. 2014; 95: 193-213.

272. Morihara K, Tsuzuki H. Specificity of proteinase K from *Tritirachium album* limber for synthetic peptides. *Agri Biol Chem*. 1975; 39(7): 1489-1492.

273. Donne D, Viles J, Groth D, *et al*. Structure of the recombinant full-length hamster prion protein PrP(29-231): The N-Terminus is highly flexible. *PNAS*. 1997; 94(25): 13452-13457.

274. Colby D, Prusiner S. Prions. *Cold Spring Harb Perspect Biol*. 2011; 3(a0068333): 1-22.

275. Smirnovas V, Baron G, Offerdahl D, Raymond G, Caughey B, Surewicz W. Structural organizaton of brain-derived mammalian prions as probed by hydrogen excange. *Nat Struct Mol Biol*. 2011; 18(4): 504-506.

276. Baron G, Hughson A, Raymond G, *et al.* Effect of glycans and GPI anchor on strain dependent conformations of scrapie prion protein: Improved purifications and IR spectra. *Biochemistry*. 2011; 50(21): 4479-4490.

277. Bauer H, Aebi U, Häner M, *et al.* Architecture and polymorphism of fibrillar supramolecular assemblies produced by in vitro aggregation of human calcitonin. *J Struct Biol*. 1995; 115(1): 1-15.

278. Goldsbury C, Cooper G, Goldie K, *et al.* Polymorphic fibrillar assembly of human amylin. *J Struct Biol*. 1997; 119(1): 17-27.

279. Goldsbury C, Goldie K, Pellaud J, *et al*. Amyloid fibril formation from full-length and fragments of amylin. *J Struct Biol*. 2000; 130(2-3): 352-362.

280. Sgourakis N, Yau W, Qiang W. Modeling an in-register, parallel "Iowa" Aβ fibril structure using solid-state NMR data from labeled samples with Rosetta. *Structure*. 2015; 23(1): 216-227.

281. Lashuel H, Wall J. Molecular electron microscopy approaches to elucidating the mechanisms of protein fibrillogenesis. In: Sigurdsson EM, ed. *Methods in Molecular Biology*. Vol 299. Totowa, NJ: Humana Press Inc.; 2005: 81-101.

282. Saibil H. Macromolecular structure determination by cryo-electron microscopy. *Acta Crystallogr Sect D Biol Crystallogr*. 2000; 56(10): 1215-1222.

283. Serpell L, Sunde M, Fraser P, *et al*. Examination of the structure of the transthyretin amyloid fibril by image reconstruction from electron micrographs. *J Mol Biol*. 1995; 254: 113-118.

284. Jimenez J, Guijarro J, Orlova E, *et al*. Cryo-electron microscopy structure of an SH3 amyloid fibril and model of the molecular packing. *EMBO J*. 1999; 18(4): 815-821.

285. Sachse C. Single-particle based helical reconstruction—how to make the most of real and Fourier space. *AIMS Biophys*. 2015; 2(2): 219-244.

286. Komatsu H, Feingold-LE E, Sharp K, Rastogi T, Axelsen P. Intrinsic linear heterogeneity of amyloid β protein fibrils revealed by higher resolution mass-per-length determinations. *J Biol Chem*. 2010; 285(53): 41843-41851.

287. Cobb N, Sonnichsen D, Mchaourab H, Surewicz W. Molecular architecture of human prion

protein amyloid : A parallel, in-register beta-structure. *PNAS*. 2007; 104(48): 18946-18951.

288. Groveman B, Dolan M, Taubner L, Kraus A, Wickner R, Caughey B. Parallel in-register intermolecular β-sheet architectures for prion-seeded prion protein (PrP) amyloids. *J Biol Chem*. 2014; 289(35): 24129-24142.

289. Wille H, Michelitsch M, Guenebaut V, *et al*. Structural studies of the scrapie prion protein by electron crystallography. *PNAS*. 2002; 99(6): 3563-3568.

290. Govaerts C, Wille H, Prusiner S, Cohen F. Evidence for assembly of prions with left-handed beta-helices into trimers. *PNAS*. 2004; 101(22): 8342-8347.

291. Gabizon R, McKinley M, Groth D, Kenaga L, Prusiner S. Properties of scrapie prion protein liposomes. *J Biol Chem*. 1988; 263(10): 4950-4955.

292. Sang J, Meisl G, Thackray A, *et al*. Direct observation of murine prion protein replication *in vitro*. *J Am Chem Soc*. 2018; 140(44): 14789-14798.

293. Carlson G, Kingsbury D, Goodman P, *et al*. Linkage of prion protein and scrapie incubation time genes. *Cell*. 1986; 46(4): 503-511.

294. Meggendorfer F. Klinische und genealogische Beobachtungen bein einem Fall von spastischen Pseudokosklerose Jakobs. *Z Neurol Psyciath*. 1930; 128: 337-341.

295. Kretzschmar HA, Neumann M, Stavrou D. Codon 178 mutation of the human prion protein gene in a German family (Backer family): sequencing data from 72-year-old celloidin-embedded brain tissue. *Acta Neuropathol*. 1995; 89(1): 96-98.

296. Clift K, Guthrie K, Klee E, *et al*. Familial Creutzfeldt-Jakob disease : Case report and role of genetic counseling in post mortem testing. *Prion*. 2016; 10: 502-506.

297. Gambetti P, Kong Q, Zou W, Parchi P, Chen S. Sporadic and familial CJD : classification and characterization. *Br Med Bull*. 2003; 66: 213-239.

298. Geschwind M. Prion diseases. *Contin (Minneap Minn)*. 2015; 21(6): 1612-1638.

299. Prusiner S, McKinley M, Bowman K, *et al*. Scrapie prions aggregate to form amyloid-like birefringent rods. *Cell*. 1983; 35(2): 349-358.

300. Ma J, Wang F. Prion disease and the "protein-only hypothesis." *Essays Biochem*. 2014; 56: 181-191.

301. Van der Horst DJ, Ryan RO. Lipid Transport, In reference Module in life Sciences. *Elsevier*; 2017; 1-26

302. Singh A, Qing L, Kong Q, Singh N. Change in the characteristics of ferritin induces iron imbalance in prion disease affected brains. *Neurobiol Dis*. 2012; 45(3): 930-938.

303. Bruckman M, Hern S, Jiang K, Flask C, Yu X, Steinmetz N. Tobacco mosaic virus rods and spheres as supramolecular high-relaxivity MRI contrast agents. *J Mater Chem B*. 2013; 1: 1482-1490.

304. Namba K, Stubbs G. Structure of Tobacco Mosaic Virus at 3.6 Å resolution : Implications for Assembly. *Science*. 1986; 231(4744): 1401-1406.

305. Saverioni D, Notari S, Capellari S, *et al*. Analyses of protease resistance and aggregation state of abnormal prion protein across the spectrum of human prions. *J Biol Chem*. 2013; 288(39): 27972-27985.

306. Kobayashi A, Satoh S, Ironside JW, Mohri S. Kitamoto T. Type 1 and type 2 human PrPSc have different aggregation sizes in methionine homozygotes with sporadic, iatrogenic and variant Creutzfeldt-Jakob disease. 2019; :237-240.

307. Cali I, Castellani R, Alshekhlee A, *et al*. Co-existence of scrapie prion protein Types 1 and 2 in sporadic Creutzfeldt–Jakob disease: Its effect on the phenotype and prion-type characteristics. *Brain*. 2009; 132: 2643-2658.

308. Tsuboi Y, Baba Y, Doh-ura K, Imamura A, Fujioka S, Yamada T. Diffusion-weighted MRI in familial Creutzfeldt-Jakob disease with the codon 200 mutation in the prion protein gene. *J Neurol Sci*. 2005; 232(1): 45-49.

309. Wieser H, Schindler K, Zumsteg D. EEG in Creutzfeldt–Jakob disease. *Clin Neurophysiol*. 2006; 117(5): 935-951.

310. Puoti G, Bizzi A, Forloni G, Safar J, Tagliavini F, Gambetti P. Sporadic human prion diseases: Molecular insights and diagnosis. *Lancet Neurol*. 2012; 11(7): 618-628.

311. Zerr I, Kallenberg K, Summers D, *et al*. Updated clinical diagnostic criteria for sporadic Creutzfeldt-Jakob disease. *Brain*. 2009; 132(10): 2659-2668.

312. Tschampa H, Kallenberg K, Kretzschmar H, *et al*. Pattern of cortical changes in sporadic Creutzfeldt-Jakob disease. *AJNR*. 2007; 28: 1114-1118.

313. Hartmann P, Ramseier A, Gudat F, Mihatsch MJ, Polasek W, Geisenhoff C. Das Normgewicht des Gehirns beim Erwachsenen in Abhängigkeit von Alter, Geschlecht, Körpergröße und Gewicht. *Pathologe*. 1994; 15(3): 165-170.

314. Cardone F, Liu Q, Petraroli R, *et al*. Prion protein glycotype analysis in familial and sporadic Creutzfeldt-Jakob disease patients. *Brain Res Bull*. 1999; 49(6): 429-433.

315. Terry C, Wenborn A, Gros N, *et al*. Ex vivo mammalian prions are formed of paired double helical prion protein fibrils. *Open Biol*. 2016; 6(160035): 1-12.

316. Parchi P, Saverioni D. Molecular pathology, classification, and diagnosis of sporadic human prion disease variants. *Folia Neuropathol*. 2012; 50(1): 20-45.

317. Prusiner S, Scott M, Foster D, *et al*. Transgenetic studies implicate interactions between homologous PrP isoforms in scrapie prion replication. *Cell*. 1990; 63(4): 673-686.

318. Kocisko D, Come J, Priola S, *et al*. Cell-free formation of protease-resistant prion protein. *Nature*. 1994; 370(6489): 471-474.

319. Hosszu L, Jackson G, Trevitt C, *et al*. The Residue 129 Polymorphism in human prion protein does not confer susceptibility to Creutzfeldt-Jakob disease by altering the structure or global stability of PrPC. *J Biol Chem*. 2004; 279(27): 28515-28521.

320. Hill A, Joiner S, Wadsworth J, *et al*. Molecular classification of sporadic Creutzfeldt-Jakob disease. *Adv Access Pub*. 2003; 126: 1333-1346.

321. Stumpf M, Krakauer D. Mapping the parameters of prion-induced neuropathology. *PNAS*. 2000; 97(19): 10573-10577.

322. Mead S, Whitfield J, Poulter M, *et al.* Genetic susceptibility , evolution and the kuru epidemic. *Philos Trans R Soc B Biol Sci*. 2008; 363: 3741-3746.

323. Tagliavini F, Lievens PM, Tranchant C, *et al*. A 7-kDa Prion Protein (PrP) Fragment , an integral component of the PrP region required for infectivity, is the major amyloid protein in Gerstmann-Straüssler-Scheinker disease A117V*. 2001; 276(8): 6009-6015.

324. Pirisinu L, Di Bari M, D'Agostino C, *et al.* Gerstmann-Sträussler-Scheinker disease subtypes efficiently transmit in bank voles as genuine prion diseases. *Sci Rep*. 2016; 6(20443): 1-9.

325. Mercer R, Daude N, Dorosh L, *et al.* A novel Gerstmann- Sträussler disease mutation defines a precursor for amyloidogenic 8 kDa PrP fragments and reveals N-terminal structural changes shared by other GSS alleles. *PLoS Pathog*. 2018; 14(1): e1006826.

326. Jiménez-Huete A, Lievens PM, Vidal R, *et a*l. Endogenous proteolytic cleavage of normal and disease-associated isoforms of the human prion protein in neural and non-neural tissues. *Am J Pathol*. 1998; 153(5): 1561-1572.

327. Nicoll A, Collinge J. Preventing prion pathogenicity by targeting the cellular prion protein. *Infect Dis Drug Targets*. 2009; 9: 48-57.